University of Alberta

DFT Investigation on the Structure and Composition of the Phosphosulfide Overlayer on Ni_2P Hydrotreating Catalyst

by

Abu Saleh Muhammad Junaid ©

A thesis submitted to the Faculty of Graduate Studies and Research
in partial fulfillment of the requirements for the degree of

Master of Science

in

Chemical Engineering

Department of Chemical and Materials Engineering

Edmonton, Alberta

Fall 2006

Library and Archives Canada

Published Heritage Branch

395 Wellington Street
Ottawa ON K1A 0N4
Canada

Bibliothèque et Archives Canada

Direction du Patrimoine de l'édition

395, rue Wellington
Ottawa ON K1A 0N4
Canada

Your file Votre référence
ISBN: 978-0-494-22296-6
Our file Notre référence
ISBN: 978-0-494-22296-6

NOTICE:
The author has granted a non-exclusive license allowing Library and Archives Canada to reproduce, publish, archive, preserve, conserve, communicate to the public by telecommunication or on the Internet, loan, distribute and sell theses worldwide, for commercial or non-commercial purposes, in microform, paper, electronic and/or any other formats.

The author retains copyright ownership and moral rights in this thesis. Neither the thesis nor substantial extracts from it may be printed or otherwise reproduced without the author's permission.

AVIS:
L'auteur a accordé une licence non exclusive permettant à la Bibliothèque et Archives Canada de reproduire, publier, archiver, sauvegarder, conserver, transmettre au public par télécommunication ou par l'Internet, prêter, distribuer et vendre des thèses partout dans le monde, à des fins commerciales ou autres, sur support microforme, papier, électronique et/ou autres formats.

L'auteur conserve la propriété du droit d'auteur et des droits moraux qui protège cette thèse. Ni la thèse ni des extraits substantiels de celle-ci ne doivent être imprimés ou autrement reproduits sans son autorisation.

In compliance with the Canadian Privacy Act some supporting forms may have been removed from this thesis.

While these forms may be included in the document page count, their removal does not represent any loss of content from the thesis.

Conformément à la loi canadienne sur la protection de la vie privée, quelques formulaires secondaires ont été enlevés de cette thèse.

Bien que ces formulaires aient inclus dans la pagination, il n'y aura aucun contenu manquant.

Canada

Abstract

Ni_2P is one of the most active hydrodesulfurization (HDS) catalysts among the group of transition metal phosphides, and has previously shown significantly higher activity and conversion compared to conventional HDS catalysts on both a weight and active site basis. Previous experimental studies using XRD and EXAFS have indicated the formation of a surface phosphosulfide phase of unknown structure on top of a Ni_2P core during HDS. This study represents a systematic investigation of the relative energetics of possible surface compositions of Ni_2P under hydrotrdesulfurization conditions (i.e. H_2S/H_2, temperature) using density-functional theory (DFT) calculations. Using a systematic and sequential approach to study the energetics of sulfur incorporation on the Ni_3P_2 termination of $Ni_2P(001)$ as a function of concentration and atomic location, the a thermodynamically stable phosphosulfide surface consistent with a surface stoichiometry of Ni_3PS plus adsorbed sulphur atoms has been identified. CO absorbance frequencies on the Ni_3P_2 and Ni_3PS surface are calculated as a function of surface coverage, and are shown to be in excellent agreement with previously published experimental CO infrared spectroscopy (IR) data on spent Ni_2P (i.e phosphosulfide surface) HDS catalysts.

Acknowledgement

I would like to appreciate the supervision and effort of Dr. Alan E. Nelson, former faculty member, Department of Chemical and Materials Engineering, University of Alberta. His persuasion and enthusiasm had mobilized the progression of the work to a great extent. I would also like to express my gratitude to Dr. Mingyong Sun, former group member, for his help and affiliation with the project.

I am more than indebted to my former and current group members, who had been wonderful in so many ways in the past one and half years or so. I am delighted to acknowledge particularly, in alphabetical order, Alex Abraham, Brian Greenhalgh, Claudia Guarino, Joyce Funk, Ling Yang, Mildred Becerra, Dr. Peter Unwin, Dr. Shaofeng Yang, Dr. Wa'el Abdallah, Dr. Yadollah Maham, Zhenhui Wang and Dr. Zhiming Liu. I also acknowledge Martina Rusnacik and Shahram Sharafnia as being my former group members.

I am grateful for the cooperation of Bob Barton and Jack Gibeau of the computer support, and the help of Mohammed Al-Saleh regarding the formatting of this thesis.

I want to mention the constant mental support of Enayet Bin Halim, my room-mate, who had been my family here, away from my home. I want to express my gratitude to Saikat and the rest of the Bangladeshi students' community here in U of A, for the good times. And of course, I do not have words to express my gratitude to my family – my parents, Anup, Shumon, Shoumi and Moumi, back in Bangladesh; I cannot wait to see you again.

Mita, everything was not fair to us, and only we know what we had to go through in the past morbid times. I wish I could uplift every uncertainty, torment, and frustrations I have inflicted upon you, and still do not have any answers for. But this work is only a legacy of your sacrifice. And I am grateful to you Almighty, for being with us through this very very difficult phase of our lives.

A. S. M. Junaid
September 26, 2006.

To Mita and my family—those who suffered

TABLE OF CONTENTS

CHAPTER 1: INTRODUCTION

1.1 Sulfur in Petroleum Hydrocarbons 1

1.2 Current Technology for Sulfur Removal 2

1.3 Developments in HDS Processes and Catalysts 3

1.4 Nickel Phosphide and Objective of This Study 3

CHAPTER 2: LITERATURE REVIEW

2.1 Introduction 6

2.2 The Hydrodesulfurization Process 8

2.3 Development of Conventional HDS Catalysts 9

2.4 Novel HDS Catalysts and Processes 12

2.5 The Nickel Phosphide Catalyst 17

2.6 Summary 24

CHAPTER 3: EXPERIMENTAL METHODS

3.1 Introduction 25

3.2 Molecular Modeling: Development of DFT 25

3.2.1 Quantum Mechanics and Schrödinger's Wave Equation 25

3.2.2 The Earlier Approaches 27

3.2.3 The *Ab Initio* Methods 30

3.2.4 The Semiempirical Methods 34

3.2.5 The Density Functional Theory 35

3.3 DFT Simulation: Procedures and Parameters 40

3.3.1 Simulation Procedures 40

3.3.1.1 Geometry Optimization 41

3.3.1.2 Surface Energetics 41

3.3.1.3 Thermodynamic Calculations 42

3.3.1.4 Vibrational Frequency Calculations 44

3.3.1.5 Transition State Search 45

3.3.2 Salient DFT Parameters Used in the Study 45

CHAPTER 4: RESULTS

4.1 Introduction 49
4.2 Summary of Parameters 49
4.3 The Structure and Surface of Ni_2P 51
4.4 Incorporation of Sulfur in the Ni_2P Structure 52
4.4.1 Molecular and Dissociative Adsorption of H_2S 53
4.4.2 Replacement of Phosphorus Atoms from the Surface 63
4.4.3 Complete Sulfidation 65
4.4.4 Summary of the Studies on Sulfur Incorporation in Ni_2P 65
4.5 CO Adsorption 72
4.5.1 Modes of CO Adsorption 72
4.5.2 Adsorption Energy 73
4.5.3 Vibrational Frequency Analysis 74
4.6 Hydrogen Adsorption 79
4.6.1 Modes of Adsorption 79
4.6.2 Adsorption Energy 80
4.6.3 Transient State Search 81
4.7 Summary of the Results 84

CHAPTER 5: DISCUSSION

5.1 Introduction 85
5.2 Structure and Surface of Pristine Ni_2P 85
5.3 Incorporation of Sulfur in Ni_2P Structure 85
5.3.1 Molecular and Dissociative Adsorption of H_2S 86
5.3.2 Replacement of phosphorus atoms from the surface 88
5.3.3 Complete Sulfidation 90
5.4 CO Adsorption 90
5.4.1 Adsorption Energy 91
5.4.2 Vibrational Frequency 92

5.5 Hydrogen Adsorption 96

CHAPTER 6: CONCLUSIONS

6.1 Conclusions from the Current Study 98

6.2 Recommendations and Future Works 99

BIBLIOGRAPHY 101

APPENDIX A 107

APPENDIX B 108

APPENDIX C 109

APPENDIX D 111

APPENDIX E 114

LIST OF TABLES

Table 4.1	Total Energy of the structures and the chemical species for determining the relative stability of Ni_3P_2 and Ni_3P surfaces.	55
Table 4.2	Energy changes for the most stable configurations for the replacement of different number of phosphorus atoms from the surface.	68
Table 4.3	Adsorption energies of CO on the pristine Ni_3P_2, and the 50% phosphorus replaced Ni_3PS surfaces, corresponding to different surface coverages.	78
Table 4.4	Calculated vibrational frequencies (cm^{-1}) of adsorbed CO molecule on the pristine Ni_3P_2 and the 50% phosphorus-replaced Ni_3PS surfaces, corresponding to different surface coverages.	78
Table A.1	Variation of adsorption energy and frequency values for 1 ML CO adsorbed on the sulfided and unsulfided Ni_2P unit cell surface, for changing k-point parameters.	107
Table B.1	Calculated data for dissociative adsorption of H_2S as atomic sulfur on pristine Ni_2P supercell surface.	108
Table C.1	Calculated data for the replacement of the phosphorus atoms from the Ni_3P_2 surface by the sulfur atoms from the gas phase H_2S.	109
Table D.1	Calculated data for the stable modes of CO adsorption on the pristine Ni_2P surface, for different surface coverages.	111
Table D.2	Calculated data for the stable modes of CO adsorption on the partially phosphorus replaced Ni_2P surface, for different surface coverages.	113
Table E.1	Calculated data for the stable modes of hydrogen adsorption on the pristine Ni_2P unit cell surface.	114
Table E.2	Calculated data for the stable modes of adsorption of molecular hydrogen on the partially replaced Ni_2P unit cell surface.	115
Table E.3	Calculated data for the stable modes of adsorption of hydrogen atoms on the partially replaced Ni_2P unit cell surface	115

LIST OF FIGURES

Figure 2.1	Major sulfur contaminants in petroleum and coal–derived products: Polycyclic Aromatic Sulfur Heterocycles (PASH).	7
Figure 2.2	(a) Comparative HDS and HDN activity (per unit active site basis) of transition metal phosphide catalysts in the hydroprocessing of a model feed at 643 K and 3.1 MPa; (b) Comparative Thiophene HDS activity (per unit weight basis) of nickel phosphide and the conventional hydrotreating catalysts.	19
Figure 2.3	EXAFS of fresh and spent Ni_2P/SiO_2 catalyst (initial Ni/P=1) before (left) and after (right) DBT reaction.	20
Figure 2.4	Comparison of X-ray diffraction patterns for fresh (lower) and spent (upper) samples for different initial Ni/P ratios.	21
Figure 2.5	IR spectra of CO adsorbed at room temperature on phosphide catalysts: (left) reduced by flowing H_2 at 873 K for 2 hours; (right) sulfided with a 10 mol% H_2S/H_2 mixture at 593 K for 1 hour.	23
Figure 4.1	Unit Crystal of Ni_2P and the two possible terminations in (001) direction. Nickel and phosphorus atoms are presented in cyan and purple colors, respectively.	54
Figure 4.2	Five layered unit cells with either Ni_3P_2 or Ni_3P termination and constrained middle layers. The cells are constructed by cleaving the unit crystal along the (001) plane, for surface energetics calculations.	54
Figure 4.3	The construction of a four layered 2x2x2 supercell from the periodic repetition of the unit crystal along the x and y-directions.	56
Figure 4.4	Top view of the Ni_3P_2 surface of the Ni_2P supercell. The nickel atoms on the Ni_3P_2 surface form three fold hollows (TFH) on the surface. Nickel and phosphorus atoms are presented in cyan and purple colors, respectively.	56
Figure 4.5	The stable modes of adsorption of H_2S as a molecule on the Ni_3P_2 surface. Cyan, purple, yellow and white represent nickel, phosphorus, sulfur and hydrogen atoms respectively.	57
Figure 4.6	The stable modes of dissociative adsorption of H_2S on the Ni_3P_2	60

surface as adsorbed –SH species. Cyan, purple, yellow and white represent nickel, phosphorus, sulfur and hydrogen atoms respectively.

Figure 4.7 Dissociative adsorption of H_2S as sulfur atom on the Ni_3P_2 surface. Cyan, purple, and yellow represent nickel, phosphorus and sulfur atoms respectively. 61

Figure 4.8 Free energy change for molecular and dissociative adsorption of H_2S on the Ni_3P_2 (001) surface, as a function of temperature at 5.0 MPa hydrogen and 0.1 MPa H_2S pressure. The pristine Ni_3P_2 surface, and gas-phase H_2S and H_2 are taken as the energetic references. 62

Figure 4.9 Energy changes related to the steps for replacement of phosphorus on the Ni_3P_2 surface by sulfur atoms from the gas phase H_2S. 67

Figure 4.10 The Ni_3P_2 surface of the 2x2x2 Ni_2P supercell. The Phosphorus atoms are purple and numbered. 68

Figure 4.11 The 50% phosphorus replaced Ni_3P_2 surface (Ni_3PS). Replacements took place at all the available distant positions. Cyan, purple and yellow represent nickel, phosphorus and sulfur atoms respectively. 69

Figure 4.12 Free energy change of 50% phosphorus replaced Ni_2P (001) surface (Ni_3PS) as a function of temperature at 5.0 MPa hydrogen and 0.1 MPa H_2S. The pristine Ni_3P_2 surface, and gas phase H_2S and H_2 are taken as the energetic references. 69

Figure 4.13 The 62.5% phosphorus replaced Ni_3P_2 surface, resulting from the replacement at a neighboring position, after replacing the phosphorus atoms from all the available distant positions on the supercell surface. Cyan, purple and yellow represent nickel, phosphorus and sulfur atoms respectively. 70

Figure 4.14 Replacement of a phosphorus atom from the bulk with a sulfur atom, after all the distant phosphorus atoms are replaced from the surface. Cyan, purple and yellow represent nickel, phosphorus and sulfur atoms respectively. 70

Figure 4.15 Free energy change for complete sulfidation of Ni_2P to Ni_3S_2, as a function of temperature at 5.0 MPa H_2 and 0.1 MPa H_2S, and with different PH_3 concentrations in the gas phase. 71

Figure 4.16 Top view of the surfaces of the unit cell models replicating the original supercell geometries, constructed for the CO adsorption studies: (a) pristine Ni_2P surface; (b) partially phosphorus replaced Ni_2P; and (c) Ni_2P surface with adsorbed atomic sulfur. Cyan, purple and yellow represent nickel, phosphorus and sulfur atoms respectively. 75

Figure 4.17 Preferred configurations for adsorption of CO on the pristine Ni_3P_2 or partially sulfided Ni_3PS surfaces, corresponding to different surface coverages. Carbon, oxygen and nickel atoms are in gray, red and cyan respectively. White indicates phosphorus or sulfur atoms. 76

Figure 4.18 Configurations of CO adsorption on the Ni_3P_2 surface with adsorbed solid sulfur. Gray, red, cyan, purple and yellow represent carbon, oxygen, nickel, phosphorus and sulfur atoms, respectively. 77

Figure 4.19 The most stable configuration for adsorption of hydrogen on the pristine Ni_3P_2 surface. Cyan, purple and white represent nickel, phosphorus and hydrogen atoms respectively. 82

Figure 4.20 The most stable configuration for adsorption of: (a) hydrogen molecule; (b) hydrogen atoms on the Ni_3PS surface. Cyan, purple, yellow and white represent nickel, phosphorus, sulfur, and hydrogen atoms respectively. 82

Figure 4.21 Input configuration for the reactant in the transient state search for the hydrogen dissociation reaction. Cyan and white represent nickel, and hydrogen atoms respectively. 83

Figure 5.1 A qualitative representation of the true active phase of Ni_2P at hydrotreating conditions, a combination of the partial replacement model, and the model with adsorbed sulfur atoms: (a) top view; (b) side view. Cyan, purple and yellow represent nickel, phosphorus and sulfur atoms respectively. 95

LIST OF SYMBOLS, NOMENCLATURE, AND ABBREVIATIONS

a_0, b_0, c_0	Lattice Constants
C	Coefficient Matrix
c_{ij}	Mixing Coefficient for j^{th} Basis Function for the i^{th} MO
dr	Differential Distance
$d\tau$	Differential Volume Element
E	Value of energy of a state in the system
F	Reduced Density Gradient for Spin
G	Free Energy
H	Energy Element Matrix
$\hat{H}$	Hamiltonian Operator
$\hat{h}^{KS}$	Kohn Sham Fock Operator
$\hbar$	Planck's Constant Divided by 2
ln	Natural Logarithm
M	Mass of Nucleus; Number of Nuclei
m_e	Mass of Electron
N	Number of Electrons
p	Partial Pressure
R	Inter Nuclear Distances/ Universal Gas Constant
r	Distance between Particles
S	Overlap Matrix
s_σ	Local Inhomogeneity Parameter

T	Temperature
$\hat{T}_E$	Kinetic Energy of Electrons
$\hat{T}_N$	Kinetic Energy of Nuclei
$\hat{U}$	Electron-Nuclear Electrostatic Interaction Energy
v	External Potential
$\hat{V}_E$	Inter-electronic Electrostatic Potential Energy
$\hat{V}_N$	Inter-nuclear Electrostatic Potential Energy
x	Collective Coordinate
x, y, z	Cartesian Coordinates
Z	Charge in a single nucleus

Greek Letters

α	Coulomb Integral
β	Resonance/Bond Integral
Δ	Difference
δ	Differential Amount
∇	Gradient of Space
ε_0	Vacuum Permittivity Constant
ψ_i	Wave Function Containing Information about ith Quantum State
ϕ_j	Atomic Orbital or the Basis Function
π	Pi
ρ	Electron Density

Abbreviations

AER	All Electron Relativistic
API	American Petroleum Institute
BOA	Born Oppenheimer Approximation
CI	Configuration Interaction
DBT	Dibenzo Thiophene
DFT	Density Functional Theory
DN	Double Numerical
DNP	Double Numerical Plus Polarization
ECE	Exchange Correlation Energy
ECP	Exchange Correlation Potential
EHM	Extended Hückel Method
EHT	Extended Hückel Theory
EPA	Environmental Protection Agency
EXAFS	Extended X-ray Adsorption Fine Structure
GGA	Generalized Gradient Approximation
HC	Hydrocarbon
HDA	Hydrodearomatization
HDN	Hydrodenitrogenation
HDO	Hydrodeoxygenation
HDS	Hydrodesulfurization
HF	Hartree Fock
HYD	Hydrogenation

HYT	Hydrotreating
IEM	Independent Electron Model
IR	Infrared
KS	Kohn Sham
LCAO	Linear Combination of Atomic Orbitals
LDA	Local Density Approximation
LEED	Low Energy Electron Diffraction
LSDA	Local Spin Density Approximation
LST	Linear Synchronous Transit
MO	Molecular Orbital
NMR	Nuclear Magnetic Resonance
OA	Orbital Approximation
PASH	Polycyclic Aromatic Sulfur Heterocycles
PES	Potential Energy Surface
PM	Particulate Matters
QST	Quadratic Synchronous Transit
SCF	Self-Consistent-Field
SHM	Simple Hückel Method
SHT	Simple Hückel Theory
ST	Synchronous Transit
STM	Scanning Tunnelling Microscopy
SWE	Schrödinger's Wave Equation
TFH	Three Fold Hollow

TPR	Temperature-Programmed Reduction
TS	Transition State
TSS	Transition State Searching
XANES	X-ray Absorption Near-edge Spectroscopy
XPS	X-Ray Photoelectron Spectroscopy
XRD	X-Ray Diffraction
UAE	United Arab Emirates
UHV	Ultra High Vacuum
ULSD	Ultra-Low Sulfur Diesel
US	United States
VP	Variational Principle
WHSV	Weight-Hourly Space Velocity
ZPE /ZPVE	Zero Point Vibrational Energy

Chemical Formula

Al_2O_3	Alumina
CO	Carbon Monoxide
Co	Cobalt
CoP	Cobalt Phosphide
Fe	Iron
Fe_2P	Ferrus Phosphide
H_2	Molecular Hydrogen
H_2O	Water
H_2S	Hydrogen Sulfide

Mo	Molybdenum
Mo_2C	Molybdenum Carbide
MoP	Molybdenum Phosphide
MoS_2	Molybdenum Sulfide
Na_2HS	Sodium Hydrogen Sulfide
Na_2S	Sodium Sulfide
NH_3	Ammonia
Ni	Nickel
Ni_2P	Nickel Phosphide
Ni_3P_2	A Particular Termination of Ni_2P Crystal along (001) Plane
Ni_3P	A Particular Termination of Ni_2P Crystal along (001) Plane
Ni_3PS	50% Phosphorus Replaced Ni_3P_2 Surface
NiP_xS_y	Nickel Phosphosulfide
Ni_3S_2	Nickel Sulfide
NO_X	Oxides of Nitrogen
Pd	Paladium
PH_3	Phosphine
Pt	Platinum
Ru	Ruthenium
-SH	Mercapto Radical
SiO_2	Silica
U	Uranium
V	Vanadium

W	Tungsten
WP	Tungsten Phosphide
WS_2	Tungsten Sulfide

Units

Å	Angstrom
/Å	Per Angstrom
Bbl/day	Barrel per Day
cm	Centimeter
cm^3	Centimeter Cube
cm^{-1}	Per Centimeter (Frequency or Wavenumber)
cm^3h^{-1}	Centimeter Cube per Hour
°C	Degree Celsius
eV	Electron Volt
$eV/Å^2$	Electron Volt per Angstrom Square
h	Hour
h^{-1}	Per Hour
Ha	Hartree
Ha/Å	Hartree per Angstrom
Gallon	Gallon
K	Kelvin
$kJmol^{-1}$	Kilo Joule per Mol
ML	Monolayer Adsorption

m^2/g	Meter Square per Gram
nm	Nanometer
Pa	Pascal Pressure
kPa	Kilo Pascal Pressure
MPa	Mega Pascal Pressure
Ppm	Parts per Million
Psi	Pound per Square Inch Pressure
μmol	Micro Mol
v	Related to External Potential
%	Percent
Wt%	Weight Percent
Mol%	Mol Percent

Superscript

0	Evaluated at Ground/Reference State
KS	Kohn Sham
Total	Corresponding to A Total Quantity

Subscript

0	Evaluated at Ground State/Vacuum
0 K	At 0 K Temperature
A or B	Corresponding to Particular Nucleus
AB	Related to Two Particular Nuclei

ads	Related to Adsorption
C	Related to Correlation Function
Corr	Related to Electron Correlation
E	Related to Energy
HF	Corresponding to A Hartree Fock Quantity
i	Corresponds to Particular Energy Level/Quantum State/Electron/MO
j	Corresponds to Particular Electron/Basis Function
iA	Related to A Particular Electron and A Particular Nucleus
ij	Related to Two Particular Electrons
r	Corresponding to A Particular Radius
t	Corresponding to A Particular Trial Value
T_{Corr}	Evaluated at A Corrected Temperature
X	Related to Exchange Function
XC	Corresponding to Exchange Correlation

1 Introduction

1.1 Sulfur in Petroleum Hydrocarbons

During the 1950's in North America, health and environmental problems were first recognized to be associated with air pollution. This was discovered when motor vehicle emissions were found to be major contributors to the formation of the photochemical smog over California.[1] With the adoption of the US Clean Air Act in 1970, a program was implemented to reduce the air pollution from motor vehicles by 90% compared to a 1960 model year car.[1] Success was achieved to some extent by making mechanical improvements, such as engine modifications. Similar reduction in emission levels had been stipulated in Europe, when the first passenger car emissions directive of 1970 and the first heavy duty vehicle emissions directive of 1988 successfully restricted emissions of carbon monoxide (CO), unburned hydrocarbon (HC), oxides of nitrogen (NO_X) and particulates (PM).[2] However, these modifications failed to reach the desired reduction level, necessitating alternative techniques in this regard.[1] Automotive catalysts have been used as a possible solution to the problem, but in addition to having short life span the catalysts also fail to restrict the emission of sulfur oxides resulting from combustion of the fuel-bound sulfur, which are major sources of air pollution from vehicular emissions.[1] Based on these facts, it is necessary to formulate better fuels with fewer pollutants and reduced pollutant levels, which can be complementary to the mechanical adjustment and catalytic after treatments.[3]

In 1943, the first industrial application of the sulfide catalyst took place.[4] Sulfide catalysts had been found to be efficient in removing the sulfur contaminants from the petroleum and petroleum derivative technical raw materials with different catalytic chemical processes. The presence of sulfur in these materials caused deactivation, poisoning, and problems in regeneration of the conventional catalysts used in different processes. When acid rain and associated issues were discovered in the 1950's and started

being noticed in the 1960's, in addition to the health related issues, removal of sulfur from diesel fuels gained much importance. Sulfur oxides had been found to cause serious respiratory damage and diseases, nausea, and irritation to human body.[5] In 1988, as part of the United Nations-sponsored Long Range Transboundary Air Pollution Agreement, the U.S.A. and other nations agreed to limit nitrogen oxide emissions to 1987 levels.[6] Changes to the Clean Air Act in 1990 set rules to reduce the release of sulfur dioxide from power plants down to 10 million tonnes by January 1, 2000.[6] Removal of sulfur from fuels is now a major concern in petroleum industries.

1.2 Current Technology for Sulfur Removal

By far, catalytic hydrodesulfurization (HDS) processes are the most effective and proven procedures to remove sulfur from the petroleum and petroleum products. As compared to the other alternatives for sulfur removal which do not employ hydrogenation, such as the thermal processes where the sulfur content is concentrated in coke or residuum, HDS possesses a significant advantage since it removes the sulfur as gas phase H_2S.[7] It is essentially a catalytic hydrogenation reaction of a pre-dominantly hydrocarbon feed to produce desulfurized hydrocarbon products and hydrogen sulfide.[7] The most common types of catalysts used in this process are transition metal sulfides of one or more metals. To date, the bi-metallic Ni/Co promoted Mo sulfides are the most widely used catalysts, and are known as the 'work horse' of the HDS industries.[8]

However, with the increase in the demand of petroleum, and with the rise in environmental concerns, more stringent regulations are continuously being imposed for steeper reduction of sulfur in transportation fuels.[2,9] In 1999, the US Environmental Protection Agency (EPA) established new, nationwide limits for sulfur levels in gasoline to a 30 ppm per gallon average beginning in 2005 and an 80 ppm per gallon cap beginning in 2006. The EPA is now attempting to limit the sulfur content in motor and diesel fuels below 15 ppm, far below the current cap of 500 ppm.[9,10] The conventional technology and catalysts are unable to reduce the sulfur content of petroleum to this extent. This has necessitated, initiated and mobilized numerous research in desulfurization processes and catalysts in the hydrocarbon processing industries.

1.3 Developments in HDS Processes and Catalysts

The multi-step deep desulfurization process, introduced in the 1990's, is capable of eliminating sulfur from the diesel fuels to a significantly low amount.[11] As a result of extensive research and studies, several new catalysts and processes have been developed for hydrodesulfurization, but many of them are still being tested. Among the prospective hydrodesulfurization catalysts, noble metals, transition metals, and modification of transition metals with main group elements have been much studied and discussed. Recently, processes using base metals and base metal hydrides, particularly sodium and sodium hydride, had been patented for sulfur removal.[12,13] Biodesulfurization is currently being studied by several researchers, and is expected to be a potential method for sulfur removal.[14,15] Some other unconventional methods that are currently under study include ultrasonic waves and oxidative desulfurization.[14]

Among all the possible future HDS catalysts, the transition metals modified by the main group element phosphorus have demonstrated substantial promise to be the next generation HDS catalysts.[16] Because of their high hydrodesulfurization and hydrodenitrogenation (HDN) activities, they are currently the new focus of research within the catalysis community. Nickel phosphide has shown the highest HDS activity among all these transition metal phosphide catalysts.[17,18] Comparative studies have shown that it possesses higher activity even compared to the proven and industrially used bi-metallic transition metal sulfide catalysts.[17,18] Such a potential can mean substantial reduction of the cost of processing in petroleum industries, and hence, nickel phosphide catalysts demand further investigation and research.

1.4 Nickel Phosphide and Objective of This Study

Despite the impressive activity of nickel phosphide (Ni_2P), the stability of the catalyst is questionable during long operation at industrial conditions. In order to have a better understanding of the underlying relation between the activity and stability of Ni_2P, the active phase of the catalyst at actual hydrotreating conditions has to be determined. Based on experimental evidence, several researchers have suggested the presence of

sulfur within the active phase of the catalyst. Oyama et al.[16] compared the extended X-ray absorption fine structure (EXAFS) spectra of the fresh and spent samples of Ni_2P/SiO_2 with different Ni/P ratios with bulk sulfide samples. In a following study, they also conducted elemental analysis of the spent samples.[19] The results from these studies suggested that the original Ni_2P phase, as present in the fresh samples, was disrupted and some sulfur in the reactant had been taken up by the catalyst in course of HDS reactions. However, XRD analysis on the spent samples, and comparison of the diffraction patterns with those of fresh samples, indicated no change in the bulk phase. Two different infrared (IR) spectroscopic studies[16,20] performed on reduced and sulfided Ni_2P/SiO_2 also supported these results. Similar conclusions were deduced by Layman and Bussell [21] based on an IR study done on the reduced and sulfided Ni_2P/SiO_2 catalyst samples using CO as the probe molecule.

The deductions from the EXAFS and IR studies and the elemental analysis indicate the partial sulfidation of the Ni_2P surface, and the possibility of formation of a nickel phosphosulfide surface at hydrotreating conditions. Combined with the XRD patterns which show that the bulk phase of the catalyst remained unchanged, it may be postulated that the stable and active phase of Ni_2P at hydrotreating condition is a NiP_xS_y overlayer. However, the exact form of the active phase is unknown, and current experimental characterization techniques are unable to determine its exact form. Oyama et al. [19] reported that the characterization of the phosphorus and the sulfur components of the overlayer were not possible by direct EXAFS or X-ray absorption near-edge spectroscopy (XANES) measurements, the best available experimental techniques for such measurement, because of the low energy of the K- and L-edge transitions.

The objective of this study is to utilize Density Functional Theory (DFT) calculations to determine the form of the active phase of nickel phosphide at typical hydrotreating conditions. Using the quantum mechanical calculations, it is possible to determine the forms of materials from first principles, which experimental methods are unable to determine at present. This study was directed to determine the active phase of Ni_2P in hydrotreating conditions from the *ab initio* calculations, develop a fundamental understanding of the formation, activity, and stability of this phase, and observe the adsorption and HDS reaction phenomena over the phase using model compounds. A

literature review of the hydrotreating catalyst development research and transition metal phosphides is provided in Chapter 2. A detailed description, history and development of DFT and associated experimental methods used in this study are available in Chapter 3. The results of the calculations done in this study are presented in Chapter 4. Subsequently, the calculations are analyzed, discussed, and compared to the previously reported experimental observations in Chapter 5. Finally, the conclusions drawn from this study are summarized in Chapter 6.

2 Literature Review

2.1 Introduction

Air pollution in urban areas has become a major problem. The rising environmental concerns, combined with the increase in the demand of petroleum products are continuously imposing more stringent regulations for the increased reduction of sulfur in transportation fuels.[2,9] In the 21st century, the demand for gasoline and middle distillates is anticipated to increase two-fold.[22] Most of the advanced countries in the world have adopted strict policies to control the sulfur content in petroleum products. For example, the sulfur content of distillate in Japan was regulated to 0.05 wt% in 1997.[11] The US Environmental Protection Agency (EPA) is now attempting to limit the sulfur content in motor and diesel fuels below 15 ppm, far below the current cap of 500 ppm.[9,10,14] This future specification, known as the Ultra-Low Sulfur Diesel (ULSD) specification, is supposed to be in effect from June 2006.[14] This is indeed mobilizing current research, and causing breakthroughs in desulfurization processes in current hydrocarbon processing industries. At present, the major developers of desulfurization processes and catalysts who have achieved considerable progress are Haldor Topsoe, Criterion Catalysts, and MAKFining (a consortium effort of Mobil, Akzo Nobel, Kellogg Brown and Root, and TotalFinaElf Research).[14]

Sulfur contaminants result mainly from the polycyclic aromatic sulfur heterocycles (PASH), the major components in petroleum and coal–derived products, and also from the non-heterocyclic thiols, sulfides and disulfides.[11] Examples of the PASH components are presented in Figure 2.1[11,23]. The sulfur content of the petroleum crude usually varies depending on the location. For example, Athabasca crude oil has a sulfur-content of 4.5 wt%.[7] Moreover, sulfur-content also varies in different petroleum fractions, depending upon the type of fraction, and the stage of treatment.

Components	Structures
Thiophene	
Benzothiophene	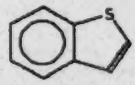
Dibenzothiophene	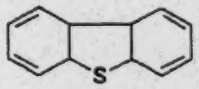
Benzo[b]naphtha[1,2-d]thiophene	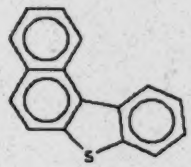
4-Methyldibenzothiophene	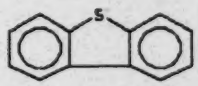
4,6-Dimethyldibenzothiophene	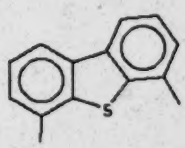
Benzo[b]naphtha[2,3-d]thiophenes	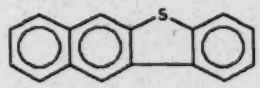

Figure 2.1 Major sulfur contaminants in petroleum and coal–derived products: Polycyclic Aromatic Sulfur Heterocycles (PASH).[11,23]

2.2 The Hydrodesulfurization Process

Hydroprocessing of petroleum crude and fractions usually involves hydrocracking and hydrotreating (HYT), consisting of hydrodesulfurization (HDS), hydrodenitrogenation (HDN), hydrodeoxygenation (HDO), and hydrogenation (HYD) reactions. Hydrodesulfurization, one of the most important reactions in the process, is also the key to the production of cleaner fuels.[11] It is essentially a hydrogenation reaction of a pre-dominantly hydrocarbon feed to produce desulfurized hydrocarbon products and hydrogen sulfide.[7] The process can be 'destructive', which involves cleavage of carbon-carbon bonds at severe reaction temperature (usually of the order of 360 to 410 °C), with concurrent high pressure hydrogen added to the fragments to minimize undesired reactions in order to produce saturated products with low boiling points.[7] This is usually employed for heavier feedstocks, like heavy oils and residua. The tendency to form coke is high, but preventable using a higher hydrogen pressure (750 to 2000 psi).[7] On the other hand, 'nondestructive' or 'simple' hydrogenation is used for improving the product quality at mild processing conditions (temperature on the order of 170 to 330 °C and hydrogen partial pressure of 100 to 500 psi).[7] Unstable species are attacked, and the H_2S, NH_3, and H_2O from sulfur, nitrogen, and oxygen-compounds are usually produced by hydrogenolysis within the process.

As compared to the other alternatives for sulfur removal that do not employ hydrogenation, such as thermal processes where the sulfur content is concentrated in coke or residuum, HDS possesses a significant advantage since it removes the sulfur as gas phase H_2S.[7] Moreover, the desulfurization level achieved in this process is significantly higher than the other methods. Apart from being a more extensive and convenient method, hydrodesulfurization also plays an important role in reducing catalyst poisoning in catalytic reformers and hydrocracker feedstocks.[7] The HDS process also increases the octane number of the fuel, and may promote the ignition quality of gasoline for particular feedstocks. All these concurrent factors make HDS one of the most important catalytic processes, and this has motivated extensive research in the field in order to understand the reaction mechanism, catalyst structure, and process engineering related to it.[7]

In a typical single stage HDS process, the feed is brought to a pressure slightly higher than that of the reactor (150 to 3000 psi higher), mixed with the hot recycle gas and pre-heated to the temperature of the reactor inlet (on order of 290 to 455 °C).[7] During processing, the gas or the liquid feed is flowed downward through the fixed bed of solid catalyst particles in the reactor.[11] The reaction products are separated into liquid and gas, and liquid products are further separated by fractional distillation. The hydrogen rich gas is used as a recycle hydrogen stream, with more fresh hydrogen added to it, and then H_2S and light hydrocarbon gases are removed.[5,] The recycling process minimizes the loss of hydrogen, which is a very expensive commodity in petroleum industries, and helps keeping high partial pressure of hydrogen in order to promote high desulfurization rate and to prevent coke deposition on the catalyst surface. Hydrogen must be fed to the reactor several times the rate at which it's consumed.[7]

However, it is generally believed that in order to produce ULSD, a two-stage deep desulfurization process is required in place of the above-described single stage processes.[11,14] Modification of the processes will not be sufficient to reach the desired desulfurization levels. Therefore, more efficient hydrodesulfurization catalysts are required to achieve this low sulfur level in fuels. The current conventional catalysts are either not sufficient to meet the targeted regulatory standards, or not economically viable.

2.3 Development of Conventional HDS Catalysts

Hydrodesulfurization catalysts were discovered while developing catalysts for processing coal and coal-derived liquids.[11] Early in the 20th century, the deactivation and catalyst poisoning by the presence of sulfur in the raw materials used in different catalytic processes was a significant problem. The development of HDS catalysts was based on a series of observations and studies by a number of researchers[4], who found that the pre-removal of sulfur for most of these processes was economically not viable, but a satisfactory solution was achieved by using sulfur-compounds either as original constituent or by intentional addition.

In 1906 and 1912, respectively, Day and Theodorin observed the catalytic activities of noble and transition metals[4]. In 1910, according to Landsberg's suggestion, Bergius experimented with the hydrogenation of heavy petroleum distillate using molecular hydrogen, and observed the fractionation of gasoline by bond cleavage.[4] A breakthrough was achieved by Bergius and Billwiller in 1913, when the hydrogenation of coal obtained an 80 % yield in fractionation at 400-450 °C at a hydrogen pressure of 1 atmosphere. Bergius deduced that the sulfur-compounds in the feed contribute a polymeric effect to the process.[24] Based on the work of Bergius and Billwiller, the researchers at Badische Anilin u. Sodafabrik, especially Krauch and Pier, discovered the importance of Mo and W sulfide catalysts. Varga also discovered the same a little later in 1933.[4] This unique discovery gave rise to a large number of patents and reports during that time period.

After 1930, the research spread outside of Germany.[4] The bi-metallic catalysts were invented around this time, and the first industrial application of Co-Mo/Al_2O_3 catalyst took place in 1943.[25] During, and particularly after, the Second World War sulfide catalysts were introduced to petroleum processes. In the post war period, the developments spread world-wide. Outstanding achievements were contributed by a number of American and European companies, namely HC Research Corp., Gulf Research Corp., Esso Research & Eng., Universal Oil Prod. Co., BASF, BP, IFP, Leuna Werke (GDR), and some other Soviet organizations.[4]

To date, the most commonly used active phase of an HDS catalysts is a sulfided form of unpromoted or cobalt/nickel promoted transition metals (generally molybdenum or tungsten; nickel, iron, and chromium are also used) or their oxides.[7] MoS_2 and WS_2 are the most widely used among the unpromoted sulfides. However, the activity of these catalysts increases significantly when promoted by cobalt or nickel. Researchers have attributed this increase to the 'synergic effect', which is related to the change in the strength of the metal-sulfur bond according to the combination of metals.[26] According to this idea, Ni/Mo, Co/Mo, Ni/W or Co/W can be said to behave as 'synergic pairs', meaning that the members of each of these pairs work together or cooperate. The pairs provide enhancement of activity far greater than that expected by simultaneous individual presence of each of them as non-interacting phases.[26] The structures of promoted sulfide

catalysts are more complicated than the conventional sulfide catalyst. A variety of structures had been proposed, among which the 'monolayer model', 'pseudo-interaction model', 'contact synergy model' and 'edge decoration/CoMoS phase model' are prominent. It has been found that cobalt-atoms adsorbed on MoS_2 to produce the CoMoS phase, and hence, the last explanation has gained the greatest recognition.[11] In Al_2O_3 supported catalysts, it is suggested that the CoMoS phase stays as a single sheet, with Co most likely to be present at the Mo site. However, a recent theoretical study shows that the Co is adsorbed at the sulfur-edge, whereas nickel promoted catalysts have nickel at the metal edges.[27]

Whatever the exact local structures are, the cobalt or nickel promoted transition metal sulfide catalysts had been by far the 'workhorse' of HDS industries.[8] Some of the commercial examples of Co-Mo catalysts are: KF 752 (able to deal 500 ppm sulfur cap), KF 756 (405 ppm), and KF 757 (270 ppm), and KF 842 (160 ppm) by Akzo Nobel (KF 757 and KF 842 are said to be using STARS technology: Super Type II Active Reaction Sites), HR 306, and HR 406 by Axens. Axens also offers a mixture of Co-Mo and Ni-Mo catalyst called HR 468, and a Ni-Mo catalyst called HR 448.[8] Very recently, Haldor Topsoe has leveraged the BRIM technology platform to optimize and launch two new high performance Ni-Mo catalysts, namely TK-575 and TK-605.[28] The first one is tailored for removing the refractive organic compounds, and the second one has been optimized for high-performance hydrocracker pretreatment.

The supports used for HDS catalysts are usually alumina, silica, carbon, kieselguhr, titania, magnesia, or zeolites.[7] To improve the activity of the support, decoration with phosphorus, fluorine, etc. has been attempted, as well as using metallic bi-oxides as supports. Sometimes, the hydrocracking process requires a bi-functional catalyst with both acidic (cracking) and metallic (hydrogenation) components. Usually the amorphous silica-alumina support, crystalline zeolite material, or acid-treated clay works as the cracking component. The typical surface area of HDS catalysts is 200-300 m^2/g, which is almost entirely contained within the pore space of the support (in this case alumina). Typical pore volumes and pore diameters are 0.5 to 1.0 cm^3 and 10 nm, respectively.[7,11] The current world-wide demand of HDS catalysts is approximately 70,000 tons per year.[11]

2.4 Novel HDS Catalysts and Processes

With the invention of the deep desulfurization process of the middle distillate in the 1990's, the interest in this field had been rejuvenated.[11] Several new catalysts and processes had been invented, a number of which are still to find industrial applications. Within the last decade, noble metals, transition metal phosphides, carbides and nitrides, metallic sodium, and zeolites have been under study as potential HDS catalysts.

Among the sulfided noble metal catalysts, ruthenium (Ru) had been found to be most active for HDS of DBT.[29] However, while some of the catalysts made from sulfided ruthenium showed good activity, the others did not probably because of incomplete sulfidation or instability of RuS_2 in presence of hydrogen. Other noble metals had been tried and it has been observed that a volcanic periodic trend exists for HDS activities of these metals. Sulfided rhodium, osmium, iridium, palladium and platinum were considered to be potential HDS catalysts, but they have been proven as better HDN catalysts than HDS catalysts.[11] Precious metal catalysts are also very effective at desulfurizing sterically hindered compounds.[8] Bimetallic catalysts using Ru-U, Pd-U, V-U, Co-Ru, Ni-Ru, Fe-Ru, Ru-Mo, Pd-Ni, and Pt-Pd had been studied. It has been found that the 'synergic effect' also exists for noble bimetallic catalysts.

Despite their high activities, noble metals are not widely used mainly because of their cost. The activity increases linearly with the metal loading to some extent, indicating that more metal has to be provided in order to attain extensive removal.[11] Moreover, in order to reduce the metal amount while maintaining the same activity, supports with large surface areas (e.g. zeolites) are required. Although this increases the activity per unit site, the volume of the catalyst becomes substantially large to handle. Currently, noble metals are used in two-step deep desulfurization processes in combination with a commercial HDS catalyst reducing the sulfur-content below a certain level.[30] An example of precious metal catalysts is the ASAT catalyst developed by United Catalysts and Sud-Chemie AG, which uses both platinum and palladium.[8]

In 2001, implementing a different method to make coatings, Akzo Nobel introduced a highly active catalyst named NEBULA (New Bulk Phase Activity). The catalyst is formed by concentrating the metal coating to a greater extent than the typical

catalysts and reducing the generally inactive substrate phase.[8,31] Because of the high metal content in the bulk phase, NEBULA achieved higher activity at the expense of costs several times more than the conventional catalysts. In addition to that, the higher activity leads to an increased tendency for coking, which must be countered by using a high hydrogen partial pressure, resulting into higher hydrogen consumption. However, it has been claimed that the 15 ppm sulfur standard can be met by simply replacing a part of or all of its existing catalyst with this new bulk phase and providing significantly more hydrogen. Moreover, it may significantly reduce the capital investment for meeting this standard. In 2003, a modified form of this bulk phase activity catalyst containing 15-20% less metals and possessing the same activity was introduced.[8] This modified form, known as NEBULA 20, handles the heavier feeds more efficiently. However, the higher activity of both the modified and unmodified form of the catalyst is questioned by the fact that it is measured per unit volume basis, not per unit weight. Therefore, the weight of these catalysts may necessitate an increase in the weight bearing capacity of the reactors and an increase in capital investment, while used in industrial hydrotreating operations.

Researchers have tried to invent new hydrotreating catalysts by modifying the transition metal properties by combining them with the main group elements. In the last decade or so, much progress had been made on developing carbides and nitrides as potential HDS catalysts.[32] Because of the incorporation of nitrogen and carbon in the metal lattice, transition metal carbides and nitrides have altered physical and chemical properties that make them unique compared to their parent metals. Studies indicate that the high activity of these catalysts is not due to their structure sensitivity, but rather because of the optimal binding energy available in the group 6 compounds. They follow the Sabatier's principle, since the overall activity of the catalysts for HDN and HDS follow this Sabatier relationship:

Group 6 > Group 5 > Group 4

Mo_2C, in particular, has shown excellent HDN and reasonable HDS activities, as compared to the available commercial catalysts. Another advantage of these catalysts is better tolerance of sulfur, as XPS studies showed evidence of little or no sulfur

incorporated on their surface.[32] However, although better for HDN reactions, the HDS activities of most of the carbides and nitrides are not fairly above those of the traditional catalysts.

Desulfurization, and combined desulfurization and conversion of petroleum, heavy oils and residua, using metallic sodium or sodium hydride had been attempted using several processes.[12] The reactions are not strictly catalytic as sodium is consumed in the reactions to give Na_2S or NaSH. Low-pressure and/or excess hydrogen is used to stabilize the products, which would otherwise tend to polymerize as the sulfur is removed. Recently, a modified process had been proposed[13] involving contacting the petroleum feed with sodium metal (in a liquid or molten state) using staged addition at a temperature of 325-400 °C in the presence of a molar excess of hydrogen to sodium metal of at least 1.5:1, and at a molar ratio of sodium to unreacted sulfur of up to 1:1. This suppresses the formation of Na_2S substantially and promotes the formation of NaSH during the desulfurization process. The process operates at a hydrogen pressure range of 2-7 MPa. Sulfur removed from the petroleum feed is recovered as NaHS, using a two phase liquid-liquid separation of the molten salt at temperatures of about 350 °C. One molar equivalent of sodium metal is consumed per equivalent of sulfur removed from the petroleum feed, making the process to be suitable for petroleum feed of the group consisting of heavy oil, naphtha and distillate fractions. However, application of this process to lower sulfur (<2,000 ppmw) containing feeds (e.g., naphthas, distillate fractions) may not be economic in terms of sodium regeneration. Therefore, a once-through process may be utilized.

Based on the ring opening activity of microorganisms and their ability to bioconvert sulfur compounds in petroleum, there has been interest to develop biocatalysts for removal of sulfur from fuels. In a biodesulfurization process, organosulfur compounds are oxidized with genetically engineered microbes and the sulfur is removed as a water-soluble sulfate salt.[14] Recent studies using gas chromatographic tracing showed that *Rhodococcus* IGTS-8 successfully removed DBT and other sulfur contaminants from two middle distillates containing 560 and 1860 ppm of initial sulfur-content.[15] However, these systems are usually more costly than the conventional methods, and/or are not sufficiently active against gasoline range sulfur.[14,15] The studied

bacteria are still not able to tolerate high solvent concentrations and potentially toxic aromatics that are expected in gasoline desulfurization processes. No biocatalysts have been found that can specifically remove sulfur compounds from the thiophenes in gasoline. However, very recently Energy & Environmental Partners has managed to produce a low cost biodesulfurization process for high sulfur crude, bitumen, oil shale and tar sands in low-temperature bioreactors.[14] According to such EMULSOx patents, a microorganism recovered from a petroleum-waste settling demonstrated up to 47 % sulfur removal from the distillate vs. control samples treated conventionally.[14] However, more efficient new biocatalysts need to be discovered and engineered, while additional work need to be done on the economic aspects of biodesulfurization processes, to make the process commercially viable. [14,15]

Currently, some unconventional methods of desulfurization are also being considered as potential alternatives. SulphCo Inc. has recently completed the commercial-scale demonstration of its patented Sonocracking technology which uses ultrasound to desulfurize and hydrogenate crude oil and other oil-related products.[14] The process utilizes high-power ultrasound to alter naturally occurring molecular structures in hydrocarbons (HCs) and in water in the presence of inexpensive conventional catalysts. The high-power ultrasonic waves create bubbles in the liquid, cause those to grow, contract and eventually implode, breaking the molecular bonds of the HCs. The value of the HC fractions is reported to increase due to the increase in the product volume and API gravity. A recent distillation modeling shows that an API heavy crude with 45 % residuum on three 5,000 bbl/day sonocracking units can reduce the residuum content to 15 %, translating an increase of 14-15 gallons of diesel and kerosene when that crude is refined.[14] The viscosity of the crude is also reduced by 25 %. The constructions of test scale-plants are currently underway in U.S. and U.A.E.

Another new process is oxidative desulfurization which creates a petroleum and water emulsion in which hydrogen peroxide or another oxidizer is used to convert the sulfur to sulfone.[14] The sulfone is then separated from the HC for post-processing, and most of the peroxide can be recovered. The technology preferentially treats DBT, one of the molecules that is difficult to desulfurize. The process also operates at very low temperatures and pressures, and is a low-cost technology. However, it does not work very

well on straight-run distillate. Moreover, because it removes sulfur containing molecules, some volume losses also occur.

The use of phosphorus in HDS processes to increase hydrotreating activities is available in literature and well studied, but the role of phosphorus is yet to be understood clearly.[11,33] Although a number of effects of phosphorus addition to the conventional catalytic systems had been suggested, the chances of *in situ* formation of phosphide catalysts has not been widely investigated. Recent studies have shown that the transition metal phosphides posses substantial promise to be the next-generation HDS and HDN catalysts.[16] Because of their high HDS and HDN activities, they are currently the new focus of research within the HDS catalysis community.[26] A comparative study by Oyama et al.[16] done on the HDN and HDS catalytic activities of a series of phosphides on silica support in a trickle bed reactor operated under industrial conditions used a model feed containing quinoline (2000 ppm N), dibenzothiophene (3000 ppm S), tetralin (20%), and tetradecane (balance). The results are presented in Figure 2.2 (a)[16]. This study shows that the Ni_2P has better HDS and HDN activities than the other transition metal phosphides per unit active site basis. Apparently, the activity for HDS reactions for different phosphide catalysts decreases in the following comparative manner:

$$Ni_2P > WP > MoP > CoP > Fe_2P$$

The most active of the phosphide catalysts, Ni_2P, shows higher activity even compared to the commercial bimetallic Ni-Mo-S/Al_2O_3 catalyst (Shell 324).[17] On the other hand, the undesirable hydrodearomatization (HDA) conversion by Ni_2P was only 19 % as compared to the 50 % by the Ni-Mo-S/Al_2O_3 catalyst. Lower HDA conversion is preferred to limit the H_2 consumption in the final stage of the processing and to prevent the disruption of hydrocarbon (HC) structure which may lead to cracking. The bed volume, liquid feed, and gas flow rates used in the study were 1 cm^3, 5 cm^3h^{-1}, and 150 cm^3 respectively. The reactor had been loaded with an amount corresponding to 70 μmol of chemisorption sites.

The same study also evaluated the comparative potential of Ni_2P/SiO_2 and commercial Co-Mo-S/Al_2O_3 catalyst (Ketjenfine 756) subjected to an industrial feed (gas

oil designated F-942, with a sulfur and nitrogen content of 440 ppm and 8 ppm, respectively).[17] Under realistic conditions of 593 K and 3.9 MPa Ni_2P/SiO_2, the Ni_2P catalyst gave an HDS conversion of 85 % with a reduction of the sulfur content from 440 to 66 ppm. This was indeed very good compared to the 80 % conversion and a reduction of the sulfur to 86 ppm by the commercial catalyst. The comparison was done on equal weight-hourly space velocity (WHSV) of 4 h^{-1}. It was found that Ni_2P/Si_2O, with a low density support and low surface area of 90 m^2/g was better than the commercial Co-Mo-S/Al_2O_3 with a surface area of 218 m^2/g. The HDA conversion of Ni_2P and the commercial catalyst were 0.7 % and 1.1 % respectively. Moreover, the phosphide attained a steady state more rapidly (mild activation beginning from 40 h) and was more active, while the sulfide showed a slow decline in activity as it approached steady state at 130 h. Very surprisingly, the single-metal and unpromoted Ni_2P placed over a relatively unattractive support was found to be far superior to the proven commercial catalyst.

A more recent study[18] done on thiophene HDS, however, found that the Ni_2P/SiO_2 catalyst is more active than other conventional HDS catalysts over SiO_2 support, even per unit weight basis. A 30 wt% Ni_2P catalyst showed 3.5 times more activity than the sulfided Ni-Mo/SiO_2 catalyst with a Ni to Mo ratio of 0.5. A comparison of the HDS activities found from the study is presented in Figure 2.2 (b)[18]. Such properties and activities of Ni_2P are sufficient to present its potential to be a promising next generation HDS catalyst.

2.5 The Nickel Phosphide Catalyst

The property that is responsible for the high activity of the phosphides is likely their more isotropic crystal morphology. The metal rich phosphides are based on trigonal prisms, and can well accommodate the relatively large phosphorus atoms.[16] Unlike the sulfides, which possess flat two-dimensional crystal habits that expose saturated basal planes, the prisms in the phosphides are not build layered structures[17] and posses a more isotropic structure and potentially better exposure of surface metal atoms to fluid phase reactants[16,17]. This catalytic activity is substantial, exposing a greater number of coordinative unsaturated surface atoms, and hence gives rise to higher site densities.

Although the activity of Ni_2P is impressive, the stability of the catalyst is not proven for long operation at industrial conditions. Recent studies on thiophene HDS by Sawhill et al.[18] and Layman and Bussell[21], however, have confirmed the stability of the activity of Ni_2P up to 110 hours of operation at industrial conditions. Additional studies have been performed on a 30 wt% Ni_2P/SiO_2, sulfided Ni/SiO_2, Mo/SiO_2 and Ni-Mo/SiO_2 (Ni/Mo=0.5) catalysts. It has been reported that the Ni_2P/SiO_2 catalyst is 14.8, 31.4 and 3.5 times more active than the sulfided Mo/SiO_2, Ni/SiO_2 and Ni-Mo/SiO_2 respectively, even after 100 hours of operation.

In order to have a better understanding of the underlying relation between the activity and stability of Ni_2P, the active phase of the catalyst in actual hydrotreating conditions has to be determined. Several researchers[16,20,21] have suggested the form of the active phase based on their experimental results. Oyama et al.[16,19,34] compared the extended X-ray absorption fine structure (EXAFS) spectra of the fresh and spent samples of Ni_2P/SiO_2 with different Ni/P ratios with bulk sulfide samples. Details of the results are presented in Figure 2.3[16,21]. The HDS reaction involved DBT as the sulfur containing (3000 ppm) reactant in the model feed. Clearly, for all the spent samples with different Ni/P ratio, there had been diminution in the intensity of the Ni-Ni peak accompanied with a shift to a lower distance. The Ni-P peak also diminished in distance slightly, and a signal appears in between the Ni-Ni and Ni-P peaks. These evidences signify that the original Ni_2P phase, as present in the fresh samples, was disrupted. Comparisons of the spent catalysts with the bulk sulfide samples confirmed the new appearance as a Ni-S signal, which clearly indicates the presence of sulfur in some form incorporated in Ni_2P. The same study also involved the elemental analysis of the spent samples.[21] It was found that some sulfur in the reactant had been taken up by the catalyst. However, XRD analysis on the spent samples, and comparison of the diffraction patterns with those of fresh samples Figure 2.4 indicated no change in the bulk phase of Ni_2P crystals.

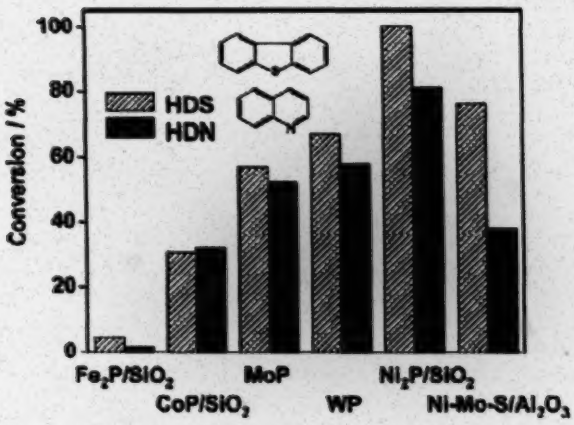

(a)

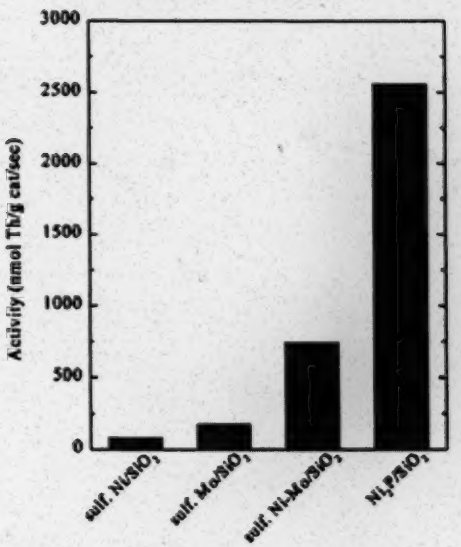

(b)

Figure 2.2 (a) Comparative HDS and HDN activity (per unit active site basis) of transition metal phosphide catalysts in the hydroprocessing of a model feed at 643 K and 3.1 MPa.[16] *

(b) Comparative Thiophene HDS activity (per unit weight basis) of nickel phosphide and the conventional hydrotreating catalysts.[18] **

* *Reprinted from the Journal of Catalysis, Vol 216, S.T. Oyama, Novel catalysts for advanced hydroprocessing: transition metal phosphides, Pages 343-352, Copyright (2003), with permission from Elsevier.*

** *Reprinted from the Journal of Catalysis, Vol 215, Sawhill et al., Thiophene hydrodesulfurization over supported nickel phosphide catalysts , Pages 208-219, Copyright (2003), with permission from Elsevier.*

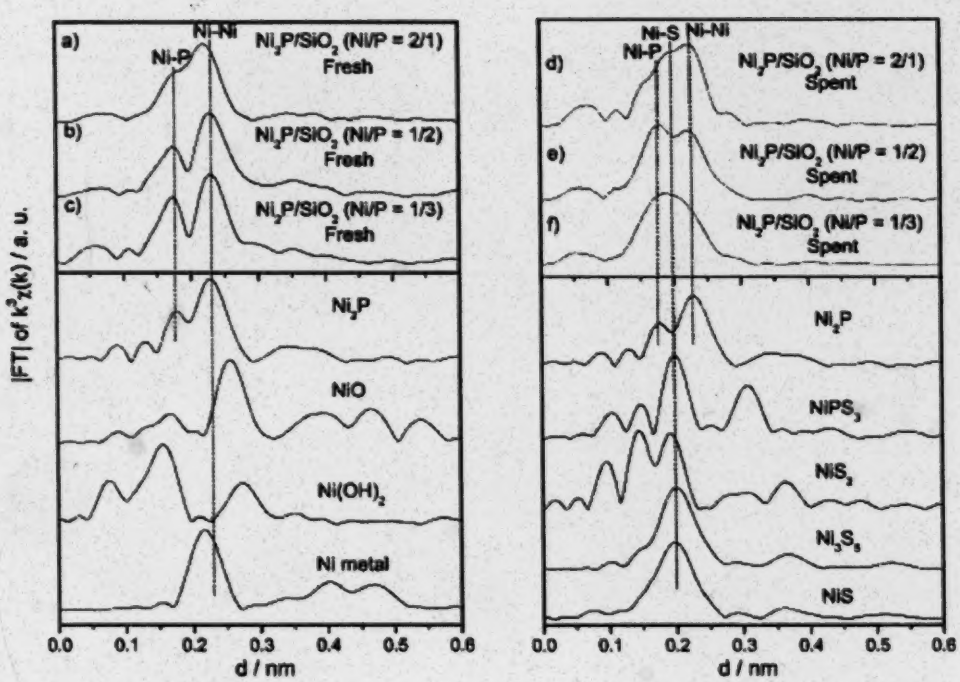

Figure 2.3 EXAFS of fresh and spent Ni_2P/SiO_2 catalyst (initial Ni/P=1) before (left) and after (right) DBT reaction.[19] *

* *Reprinted from the Journal of Catalysis, Vol 210, Oyama et al., Effect of Phosphorus Content in Nickel Phosphide Catalysts Studied by XAFS and Other Techniques, Pages 207-217, Copyright (2002), with permission from Elsevier.*

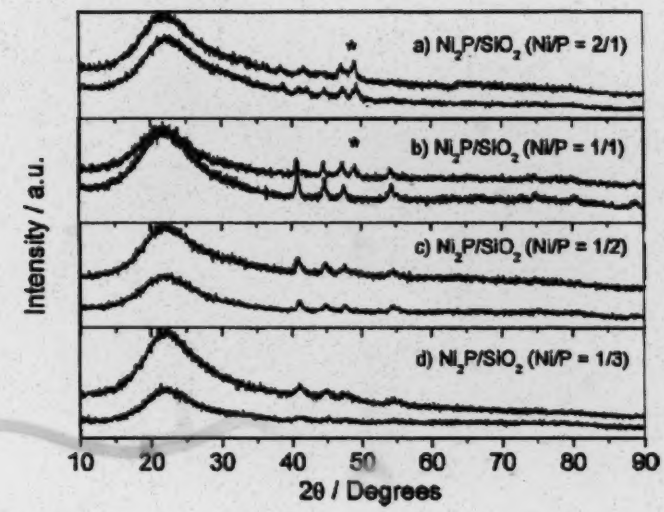

Figure 2.4 Comparison of X-ray diffraction patterns for fresh (lower) and spent (upper) samples for different initial Ni/P ratios.[19] *

* *Reprinted from the Journal of Catalysis, Vol 210, Oyama et al., Effect of Phosphorus Content in Nickel Phosphide Catalysts Studied by XAFS and Other Techniques, Pages 207-217, Copyright (2002), with permission from Elsevier.*

Two different infrared (IR) spectroscopic studies[19,20] performed on reduced and sulfided Ni_2P/SiO_2 confirmed to the results of the previously discussed EXAFS and XRD analyses. With a Ni_2P/SiO_2 sample reduced by flowing H_2 at 873 K for 2 hours, and another sulfided by a pre-treatment with a mixture of 10 mol% H_2S/H_2 for 1 hour at 593 K, Sun et al. performed CO adsorption on the surfaces of both the samples.[20] The IR spectra representing the vibrational frequencies of CO and the intensities of adsorption are provided in Figure 2.5. It had been found that for the sulfided catalyst, a large decrease in the intensity was present along with an upward shift in one of the frequencies from 2082 to 2094 cm^{-1} as compared to the reduced sample. The reduction in intensity is attributed to the blockage of some of the adsorption sites, by sulfur deposition, whereas the increase in frequency can be considered as a result of decrease in adsorption strength of CO on the surface due to the withdrawal of electron density from the nickel sites by the deposited sulfur. These results indicate partial sulfidation occurring on the surface. A similar conclusion was deduced by Layman et al.[21] from an IR study done on reduced and sulfided Ni_2P/SiO_2 catalyst samples, using CO as the probe molecule.

The deductions from EXAFS, IR and elemental analyses are congruent, all indicating towards the partial sulfidation of the Ni_2P surface and formation of a nickel phosphosulfide phase at the outer region of the catalyst at hydrotreating conditions. Combined with the XRD patterns, which shows that the bulk phase of the catalyst remains unchanged, we can conclude that the stable and active phase of Ni_2P at hydrotreating condition is a NiP_xS_y overlayer. This is also in agreement with the findings of Korányi[35], who indicated the presence of a type of "PS" compound similar to Ph_3PS in fresh $NiPS_3$ sample, based on the characterization results of X-ray Photoelectron Spectroscopy (XPS). However, the exact form of the active phase remains unknown, and experimental characterization techniques are unable to determine it. Oyama et al. reported that characterization of the phosphorus and sulfur components of the overlayer was not possible by direct EXAFS or X-ray absorption near-edge spectroscopy (XANES) measurements, because of the low energy of the K- and L-edge transitions.[19]

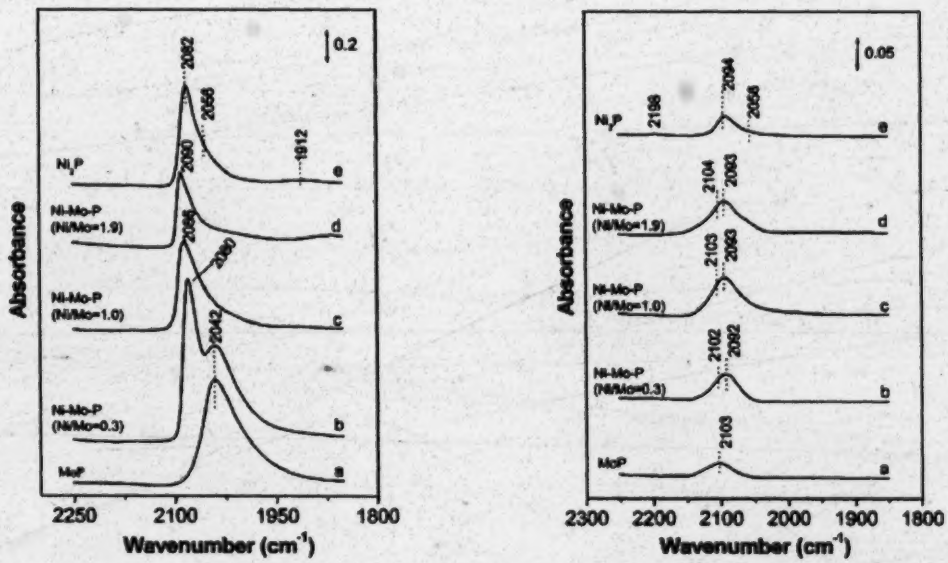

Figure 2.5 IR spectra of CO adsorbed at room temperature on phosphide catalysts: (left) reduced by flowing H_2 at 873 K for 2 hours; (right) sulfided with a 10 mol% H_2S/H_2 mixture at 593 K for 1 hour.[20] *

* *Reprinted from the Journal of Catalysis, Vol 228, Sun et al., Dibenzothiophene hydrodesulfurization activity and surface sites of silica-supported MoP, Ni_2P, and Ni_Mo_P catalysts, Pages 298-310, Copyright (2004), with permission from Elsevier.*

2.6 Summary

The worldwide increase in the demand of petroleum, and the rising environmental concerns are imposing strict regulations to decrease the sulfur and nitrogen contents in petroleum fractions.[2,9,10] To date, hydrodesulfurization (HDS) is the most effective method for removal of sulfur from petroleum.[11] The most commonly used HDS catalysts are promoted or unpromoted sulfides of transition metals.[7] To attain the new standards of sulfur content in petroleum fractions, more efficient HDS catalysts and processes are required. Transition metal phosphides, especially Ni_2P, has shown promise to be the next generation HDS catalysts because of its high activity,[16,26] although the stability of Ni_2P in industrial hydrotreating environment is not established. Researchers have found evidence of the presence of sulfur in the Ni_2P structure during the HDS process.[16,20,21] It is evident from their work that a phosphosulfide overlayer forms over the Ni_2P structure during hydrotreatment, while the bulk phase of the catalyst remains unchanged. Experimental techniques, however, are unable to determine the composition and exact form of this active phase.[19]

In the last decade, advances in theoretical chemistry and computational power have developed molecular modeling and simulation as important tools for catalysis research.[36] In heterogeneous catalysis, molecular modeling is a complement to the experimental techniques, which helps bringing information for a given system from different experimental techniques to a coherent picture.[37] A dual-feedback strategy that uses experiments to validate the modeling calculations, and modeling to explain experimental results, has been proven to be a very effective methodology.[37] Among all molecular modeling and simulation techniques, quantum mechanical calculations provide information about the smallest length scale and are able to probe the details of catalytic and surface chemistry in an explicit manner. The experimental findings can also be incorporated with periodic boundary conditions and long range interactions to treat infinite solids.[37] Density Functional Theory (DFT) is a very effective and accurate, and hence one of the most popular quantum chemical approach to date.

Therefore, the objective of this study is to determine and study the exact atomic structure of Ni_2P at hydrotreating conditions, using DFT calculations.

3 Experimental Methods

3.1 Introduction

This study involves the calculation of all geometries, energies and frequencies by DMol^3 DFT quantum mechanical model[38] engine in Materials Studio® molecular simulation software version 3.2 by Accelrys®. Being one of the fastest *ab initio* codes existing and possessing extensive functionalities, DMol^3 is able to attend gas phase, solvent, and solid state computational problems with an accuracy of quantum mechanical methods for non-periodic and three dimensional periodic structures.[38,39]

3.2 Molecular Modeling: Development of DFT

Molecular Modeling is a compilation of computational simulation techniques to study molecular systems of all dimensions and material assemblies,[40] which can contribute greatly to the fields of computational chemistry, biology and materials science. The inception of molecular modeling and the development of quantum mechanics have made significant progress in the last few decades.[41] A brief focus on the historical and conceptual backgrounds is discussed in the following sections, before the current molecular modeling approaches used in this study are presented.

3.2.1 Quantum Mechanics and Schrödinger's Wave Equation

Failure of classical physics to explain certain observed phenomena (Blackbody Radiation, Photoelectric Effect, and Line Spectrum of Atomic Hydrogen) initiated a revisit to the ideas of classical physics. By the first half of the twentieth century, the concepts of quantized energy and wave-particle duality of light were confirmed, and the basics of quantum mechanics were established by Max Planck, Niels Bohr, Werner Heisenberg, Erwin Schrödinger and others.[40,42] In 1925 Edward

Schrödinger represented the wave characteristics of electrons by the "Wave Equation" to describe a quantum mechanical system. The basic and time independent form of the many particle Schrödinger Wave Equation (SWE) can be represented as follows:

$$\hat{H}\psi_i(\bar{x}_1, \bar{x}_2, \ldots\ldots\bar{x}_N, \bar{R}_1, \bar{R}_2, \ldots\ldots\bar{R}_M) = E_i\psi_i \tag{3.1}$$

where $\hat{H}$ represents the Hamiltonian operator of the molecular system with M nuclei and N electrons, ψ_i is the wave function containing all information about the i^{th} quantum state, and E_i is the numeric value of the energy of the i^{th} state of the system. ψ_i depends on 3N Spatial Coordinates and N Spin Coordinates of N electrons in the state, collectively termed as x, and 3M Spatial Coordinates of M nuclei of the system.[43] The Wave Function is related to the probability of finding electrons as:

$$\int \psi^* \psi d\tau = \langle \psi | \psi \rangle = 1 \tag{3.2}$$

Although Equation (3.1) appeared deceptively simple, the difficulties in obtaining the exact solution were soon obvious from the complicated form of the Hamiltonian operator:

$$\hat{H} = \underbrace{-\frac{\hbar^2}{2}\sum_{A=1}^{M}\frac{1}{M_A}\nabla_A^2}_{\text{Kinetic Energy of Nuclei, } \hat{T}_N} \underbrace{-\frac{\hbar^2}{2m_e}\sum_{i=1}^{N}\nabla_i^2}_{\text{Kinetic Energy of Electrons, } \hat{T}_E} + \underbrace{\frac{1}{4\pi\varepsilon_0}\sum_{A=1}^{M}\sum_{B>A}^{M}\frac{Z_A Z_B}{R_{AB}}}_{\text{Inter-nuclear Electrostatic Potential Energy, } \hat{V}_N} + \underbrace{\frac{1}{4\pi\varepsilon_0}\sum_{i=1}^{N}\sum_{j>1}^{N}\frac{1}{r_{ij}}}_{\text{Inter-electronic Electrostatic Potential Energy, } \hat{V}_E} \underbrace{-\frac{1}{4\pi\varepsilon_0}\sum_{i=1}^{N}\sum_{A=1}^{M}\frac{Z_A}{r_{iA}}}_{\text{Electron-Nuclear Electrostatic Interaction Energy, } \hat{U}}$$

+ Spin Orbital Coupling and other negligible terms (3.3)

Thus, for a large system involving a large number of electrons, the complexity to arrive at an exact solution to the equation is readily apparent.

3.2.2 The Earlier Approaches

An earlier approach to simplify the solution to SWE was the Born-Oppenheimer Frozen Nuclei Approximation (BOA), which treats the nuclear and inter-atomic motion entirely separately based on the much faster movement of the electrons as compared with the nucleus.[44] The approach assumes that the molecule is fixed at a certain internuclear separation, and then suggests carrying out calculations for the total energy as a function of inter-atomic distances, each of the result corresponding to a point on the Potential Energy Surface (PES), which is the solution to the SWE.[44,45] At a particular point on the PES, the energy corresponds to that of a particular state in the molecule. The total energy expression and the Hamiltonian are separated as follows:

$$E_{total} = E_{electronic} + E_{nuclear} \tag{3.4a}$$

$$\hat{H} = \hat{H}_{electronic} + \hat{H}_{nuclear} \tag{3.4b}$$

where,

$$\hat{H}_{electronic} = \hat{T}_E + \hat{V}_E + \hat{U} \tag{3.5a}$$

$$\hat{H}_{nuclear} = \hat{T}_N + \hat{V}_N \tag{3.5b}$$

It would be noteworthy to mention that the contributions to the translational, rotational and vibrational motion are embedded in the nuclear term in the above expressions.

The BOA reduced the complication of calculating the total energy considerably by removing the energy terms involving the nuclei, and by calculating electron energies making the nuclear energy constant. However, the treatment of the inter-electronic electrostatic potential energy still remains difficult to formulate.

The next step towards simplifying the solution was to consider each electron to move in some sort of "average potential", independent of the other electrons.[44] This Independent Electron Model (IEM) or Orbital Approximation (OA) separated the electronic Hamiltonian into components dependent only on the properties of their corresponding electron, and the nucleus, i.e,

$$\hat{H}_{electronic} = \sum \hat{H}_i \tag{3.6}$$

This major simplification led to the solution of the following form:

$$\psi_e = \psi_1 \psi_2 \ldots\ldots \psi_N \tag{3.7}$$

Thus, the many electron wave function is reduced to a series of single electron wave functions, solutions to each of which is much easier. In addition to that, based on the earlier work by Hund (1926), and the suggestions of Pauling and Lennard-Jones (1929), Mulliken approximated in 1932 that the molecular wavefunction, i.e., the Molecular Orbital (MO) is a Linear Combination of Atomic Orbitals (LCAO). These orbitals are known as the Basis Functions, and constitute a Basis Set.[46] Where ϕ_j is the Atomic Orbital (AO) or the Basis Function, and c_{ji} is the Mixing Coefficient for j^{th} Basis Function for the i^{th} MO, using the LCAO the Wave Function can be expressed as:

$$\psi_i = \sum_{j=1}^{N} c_{ji} \phi_j \tag{3.8}$$

Hückel presented a very simple, but plausible and effective method incorporating this LCAO approach in the expectation value of the orbital energy:

$$E = \frac{\int \psi^* \hat{H} \psi d\tau}{\int \psi^* \psi d\tau} \tag{3.9}$$

Here, $d\tau$ is the differential volume element. Evaluating the derivatives of equation (3.9) w.r.t. the coefficients, and determining the maxima thereafter produces the Secular Determinant with the Folk or Energy Element Matrix H as:

$$HC = S\varepsilon C \tag{3.10}$$

Here S is the Overlap Matrix describing the overlapping between the basis functions, C is the Coefficient Matrix, and H and S elements are defined as:

$$H_{ij} = \int \phi_i \hat{H} \phi_j d\tau = \alpha \text{ (for i=j) or } \beta \text{ (for i≠j)} \quad (3.11a)$$

$$S_{ij} = \int \phi_i \phi_j d\tau \quad (3.11b)$$

According to the Simple Hückel Method (SHM) or Simple Hückel Theory (SHT), Hückel proposed $\psi^* = \psi$ and $d\tau = dxdydz$, and estimated the Overlap Matrix as $\delta_i = 1$ (for $i=j$, i.e., identical Basis Functions on the same atoms) or 0 ($i \neq j$, i.e., different basis functions on the same atoms or well-separated functions on different atoms). The Coulomb Integral α (the energy of the molecule relative to a zero of energy taken as the electron and the basis function at infinite separation), and the Resonance/Bond Integral β (Energy of the electron in the overlap region) are assumed to be 0 and -1 respectively.[46] The Coefficient Matrix and the MO energies ε can then be obtained by diagonalizing equation (3.10):

$$H = C\varepsilon C^{-1} \quad (3.12)$$

The electronic contribution to the total energy is thus calculated. The total energy is determined as the following equation, by incorporating the Inter-Nuclear Potential Energy term:

$$E_{total} = E_{electronic} + E_{nuclear} = \hat{T} + \hat{V}_N \quad (3.13)$$

SHM, although simple in formulation, improperly estimates the Folk Matrix elements, incorporating the p-orbitals only as the basis sets, and treating only π electrons. However, it had been applied to predict many chemical phenomena like dipole moments, er spectra, bond lengths, redox and ionization potentials, UV and IR spectra, aromaticity, acidity/basicity, and reactivity.[46] With the availability of more sophisticated approaches, SHM is now rarely used for computational chemistry research.

Hoffmann proposed a modification to SHM, known as the Extended Hückel Theory (EHT) or Extended Hückel Method (EHM). It involves all valence s and p-orbital, and calculates smoothly varying α, β, and S integral parameters w.r.t the distance

between the orbitals and the atoms respectively.[44,46] An input geometry is provided for initial calculation of S, H and C, and the ε matrices are calculated subsequently. The mixing coefficients are transformed to those of the original basis functions' coefficient in the MO. EHM had been used to determine geometry conformation and relative energies in earlier works on SWE, and is currently widely used in solid state physics and for studying large extended systems like polymers, solids and surfaces.[46] However, it does not account for the electron spin, electron-electron repulsion, and ignores the fact that the molecular geometry is partly determined by internuclear repulsion, which cause poor geometry energy results obtained by this method.[46]

SHM and EHM are both among the initial semi-empirical methods in quantum chemistry and are basis for many of the following developments.

3.2.3 The *Ab Initio* Methods

The earlier solutions to the Schrödinger's Wave Equation focused on offering long term predictions and minimum approximations, which eventually gave birth to the *ab initio* (Latin for 'from the beginning') philosophy.[41] In the SHM, the Fock Matrix elements H_{ij} are not calculated, but are estimated according to simple rules based on atomic connectivity. In EHM, they are calculated from the relative positions through S_{ij}, but not using the first principle. In *ab initio* calculations, they are calculated directly from Equation (3.11a).

Analytical solutions for the polyelectronic systems were not possible because of the complexity of the electron-electron term. In 1928, Hartree proposed a plausible approximate polyelectronic wave function, named as the Hartree Product, as the product of one-electron wavefunctions or spatial orbitals:

$$\psi_0 = \psi(1)_0\psi(2)_0\psi(3)_0.....\psi(N)_0 \qquad (3.14)$$

The one electron SWE is solved for electron 1, where the electron-electron repulsion term is calculated from electron 1 and an average smeared out electrostatic field calculated from $\psi(2)_0\psi(3)_0.....\psi(N)$, and obtaining $\psi(1)_1$. This improved estimate for

electron 1 is then used to determine $\psi(2)_1$, taking the repulsion term resulting from electron 2, and $\psi(1)_1\psi(2)_0\psi(3)_0.....\psi(N)$, and so on until the cycle is completed to get ψ_1. The process is repeated till the difference between two consecutive values of ψ_k is insignificant, and the energy calculated from both of them are essentially the same, i.e., the later value is consistent with the former. Thus, the Hartree procedure is named as the Self-Consistent-Field (SCF) Procedure.[46]

Although the Hartree Method provided a new initiative to the solution, it didn't take the Electron Spin Property, which restricts placement of more than two electrons in a single atomic or molecular orbital according to Pauli's Exclusion Principle, and also didn't incorporate the anti-symmetric property of the electron switching, as fermions should have.[46] In 1930, modifications were proposed by Fock and Slater. Slater proposed a wavefunction, known as the Slater Wavefunction, composed as a combination of spatial and spin orbitals:

$$\psi(spin\alpha) = \psi(spatial)\alpha = \psi(x,y,z)\alpha \tag{3.15a}$$

$$\psi(spin\beta) = \psi(spatial)\beta = \psi(x,y,z)\beta \tag{3.15b}$$

The Slater Wavefunction is so constructed that it is a determinant for closed shell species, denoted as the Slater Determinant, rather than being a simple product as the Hartree Wavefunction[46]:

$$\psi_{2n} = \frac{1}{\sqrt{(2n)!}} \begin{vmatrix} \psi_1(1)\alpha(1) & \psi_1(1)\beta(1) & \psi_2(1)\alpha(1) & \psi_2(1)\beta(1) & \cdots & \psi_n(1)\beta(1) \\ \psi_1(2)\alpha(2) & \psi_1(2)\beta(2) & \psi_2(2)\alpha(2) & \psi_2(2)\beta(2) & \cdots & \psi_n(2)\beta(2) \\ \vdots & \vdots & \vdots & \vdots & \cdots & \vdots \\ \psi_1(2n)\alpha(2n) & \psi_1(2n)\beta(2n) & \psi_2(2n)\alpha(2n) & \psi_2(2n)\beta(2n) & \cdots & \psi_n(2n)\beta(2n) \end{vmatrix} \tag{3.16}$$

The Slater Determinant enforces Pauli's Exclusion Principle and the anti-symmetric nature of the electronic wavefunctions. The atomic or molecular energy is

calculated by substituting the Slater Determinant and the Electronic Hamiltonian of Equation (3.5a) in Equation (3.9), where the wavefunctons are normalized and $d\tau$ involves a spin coordinate as $d\tau = dxdydzd\xi$, and $\psi = \psi^*$. The Variational Principle (VP) levels off the calculated energy at or above the true ground state energy as:[40,46]

$$E = \frac{\int \psi \hat{H} \psi d\tau}{\int \psi \psi d\tau} \geq E_0 = \frac{\int \psi_0 \hat{H} \psi_0 d\tau}{\int \psi_0 \psi_0 0 d\tau} \tag{3.17}$$

Therefore, energy is minimized w.r.t the atomic or molecular orbitals using the Undetermined Lagrangian Multipliers[46] and the Hartree Fock (HF) Equations are obtained. The derivation of the HF Equations is summarized by Pople and Beveridge[47], and a detailed account is provided by Lowe[48]. Without discussing the derivation, the basic form of the HF Equations is shown below:

$$\hat{F} \begin{pmatrix} \psi_1(1) \\ \psi_2(1) \\ \psi_3(1) \\ . \\ . \\ . \\ \psi_n(1) \end{pmatrix} = \begin{pmatrix} \varepsilon_1 & 0 & . & . & . & 0 \\ 0 & \varepsilon_1 & . & . & . & 0 \\ . & . & . & . & . & . \\ . & . & . & . & . & . \\ . & . & . & . & . & . \\ 0 & 0 & . & . & . & \varepsilon_1 \end{pmatrix} \begin{pmatrix} \psi_1(1) \\ \psi_2(1) \\ \psi_3(1) \\ . \\ . \\ . \\ \psi_n(1) \end{pmatrix} \tag{3.18}$$

However, the HF Equations failed to prescribe a mathematically viable procedure for the initial guesses for the molecular wavefunctions, and also failed to provide a qualitatively understandable electron distribution, because of the complicated wavefunctions.[46] In 1951, Roothan[49] and Hall[50] independently suggested that the representation of the MOs should be analogical to the LCAO Approach in Equation (3.8). Thus the Roothan Hall equations are obtained by substituting the MOs in the HF Equation using the LCAO Approach as the following:

$$FC = SC\varepsilon \tag{3.19}$$

The Total Hartree Folk Energy is calculated incorporating the inter-nuclear electrostatic potential energy using the frozen nuclei approach:

$$E_{HF}^{Total} = E_{HF} + V_N \tag{3.20}$$

Since the zero energy in SWE is the energy of the electrons and the nuclei at infinite separation, the HF Energy (any *ab initio* energy) of a species is relative to the energy of the electrons and the nuclei at infinite separation. Therefore, it signifies that it is the minimum energy required to break up the molecule or atom and separate the electrons and nuclei to infinity.[46] However, it is usually the relative energy differences that are important in computational chemistry.

Since the nuclear motion (due to vibration) persists even at 0 K, an unavoidable energy term denoted as the Zero Point Vibrational Energy (ZPVE or ZPE) must be added to the Equation (3.20) in the following way:

$$E_{0K}^{Total} = E_{HF}^{Total} + ZPE \tag{3.21}$$

HF Method treated the electron-electron repulsion considering a smeared out averaged electrostatic field from all the electrons except the one under consideration. It also assumed that at a particular moment, an electron has a particular set of spatial coordinates independent of the coordinates of the other electrons. But in reality each electron moves under the influence of the repulsion of the individual electrons, not an average electron cloud,[46] and the HF method therefore overpredicts the electron-electron repulsion term, and so the electrostatic energy. The energy error associated with the HF Approximation for a given system, the Electron Correlation Energy[41], can be determined by:

$$E_{CORR} = E - E_{HF} \tag{3.22}$$

The treatment of the Correlation Energy term is very important. Based on the earlier molecular computational method by Møller and Plesset[51] in 1934, Binkley and Pople[52] proposed a treatment using the Perturbation Theory. This approach treats the

complex and realistic system as a perturbed version of the simple and manageable idealized system. Among other post Hartree Fock methods treating the Electron Correlation Energy, Configuration Interaction (CI), which suggests addition of electronic configuration terms to represent promotion of electrons from occupied to virtual MOs,[53] and the Coupled-Cluster Approach are mentionable.

The *ab initio* methods are based on fundamental principle without specific empirical adjustments or severe approximations, making them more general, reliable and satisfactory.[46] They are used to calculate molecular geometries and energies, vibrational frequencies, spectra (IR, UV, NMR), ionization potentials and electron affinities, and dipole moment related to electron distribution. Theoretical and practical examples of these applications include, but are not limited to, identification and understanding novel molecules from spectroscopic results, visualization of calculated phenomena like the vibrational frequencies, charge distribution and molecular orbitals.

Despite the relative accuracy of the *ab initio* methods, they demand greater computational resources and are extremely slow.[46] These disadvantages tend to increase with the complexity of the problem at hand, and with the level of calculation.

3.2.4 The Semiempirical Methods

In contrast to the theoretical approach of the *ab initio* methods, the semi-empirical methods offer mechanical calculation of some integrals for SWE, based on experimentally approximated quantities.[46] Conventionally, most of these methods are parameterized using the experimental values of ionization energies, heats of formation, and electron affinities. Apart from the SHM and EHM, the SCF semiempirical methods are well known for the reduced calculation time. However, the assumption that the approximated values for a parameterized species would give a more or less accurate estimation for an unparameterized species is a rather crude one, and the complication of experimental determination of quantities still remains unresolved. These problems, in addition to the practical necessity of determining the empirical parameters separately for different systems, make the application of the semiempirical methods limited.

3.2.5 The Density Functional Theory

The main difficulty faced in the *ab initio* or semiempirical methods is that they depend on the wave function, the definition of which is yet to reach a general agreement.[46] Density Functional Theory (DFT) on the other hand, is based on the probability of finding the electrons within a volume element centered on a point, an "observable" quantity known as the electron probability density function. The electronic charge is assumed to be smeared out in a fog around the molecule. It is a function of position only, and can be measured by X-ray or electron diffraction techniques.[54] Where a wave function has 4N variables for a system of N electrons, the electron density function depends on three variables irrespective of the number of atoms, although neither correct mathematical form of the functional, nor a systematic method to develop one exists. The limited intuitional and empirical parameters involved, and the possibility of finding the exact functional makes DFT *ab initio* in spirit.[46] The concept had been invigorating, and the 1998 Nobel Prize for chemistry had been awarded to Walter Kohn for the development of DFT, jointly with John Pople for his role in practical wavefunction-based methods. Standard literature on DFT are offered by Parr and Yang[55], Levine[53], Kohn et al.[56], Friesner et al.[57], and more recently by Koch and Holthausen[43].

DFT calculates all the properties of the atoms and the molecules from the Density Function. In the 1920's, the idea of calculating atomic and molecular properties was introduced independently by Enrico Fermi and Dirac, from their work on ideal electron gas. This concept gained popularity later on as the Fermi-Dirac statistics. The Thomas-Fermi-Dirac model gave surprisingly good results for atoms, but failed to make predictions for the molecules. In 1951, Slater provided a more accurate version of the model (the Xα Method), which is regarded as the first chemically useful DFT method.[58] This method is almost completely replaced later on by the Kohn-Sham type DFT methods discussed in the following sections.

The DFT calculations at present are performed utilizing the Kohn-Sham approach based on the two Hohenberg-Kohn theorems. The first of these theorems, basically an existence theorem, expect that the properties of a molecule in a ground electronic state

like the ground state energy E_0 are determined by a functional of the ground state electron density function ρ_0,[59] i.e.,

$$E_0 = E[\rho_0] \tag{3.23}$$

The second theorem is analogous to the Variation Principle[46,60] and states that any trial density function will always provide an energy higher (or equal to, if the trial function is the exact function) than the true ground state energy. Since the energy of a moving electron is due to the potential of the atomic nuclei, this potential is known as the "external potential", and is designated as v(**r**). The electronic energy E_v, a function of the trial density function, can be represented as:

$$E_v[\rho_t] \geq E_0[\rho_0] \tag{3.24}$$

However, the exact form of the functional is unknown; the approximate functionals used for calculations may give lower energies than the ground state energy, and hence may not be variational.[46]

In 1965, an analogous variational approach to the Hartree-Fock VP led to the Kohn-Sham (KS) energy equations[61], which is the basis of the current DFT calculations. This approach regards the electronic energy of the molecule as a deviation from the ideal energy of a fictitious non-interacting reference system, which is determinable. The ground state electron density in the ideal system is exactly the same as that in the real ground state system, i.e., $\rho_r = \rho_0$. The deviation is relatively small, and is approximated. The internuclear repulsion energy is added to find the "frozen nuclei" energy, and eventually the zero-point energy can be added to determine the 0 K total internal energy. The ground state electronic energy can be represented in terms of the functionals as shown in the following equation:

$$E_0 = \langle T_E[\rho_0] \rangle + \langle V_E[\rho_0] \rangle + \langle U[\rho_0] \rangle \tag{3.25}$$

Where the first, second, and the third term represent the kinetic energy of the electrons, the inter-electronic electrostatic potential energy, and the electron-nuclear electrostatic

interaction energy, respectively. The electron-nuclear interaction energy can be expressed in terms of an external potential, hence the potential corresponding to the attraction of an electron for all of nuclei A. Although not incorporated into the original DFT concept, Kohn and Sham suggested that the kinetic energy of the electrons can be expressed as a single Slater determinant of occupied (closed) spin molecular orbitals of a hypothetical non-interacting electron system. Introducing the concept of this KS spin orbital ψ_r containing KS spatial orbitals ψ^{KS} and spin functions α and β, and using Slater-Condon rules in order to simplify the integrals in the Slater determinant, Equation (3.25) can be expressed as:

$$E_0 = -\frac{1}{2}\sum_{i=1}^{2n}\left\langle \psi_i^{KS}(1)\left|\nabla_1^2\right|\psi_i^{KS}(1)\right\rangle - \sum_{nucleiA} Z_A \int \frac{\rho_0(r_1)}{r_{1A}} dr_1 + \frac{1}{2}\iint \frac{\rho_0(r_1)\rho_0(r_2)}{r_{12}} dr_1 dr_2 + \Delta\langle T_E[\rho_0]\rangle + \Delta\langle V_E[\rho_0]\rangle \tag{3.26}$$

The deviation of the real kinetic energy with the kinetic energy of non-interacting system of electrons, and the deviation of the electron-electron repulsion energy from the classical charge-cloud coulomb repulsion energy had been introduced respectively in the last two terms of Equation (3.26), in terms of functionals. The sum of the deviations is called the exchange correlation energy functional or the exchange correlation energy:

$$E_{XC}[\rho_0] \equiv \Delta\langle T_E[\rho_0]\rangle + \Delta\langle V_E[\rho_0]\rangle \tag{3.27}$$

Parr and Yang expressed the Kohn-Sham equations as the following set of one electron equations derived from (3.26), in a procedure similar to the HF method:

$$\hat{h}^{KS}\psi_i^{KS} = \varepsilon_i^{KS}\beta\psi_i^{KS} \tag{3.28}$$

The KS Fock operator $\hat{h}^{KS}$ incorporates the concept of exchange correlation potential:

$$v_{XC}(R) = \frac{\delta E_{XC}[\rho(r)]}{\delta\rho(r)} \tag{3.29}$$

The KS orbitals are expanded in terms of the basis functions, as in Equation (3.8) and the N sets of equations are used to construct the Fock matrix as in Equation (3.19). To solve the KS equations, an initial guess of the electron density function, usually a non-interacting atoms guess, is done by summing the electron densities of the individual atoms of the molecule, at the molecular geometry. An explicit expression for the KS operator is obtained, and the Fock matrix elements, which are integrals of Fock operators over the basis functions, are calculated usually numerically rather than by analytical methods. The Fock matrix is orthogonalized and diagonalized to give the initial values of c, which is again used to calculate a corrected density function as:

$$\rho_0 = \rho_r = \sum_{i=1}^{2n} \left| \psi_i^{KS} \right|^2 \tag{3.30}$$

The new estimate is used to repeat the process until the convergence criterion is reached.

The accuracy of DFT methods depends on devising good functionals for the exchange correlation term and hence the correlation potential. This is also a critical step since the exact form of the functional is unknown. The exchange correlation energy (ECE) functional and the exchange correlation potential (ECP) are functions of the electron density and therefore positions, and thus the devised functionals are presented such.[46] Usually the exchange correlation energy is split into the exchange and correlation parts[43] as:

$$E_{XC}[\rho_0] = E_X[\rho_0] + E_C[\rho_0] \tag{3.31}$$

Many approaches had been tried to devise good ECE functionals for DFT methods. The simplest approximation is the local density approximation (LDA), which assumes a homogeneous electron gas with little or no variation in density with position[43]. Another elaboration of this approach, known as the local spin density approximation (LSDA), incorporates electrons of opposite spins, and assigns them different KS orbitals. However, the electron density, particularly in molecular systems, is hardly spatially uniform, and therefore this uniform electron gas model is not valid for most situations. Most of the prominent DFT methods today utilize the variation of electron gas according

to its gradient from a particular point, along with the LSDA approach. This is known as the gradient corrected, or more widely, the generalized gradient approximation (GGA)[46]. These non-local functionals are the workhorses of current DFT methods, and the exchange part of them are usually presented with reference to the LDA approach as:

$$E_X^{GGA}[\rho_0] = E_X^{LDA}[\rho_0] - \sum_\sigma \int F(s_\sigma)\rho_\sigma^{4/3}(\bar{r})d\bar{r} \tag{3.32}$$

The argument of the function F is the Reduced Density Gradient for Spin σ, where s_σ is known as the Local Inhomogeneity Parameter:

$$s_\sigma(\bar{r}) = \frac{|\nabla\rho_\sigma(\bar{r})|}{\rho_\sigma^{4/3}(\bar{r})} \tag{3.33}$$

One of the realizations of the function F and thus the gradient corrected exchange function had been developed by Becke.[43] Related functionals to this approach are the PW91 (by Perdew, 1991, and Burke, Perdew, and Wang, 1998), CAM (Handy and coworkers), and the recent FT97 (Filatov and Thiel).[43] Other realizations produced earlier are B86 by Becke and P by Perdew, 1986. On the other hand, the most widely adopted gradient corrected correlation functionals are the empirical parameter dependent P86 (Perdew, 1986), the parameter free PW91 (Perdew and Wang, 1991), and LYP (Lee, Yang, and Parr, 1988) functional.[43]

Since the electron correlation is incorporated in DFT in its theoretical basis, rather than add-ons like MP perturbation to *ab initio* HF theory, or parameterization to the semi-empirical methods,[46] it offers more fundamental approach. The possibility of finding the true form of the exact functional makes it more theoretically promising. It's based on the concept of electron density which is easily intuitively grasped as compared to the much debated definition of wavefunction, and is the function of location only. DFT calculations offer the accuracy comparable to those of the MP2 calculations, but require less time like the less accurate HF methods.[46] It had been found to provide better IR and NMR results than the HF method, and more accurate dipole moments than the MP2 method.[46] To date, DFT appears to be the most popular and successful of all quantum mechanical

approaches, and the method of choice particularly for geometry and energy calculations for transition metal compounds, for which the other methods had been found to yield poor results.[62,63]

Based on all these advantages, DFT was the method of choice for the current study, which involves geometry, energy and IR vibrational frequency calculations, adsorption studies, and transition state search on the various unsulfided and sulfided forms of a transition metal phosphide, namely Ni_2P, at hydrotreating environment.

3.3 DFT Simulation: Procedures and Parameters

Simulation tasks performed in this study were done on systems ranging from molecules to super-cells constructed from multiple unit crystals. The parameters had been adjusted for each system and calculation. A brief discussion of the simulation calculations and the parameters follows the next sections.

3.3.1 Simulation Procedures

The tasks done in this simulation study can be classified into the following:

1) Geometry optimization
2) Surface Energetics
3) Thermodynamic calculations
4) Vibrational frequency calculations and
5) Transition state search

As mentioned earlier, the systems ranged from molecules to super-cell constructions, and the time taken for each calculation was varying depending on the systems, tasks, and parameters chosen.

3.3.1.1 Geometry Optimization

Geometry optimization is done to refine the constructed molecular or crystal structure to a stable geometry.[38] The coordinates of the atoms of the system are adjusted by a series of single-point calculations for the PES. The geometry is changed systematically until a stationary point is reached, and the energy of the structure indicates that the forces on the atoms are zero. The atoms remain relatively fixed, and the energy corresponding to a given system is calculated from first principles. The "total energy" of a molecule or crystal refers to the energy of a specific arrangement of the atoms. The zero reference energy is taken to be the infinite separation of all electrons and nuclei, so the total energy is generally negative, corresponding to a bound state. This quantity should not be confused with the "binding energy," which is the energy required to separate the individual atoms.[38] In addition to obtaining a stable geometry, optimization is required for subsequent calculation of heat of adsorption, vibrational frequency, and transition state searches. For geometry optimization calculations, if the minimum energy is attained, the total energy can be corrected for the ZPE by vibrational analysis.

3.3.1.2 Surface Energetics

If several types of surfaces are possible on a solid crystal structure, it is required to determine the most stable terminations at the conditions of the study. In this case, the Ni_2P structure has two possible terminations in the (001) direction, namely Ni_3P_2 and Ni_3P. Two approaches can be taken to determine the relative stability of these surfaces. In the first approach, the stiochiometric composition of each of the surfaces is considered, and the required energy change of the system related to its formation from the bulk phase is calculated from the chemical reactions. The chemical reactions related to the formation of the five layered structures with either Ni_3P_2 or Ni_3P_2 termination are respectively:

$$7\frac{1}{2}\,Ni_2P + \frac{1}{2}\,PH_3 = Ni_{15}P_8 + 1\frac{1}{2}\,H_2 \qquad (3.34a)$$

$$7\frac{1}{2}\,Ni_2P + 1\frac{1}{2}\,H_2 = Ni_{15}P_7 + \frac{1}{2}\,PH_3 \qquad (3.34b)$$

Therefore the energy change associated to the exposure of Ni_3P_2 and Ni_3P from the bulk phase can be calculated using the following equations respectively:

$$E_{Ni_3P_2Surf} = E_{Ni_{15}P_8} + 1\frac{1}{2}E_{H_2} - 7\frac{1}{2}E_{Ni_3P} - \frac{1}{2}E_{PH_3} \quad (3.35a)$$

$$E_{Ni_3PSurf} = E_{Ni_{15}P_7} + \frac{1}{2}E_{PH_3} - 7\frac{1}{2}E_{Ni_2P} - 1\frac{1}{2}E_{H_2} \quad (3.35b)$$

Comparing the calculated energies, it can be deduced that the surface requiring less energy to be exposed from the bulk phase is the more stable one.

The other way to determine the stability of the surfaces is to calculate the relative energy change associated with the change from one termination to the other. To change the surface termination of a five layered structure from Ni_3P to Ni_3P_2, stoichiometrically, the following chemical reaction should take place:

$$Ni_{15}P_7 + PH_3 = Ni_{15}P_8 + 1\frac{1}{2}\,H_2 \quad (3.36)$$

The related energy change to this process can be calculated using the following equation:

$$\Delta E_{Ni_3P_to_Ni_3P_2} = E_{Ni_{15}P_8} + 1\frac{1}{2}E_{H_2} - E_{Ni_{15}P_7} - E_{PH_3} \quad (3.37)$$

If the energy change is negative, thermodynamically the process for changing the surface termination from Ni_3P to Ni_3P_2 would be spontaneous, and thus the latter termination would be more stable. Otherwise, a positive energy change would mean that the Ni_3P termination is more stable.

3.3.1.3 Thermodynamic Calculations

The bond formation of species *A* to be adsorbed on the surface *S* can be represented by the following reaction scheme:

$$A + S \rightarrow A\text{-}S \quad (3.38)$$

The heat of adsorption for the proposed scheme, when the energy is expressed as *E*, is:

$$\Delta E_{ads} = E_{A-S} - E_A - E_S \tag{3.39}$$

The individual components in the expression are calculated by geometry optimization. This energy change also indicates the comparative strength of various modes of adsorption of a species on the surface, or comparative adsorption strength of different species on the surface. For example, the heat of adsorption of a free H_2S molecule on a clean Ni_2P surface can be calculated using the following equation:

$$\Delta E_{H_2S} = E(H_2S \text{ adsorbed surface}) - E(\text{clean surface}) - E(\text{free } H_2S) \tag{3.40}$$

Similarly, the energy change associated to the molecular adsorption of H_2S, and then dissociation into adsorbed –SH species plus gas-phase hydrogen, or dissociation to adsorbed sulfur plus gas-phase hydrogen are calculated using the following equations respectively:

$$\Delta E_{HS} = E(-SH \text{ adsorbed surface}) + \frac{1}{2}E(\textit{free } H_2) - E(\text{clean surface}) - E(\text{free } H_2S) \tag{3.41}$$

$$\Delta E_S = E(\textit{sulfur} \text{ adsorbed surface}) + E(\textit{free } H_2) - E(\text{clean surface}) - E(\text{free } H_2S) \tag{3.42}$$

Considering the temperature corrections and pressure effects, the free energy change for the above discussed three processes are calculated as follows:

$$\Delta G_{H_2S} = \Delta E_{H_2S} + \Delta G^0_{T_{Corr}} - RT \ln p_{H_2S} \tag{3.43}$$

$$\Delta G_{HS} = \Delta E_{HS} + \Delta G^0_{T_{Corr}} + \frac{1}{2}RT \ln p_{H_2} - RT \ln p_{H_2S} \tag{3.44}$$

$$\Delta G_S = \Delta E_S + \Delta G^0_{T_{Corr}} - RT \ln \frac{p_{H_2S}}{p_{H_2}} \tag{3.45}$$

Two other particular calculations done in this study are the partial replacements of the phosphorus atoms from the Ni_3P_2 surface to form Ni_3PS surface, and the complete replacement of the phosphorus atoms from the bulk Ni_2P structure to form bulk Ni_3S_2. Both replacements took place in the presence of gas phase H_2S and H_2, and PH_3 is formed as a gas phase product. All these schemes will be discussed in the results and discussions sections in details. However, it is noteworthy to mention that the correction to the electronic energy change of the gas phase molecules due to the enthalpy and entropy change at reaction temperatures are incorporated as $\Delta G^0_{T_{Corr}}$ terms. The electronic and free energy change of these processes are calculated using the following equations:

$$\Delta E_{Ni_3PS} = E(Ni_3PS \text{ surface}) + E(PH_3) - E(Ni_3P_2 \text{ surface}) - E((H_2S) - \frac{1}{2}E(H_2) \quad (3.46)$$

$$\Delta E_{Ni_3S_2} = \frac{2}{3}E(Ni_3S_2) + E(PH_3) - E(Ni_2P) - \frac{4}{3}E((H_2S) - \frac{1}{6}E(H_2) \quad (3.47)$$

$$\Delta G_{Ni_3PS} = \Delta E_{Ni_3PS} + \Delta G^0_{T_{Corr}} + RT(\ln p_{PH_3} - \frac{1}{2}\ln p_{H_2} - \ln p_{H_2S}) \quad (3.48)$$

$$\Delta G_{Ni_3S_2} = \Delta E_{Ni_3S_2} + \Delta G^0_{T_{Corr}} + RT(\ln p_{PH_3} - \frac{1}{6}\ln p_{H_2} - \frac{4}{3}\ln p_{H_2S}) \quad (3.49)$$

For studying the adsorption of molecular hydrogen, and dissociation of the adsorbed hydrogen species into atomic hydrogen on the surface, the following equations had been used to calculate the energy change associated to the processes respectively:

$$\Delta E_{H_2} = E(H_2 \text{ adsorbed surface}) - E(\text{clean surface}) - E(\text{free } H_2) \quad (3.50)$$

$$\Delta E_H = E(H \text{ adsorbed surface}) - E(H_2 \text{ adsorbed surface}) \quad (3.51)$$

3.3.1.4 Vibrational Frequency Calculations

The harmonic vibrational frequencies have been theoretically evaluated from the second derivatives of the total energy with respect to the Cartesian coordinates. The Hessian had been evaluated using a 2-point difference method of the analytic forces.[38,43] The elements of the Hessian are computed by displacing each atom in the model and

computing a gradient vector to build up a complete second derivative matrix.[38] All the atoms had been moved in the positive and negative directions in the Cartesian coordinates, without specifying limited Hessian atoms, in order to obtain the modes of vibration.

3.3.1.5 Transition State Search

The transition states occurring during the course of a chemical reaction are the saddle point intermediates on the potential energy surface.[41,46] For the hydrogen adsorption studies, the transition state (TS) search had been attempted using the synchronous transit (ST) method and the Newton-Raphson search, with reasonable guesses for the structures of reactants and products.[38,60] All points on the reaction coordinate have the lowest energies for all atoms in all degrees of freedom on the potential energy surface, except for the one direction along the reaction path. The point corresponding to the maximum energy along the reaction coordinate is the activated complex or the TS. According to TS theory, the activated TS complex is in thermodynamic equilibrium with the reactants, and the rate of formation of reaction is proportional to its concentration. The TS also indicates the activation energy barrier involved with the reaction. The TS is determined by a single interpolation by Linear Synchronous Transit (LST) method, and then alternating searches for a maximum by Quadratic Synchronous Transit (QST) method with constrained conjugate gradient minimization,[38] in order to refine the transition state to a higher degree. This is done using the complete LST/QST method in DMol^3 in MS package, which offers better accuracy than the LST, LST/Optimization, or the Halgren Lipscomb algorithm.[38]

3.3.2 Salient DFT Parameters Used in the Study

As stated earlier, the most important aspect of DFT calculations is the choice of the exchange correlation functional. In DMol^3 the choices offered are LDA and GGA. As discussed in Section 3.2.5, the assumption of homogeneous electron gas is unrealistic, and LDA overpredicts the molecular binding energy as well as weak bonds as hydrogen

bonds. LDA is more accurate for perfect metals but is less accurate for systems with varying electrons.[39] This study involved simulation experiments done on metal phosphide and phosphosulfide surfaces, gaseous species, and surface adsorption phenomena related to these species. Therefore, although computationally costly[38], GGA was chosen because of its accuracy for systems with changing electron density. No weak interaction like the Van Dar Waals forces was important for the study, and therefore the chances of failure using GGA were fairly limited.[64] Among the various types of GGA functionals offered in DMol^3, PW91 based on function developed by Becke (Section 3.2.4) had been chosen in particular because of its applicability in high and low density regimes[38] considered in this study.

In DMol^3, numerical basis functions with numerical values on an atomic-centered spherical polar mesh are used rather than analytical functions (e.g. Gaussian orbitals). This provides sufficiently accurate results for insulated systems. Moreover, the use of the exact DFT spherical atomic orbitals has several advantages. The molecules can be dissociated exactly in its constituent atoms within the DFT context.[38] The basis set superposition effects are also minimized, and it is possible to obtain excellent descriptions, even for weaker bonds.[38] Provision of a larger basis set ensures greater variational degrees of freedom, and generation of a second set of functions doubles the set size, which is referred to as the double-numerical (DN) set.[38] As the current study involves adsorption of hydrogen or hydrogen species on the surfaces, the double numerical plus polarization (DNP) basis set, which includes a numerical function for each occupied atomic orbital and a polarization p-function for valence atomic orbitals on valence orbitals of all hydrogen atoms, had been chosen.[38] Although computationally costly, this was necessary to maintain the highest degree of accuracy as well as consistency with all other calculations involving hydrogen adsorption. The core treatment had been set to effective core potential (ECP) which replaces all core electrons by a single effective potential to reduce the computational cost. But it introduces some relativistic correction into the core.[38] The all electron relativistic (AER) treatment offers a higher degree of accuracy by including all electrons explicitly, but demands much higher computational cost. Moreover, this small discrepancy in accuracy is neutralized for

calculations of most thermodynamic quantities and heats of adsorption, because of the cancellation of terms.

The real space cut-off limits the range of numerical integrations for the charge density and functionals over the space. Beyond this range, the atoms are non-interacting. Depending on the quality levels of DMol^3 calculations, the suggested cut-off for the species involved in this study ranged from 3.0-4.5 Å.[38] Increasing the values beyond this limit rarely imparts any significant effect on the results, although ideally the cut-off range should be the entire space. Generally the calculated absolute energy changes very little with increased cut-off, and the relative energy has little or no effect at all. Although reducing the value below the suggested level could have decreased the computational time significantly, it had been maintained at the high end range to be sufficient for the bonds involved in the study, which range from 1-2.5 Å. In this study the cut-off is set to 4.5 Å, maintaining a global scheme for all species.

The convergence tolerance specifies the threshold limit for convergence. The coarse (10^{-4} Ha for energy, 0.02 Ha/Å for force, and 0.05 Å for displacement in geometry optimization) default settings had been chosen for all calculations on supercell and unit cell systems to reduce computational time. This setting had been sufficient to provide reasonable accuracy, since the associated errors are usually cancelled out. The only exception to this setting is used in hydrogen adsorption studies on the unit cell system. For this particular study, the tolerance had been set to medium quality ($2x10^{-5}$ Ha, 0.004 Ha/Å, and 0.005 Å for energy, force and displacement respectively, in geometry optimization; 10^{-5} Ha, 10^{-4} Ha/Å, and 10^{-3} Å for energy, force and displacement respectively, in transition state search) to maintain high computational accuracy to determine the transition states of reactions, which are more difficult to detect[65].

The k-point set controls specify the number of wave vectors, i.e., the number of integration points, used to integrate the wavefunction in reciprocal space.[38] For all calculations involving larger geometries like the supercell, the individual Monkhorst-Pack parameters and an origin shift in fractional reciprocal space coordinates for the k-points had been customized to the 1x1x1 grid quality, which reduced the computational time but provided reasonably good accuracy. Because of the smaller size of structures, for all unit cell calculations, the quality had been set to a customized grid value of 4x4x1

to provide more integration points and finer control over the calculation accuracy. Some of the preliminary studies done on determining the optimum parameters for this study have found that the results for the unit cell calculations do not change significantly beyond this meshing quality. However, for the hydrogen adsorption study done on the unit cell system the default values of the k-point parameters associated with the medium settings is 4x4x1.

The Self Consistent Field (SCF) tolerance control specifies the accuracy to which the SCF equations are converged. The accuracy had been specified by the SCF tolerance level, which for this study was coarse (10^{-4}) both for supercell and unit cell geometries. For hydrogen adsorption studies, the tolerance threshold is set to medium (10^{-5}) for maintaining high accuracy for the subsequent transition state search. Since the systems involved metal atoms, and was symmetric in some aspects, degenerated levels were present due to the small HOMO-LUMO gap, and SCF convergence became a bottleneck at times. There was a necessity to use a fractional occupancy, which effectively mixes some virtual orbitals into the occupied space.[66] Therefore, the thermal smearing option, a finite-temperature Fermi function to compute fractional occupation numbers, with a small smear factor of 0.005 Ha, had been used consistently for all systems.[38,66] The integration accuracy controls the precision with which the Hamiltonian matrix elements are computed, and is usually kept at the default settings as suggested.[38] Again the coarse settings had been chosen for all geometries except for those used in the hydrogen adsorption studies, for which the settings had been kept at the medium (1000 grid points per atom) quality.

In all cases, the maximum number of iterations had been chosen as 200 for all geometry optimization cycles. The maximum step size had been set to 0.3 Å, which prevents the optimizer to take unreasonable steps with the change of Cartesian coordinates to truncate geometric displacements beyond the specified value.

4 Results

4.1 Introduction

As discussed in the previous chapter, all geometry, energy and frequency results in this study had been calculated using the DMol^3 DFT quantum mechanical model engine[38] in Materials Studio® molecular simulation software, version 3.2, by Accelrys®. The previous chapter also explained in detail the experimental methods followed in the study, along with the selected parameters, and the justification of using particular values for the parameters. It is important to refresh them in brief, which is done in the following section.

4.2 Summary of Parameters

As explained in detail in the previous chapter, taking into account the non-homogeneity of the electron density, the GGA exchange correlation functional is used consistently throughout this study. The PW91 GGA functional developed by Becke, and the DNP basis set with greater variational degrees of freedom have been selected in all cases to ensure higher degree of accuracy, and to maintain consistency with calculations involving the formation of hydrogen bonds.[38] The core treatment had been set to effective core potential (ECP) which replaces all core electrons by a single effective potential to reduce the computational cost, but introduces some relativistic corrections into the core at the same time.[38] However, this difference in accuracy is neutralized for in the calculations of thermodynamic quantities and heats of adsorption because of cancellation of terms. The real space cut-off is set to 4.5 Å, maintaining a global scheme for all species.

The convergence tolerance was set to coarse (10^{-4} Ha, 0.02 Ha/Å, and 0.05 Å for energy, force and displacement respectively, in geometry optimization) for both the

supercell and the unit cell systems. However, for the hydrogen adsorption studies done on the unit cell system, the tolerance had been set to medium ($2x10^{-5}$ Ha, 0.004 Ha/Å, and 0.005 Å for energy, force and displacement respectively, in geometry optimization; 10^{-5} Ha, 10^{-4} Ha/Å, and 10^{-3} Å for energy, force and displacement respectively, in transition state search) for transition state search calculations, which require high accuracy. The SCF tolerance level was medium (10^{-5}) for hydrogen adsorption studies on the unit cell system, and coarse (10^{-4}) for both the supercell and unit cell geometries for all the other studies. The thermal smearing option was selected with a small smear factor of 0.005 Ha consistently for all of the systems.[38,66] The integration accuracy was kept at the default settings of coarse for all supercell and unit cell geometries, with the hydrogen adsorption studies being the only exception using medium (about 1000 grid points per atom) parameters for unit cell geometries. In all cases, the maximum number of iterations was 200 for geometry optimization cycles with maximum step size of 0.3 Å.

For all calculations involving the supercell, the individual Monkhorst-Pack parameters and an origin shift in fractional reciprocal space coordinates for the k-points had been set to 1x1x1 grid quality, which reduced computational time but provided reasonably good accuracy. The choice of k-point parameter values is very important, especially when the frequency calculations are involved. Higher k-points provide more integration points along the surface, but at the expense of higher computational time. Based on some initial studies done on the adsorption of 1 ML CO on the unsulfided and sulfided surfaces, the k-point values were higher along the direction of the surface, particularly to facilitate the adsorption studies and frequency calculations in smaller geometries, i.e., unit cell systems. A summary of the results of the initial studies is presented in Table A.1 of Appendix A. The k-points had been set to the optimum grid quality of 4x4x1 for all the unit cell calculations involved in the main study to provide adequate integration points along the surface for the smaller structures, and to restrain the computational time as much as possible. It is apparent from the initial results that the frequency and adsorption energy values do not change appreciably beyond the 4x4x1 grid quality. For the hydrogen adsorption calculations on the unit cell geometry, 4x4x1 was the default settings for the k-points in medium (0.05/ Å) quality.

4.3 The Structure and Surface of Ni_2P

Transition metal phosphides posses both metallic and refractory properties,[17] and adopt many types of structures. The Ni_2P crystal has a hexagonal structure like the Fe_2P crystal,[17] and it belongs to the space group $P\bar{6}2m$ D_{3h}^2 (Structurbericht notation: revised C22) with the lattice parameters $a_0=b_0=0.5859$ nm and $c_0=0.3382$ nm.[67] The unit cell of the Ni_2P bulk crystal used in this study was constructed based on the literature data[17,67,68] and is shown in Figure 4.1. The structure was geometry optimized (energy minimized) without constraining any atoms before using it for other calculations. Along the (001) plane of this bulk structure of Ni_2P, two alternative layers had been found to exist. A recently published STM study provides direct experimental evidence for these possible terminations.[69] LEED and STM studies by Gomes et al., and recent DFT calculations by Liu et al., also confirm this structure of Ni_2P catalyst.[70]

To compare the stabilities of these two layers, namely Ni_3P_2 and Ni_3P, to exist as the surface, the energy change associated to the formation of the structures with either of these terminations from the bulk phase had been calculated separately. These two structures consisting five layers each were constructed by cleaving the unit crystal along the (001) plane. The structures are illustrated in Figure 4.2. One of them has the Ni_3P_2 layer termination as both the surfaces along the z-direction, while the other one has the Ni_3P termination as the surfaces along the same direction. The middle layer of both the structures had been constrained for faster calculation, and a vacuum of 15 Å had been provided above each termination along the z-direction to prevent interaction with the repetitive layers along that direction. The assumption made in this case was that for a slab of some appreciable thickness, only the surface energy changes according to the termination and the bulk energy remains constant regardless of the termination of the exposed plane. This is a valid assumption as the surface termination has little effect on the bulk structure, and the energy of the bulk phase is dependant only on its own structure. It was also assumed that there were no kinetic limitations for the surface to achieve the required termination. Thus, the total energy of these two structures can be used to compare the surface energies. According to the Equations (3.34a) or (3.34b), and using Equations (3.35a) or (3.35b), the total energy change related to the formation of a

structure with either of these terminations from the bulk phase can be calculated individually with reference to the bulk Ni_2P structure consisting of the same number of Ni_2P units. The structure with the lowest total energy change is considered to have the most stable termination. The geometry optimization calculations are presented in Table 4.1. The results obtained using Equations (3.35a) and (3.35b) are, respectively:

$$E_{Ni_3P_2Surf} = 3.07 \text{ eV/Å}^2$$

$$E_{Ni_3PSurf} = 3.21 \text{ eV/Å}^2$$

Alternatively, according to the scheme presented in Equation (3.36) and using the same geometry optimization results in Equation (3.37), the relative energy change associated to changing the structure with Ni_3P termination to the structure with Ni_3P_2 termination was determined:

$$\Delta E_{Ni_3P_to_Ni_3P_2} = -0.026 \text{ eV/Å}^2$$

It is apparent from both the methods that the structure with the Ni_3P_2 layer possesses lower energy, and is the more stable termination for the Ni_2P structure. The subsequent studies on the determination of the active phase, therefore, had been conducted on the Ni_3P_2 layer terminated Ni_2P structures.

4.4 Incorporation of Sulfur in the Ni_2P Structure

It had been discussed in the literature review section that previous studies found conclusive evidence of formation of an active phosphosulfide layer on the Ni_2P surface at hydrotreating conditions.[16,19-21,34,35] It has also been explained why the current experimental techniques are unable to determine the exact form of this active phase.[19] In order to determine this NiP_xS_y phase by theoretical calculations, all the possible methods of incorporation of sulfur on the stable Ni_3P_2 surface have to be considered. A four layered 2x2x2 supercell had been prepared, cleaving the unit crystal along the (001) plane exposing the Ni_3P_2 termination, and repeating the geometry in the x and y-directions as

shown in Figure 4.3. The supercell provides a reasonably larger geometry that can accommodate more possible schemes for sulfur incorporation. It can be seen from the top view of the supercell in Figure 4.4 that the nickel atoms form three fold hollows (TFH) on the exposed Ni_3P_2 surface. The sulfur-containing model molecule used in this study is hydrogen sulfide (H_2S), and the following methods of sulfur incorporation from H_2S to the Ni_2P structure were considered;

i. Molecular and dissociative adsorption of H_2S
ii. Partial and complete replacement of phosphorus atoms from the Ni_3P_2 surface by sulfur atoms
iii. Complete sulfidation of the structure

4.4.1 Molecular and Dissociative Adsorption of H_2S

The H_2S molecule had been placed initially on the Ni_3P_2 surface in all possible modes in order to determine the structure with the minimum energy by geometry optimization. It had been found that the sulfur in the H_2S molecule does not adsorb on top of the phosphorus atom of the Ni_3P_2 surface. When the sulfur atom of the H_2S molecule was placed at a bridging position between a phosphorus and a nickel atom, the molecule moved on top of the nickel atom. The same result is obtained when it is placed on the TFH site. While the sulfur atom is on top of the nickel atom, the two hydrogen atoms of the H_2S molecule prefer to point towards the two other nickel atoms of the TFH. The bridging position between two nickel atoms is less stable than the position on top of the nickel atom. Other initial modes of adsorption, including placing the hydrogen atoms closer to the Ni_3P_2 surface, either reverts back to one of the stable positions mentioned above, or causes the molecule to desorb from the surface. The most stable mode of adsorption of molecular H_2S is therefore on top of the nickel atom, with the two hydrogen atoms pointing towards the two other nickel atoms. The adsorption energy for this mode, calculated using Equation (3.40), is -0.70 eV/H_2S. All the stable modes of molecular adsorption of H_2S on the Ni_3P_2 surface are presented in Figure 4.5.

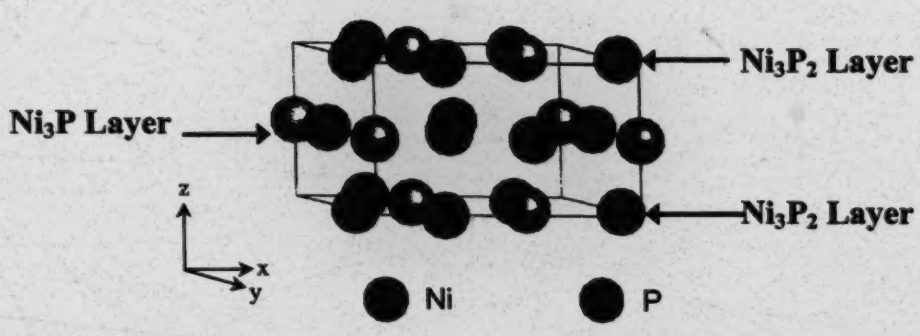

Figure 4.1 Unit Crystal of Ni_2P and the two possible terminations in (001) direction. Nickel and phosphorus atoms are presented in cyan and purple colors, respectively.

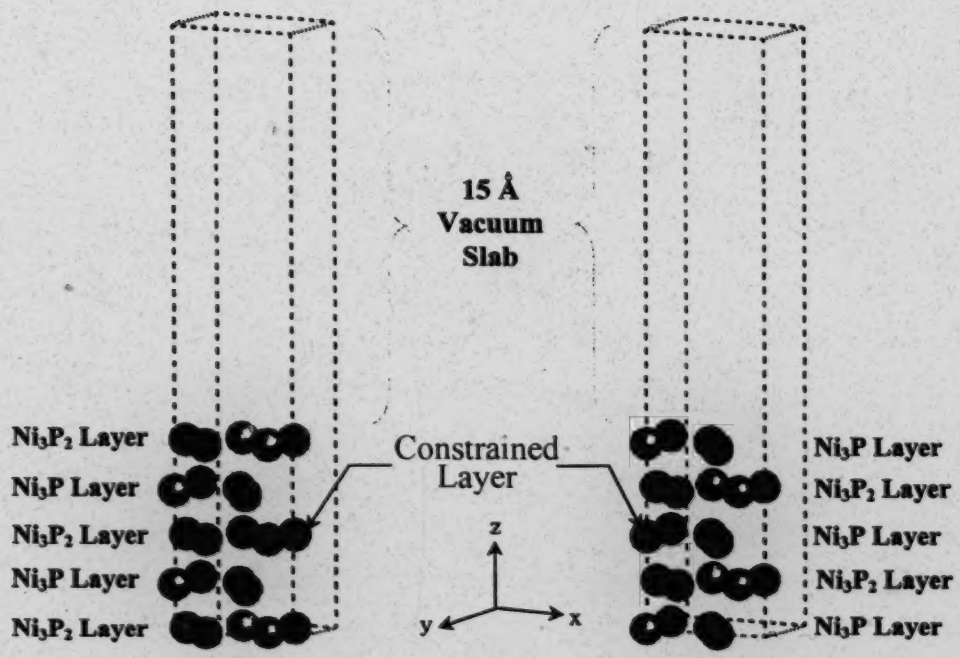

Figure 4.2 Five layered unit cells with either Ni_3P_2 or Ni_3P termination and constrained middle layers. The cells are constructed by cleaving the unit crystal along the (001) plane, for surface energetics calculations.

Table 4.1 Total Energy of the structures and the chemical species for determining the relative stability of Ni_3P_2 and Ni_3P surfaces.

Structure or Chemical Species	Total Energy (eV)
Bulk Ni_2P	-37.54
PH_3 Molecule	-10.36
H_2 Molecule	-04.56
Ni_2P with Ni_3P_2 termination	-97.08
Ni_2P with Ni_3P termination	-91.95

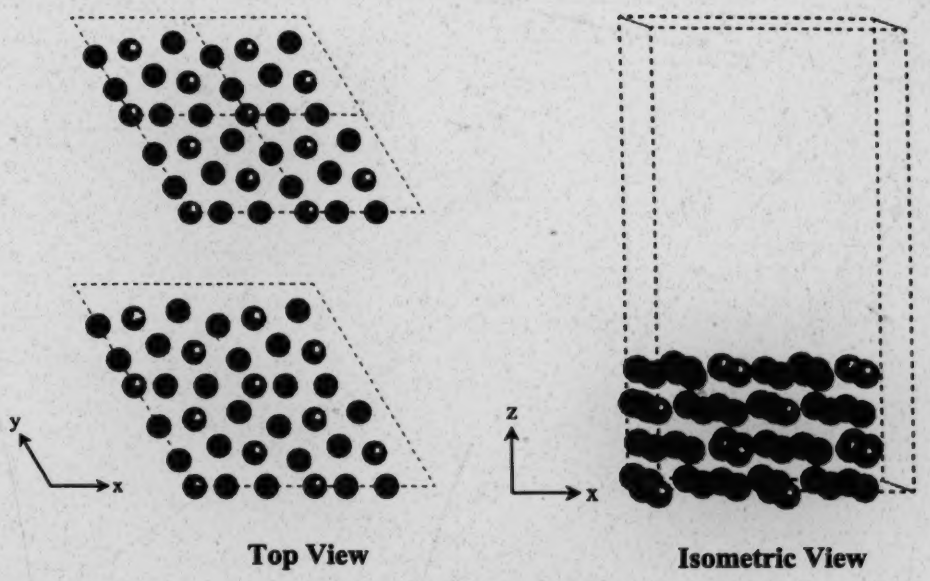

Figure 4.3 The construction of a four layered 2x2x2 supercell from the periodic repetition of the unit crystal along the x and y-directions.

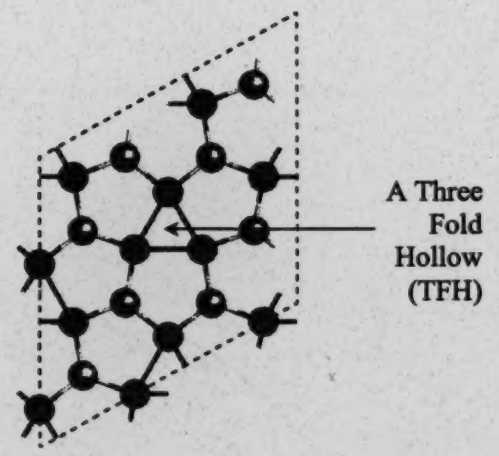

Figure 4.4 Top view of the Ni_3P_2 surface of the Ni_2P supercell. The nickel atoms on the Ni_3P_2 surface form three fold hollows (TFH) on the surface. Nickel and phosphorus atoms are presented in cyan and purple colors, respectively.

Stable Modes of Adsorption	Top View	Side View	Adsorption Energy (eV/H_2S)
H_2S adsorbed on top of a nickel site, the hydrogen atoms pointing towards the two other nickel atoms of the TFH.	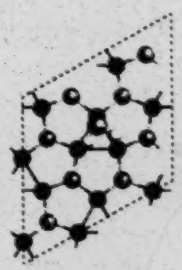	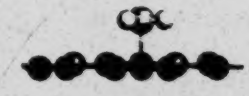	-0.70
H_2S adsorbed on top of a nickel site, while the hydrogen atoms point away from the TFH.	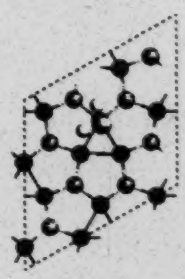		-0.68
H_2S adsorbed at the bridging position between two nickel atoms.	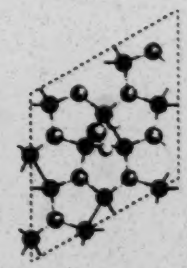		-0.54

Figure 4.5 The stable modes of adsorption of H_2S as a molecule on the Ni_3P_2 surface. Cyan, purple, yellow and white represent nickel, phosphorus, sulfur and hydrogen atoms respectively.

In addition to the molecular adsorption studies, the possibility of dissociative adsorption of H_2S molecule was considered. Dissociative adsorption can take place in many different ways. For instance, the H_2S molecule can dissociate into a smaller molecular or ionic species. Moreover, the dissociated species can remain adsorbed on the surface or can escape into the gas phase. In order to conclude whether any dissociative adsorption takes place on the Ni_3P_2 surface or not, it is important that all the configurations are considered.

A possibility for dissociative adsorption of H_2S is the formation of adsorbed –SH species and evolution of gas phase hydrogen. In the most stable structure for this adsorption scheme, the sulfur atom prefers to sit on the TFH closer to two of the trigonal nickel atoms, whereas the hydrogen atom is located almost atop the other nickel atom. When the -SH species had been placed initially on top of the nickel atom, it changed back to this configuration after geometry optimization. The adsorption strength calculated for this mode using Equation

(3.41) is -1.40 eV/H_2S. The sulfur atom forms a shorter bond of approximately 2.30 Å in length with each of the two closer nickel atoms, and a longer bond of 2.57 Å in length with the distant nickel atom in the TFH. The hydrogen atom does not form any bond with any of the nickel atoms. The -SH species also adsorbs stably at the bridge between two nickel atoms with an adsorption energy of -1.26 eV. Another stable position for adsorption of the –SH on the Ni_3P_2 surface is the bridging position between a nickel and a phosphorus atom. An initial positioning of the –SH species on top of the phosphorus atom also resulted into this mode after geometry optimization. All the stable adsorption modes of dissociative adsorption of H_2S as –SH species are presented in Figure 4.6.

Another possibility for dissociative adsorption of H_2S is the formation of atomic hydrogen and sulfur, both remaining adsorbed on the surface. However, when two hydrogen atoms and one sulfur atom are placed near the three neighboring nickel atoms that form a TFH, they always tend to combine and form an adsorbed H_2S, similar to the most stable configuration for molecularly adsorbed H_2S, as shown in Figure 4.5. This implies that the dissociation of H_2S into adsorbed atomic sulfur and hydrogen atoms is not favorable.

Dissociation can also form atomic sulfur, which is adsorbed on the surface, and gas phase hydrogen. Investigating all the probable modes, it was found that sulfur prefers the center of the TFH sites, as shown in Figure 4.7. The adsorption energies associated with all the stable modes of adsorption of H_2S as atomic sulfur are presented in Appendix B. The adsorption energies are calculated using Equation (3.42). For the most preferable position at the TFH, the adsorption energy is -1.64 eV/H_2S. The total adsorption energy increases almost linearly with the number of sulfur atoms adsorbed similarly on the Ni_3P_2 surface, until all the TFH sites are blocked by these adatoms. The number of TFH sites on the supercell surface is four. The adsorption energy per H_2S atom at this point, where one sulfur atom is adsorbed per TFH site, is -1.58 eV/H_2S. When all the TFH sites are blocked, adsorption of an additional sulfur atom at the Ni-P bridge, which is another stable position for adsorption of atomic sulfur, produces a positive energy change of +0.27 eV, taking the adsorption energy to -1.21 eV/H_2S. Addition of more than one sulfur atoms in one TFH site also produces a positive energy change.

The free energy change associated to the most stable modes of molecular and dissociative adsorption of H_2S as a molecule, -SH species, and solid sulfur on the pristine Ni_3P_2 surface, are calculated using Equations (3.43), (3.44) and (3.45), respectively. The partial pressures of H_2S and H_2 are taken to be 0.1 and 5.0 MPa, which are typical conditions for hydrotreating. The results are plotted in Figure 4.8 as a function of hydrotreating temperature. A negative ΔG value on the plot indicates that the structure with the sulfur or sulfur species on the surface is more favorable than the pristine Ni_2P surface (Ni_3P_2 surface) with the H_2S molecules in the gas phase. The relative stability at low temperature range increases in the following order:

Free H_2S (gas) + Ni_2P clean surface (Ni_3P_2) < adsorbed molecular H_2S on Ni_2P surface < adsorbed –SH+1/2 free H_2 (gas) < adsorbed S atom+ free H_2 (gas).

However, at a high temperature range, the molecularly adsorbed H_2S becomes less stable than the gas-phase H_2S and desorbs from the surface, but the dissociated sulfur species (–SH, and adsorbed sulfur atoms) are stable on the surface up to approximately 1000 K at these hydrotreating pressures of H_2 and H_2S.

Stable Modes of Adsorption	Top View	Side View	Adsorption Energy (eV/H_2S)
-SH adsorbed at the TFH site, forming bonds with the nickel atoms.	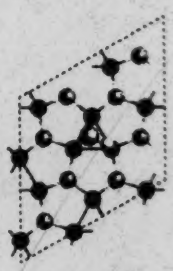		-1.40
-SH adsorbed at the bridging position between a nickel and a phosphorus atom.	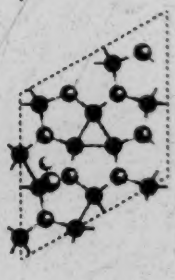	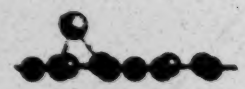	-0.41
-SH adsorbed at the bridging position between two nickel atoms in the TFH.	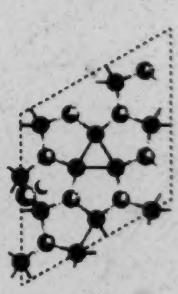		-1.27

Figure 4.6 The stable modes of dissociative adsorption of H_2S on the Ni_3P_2 surface as adsorbed –SH species. Cyan, purple, yellow and white represents nickel, phosphorus, sulfur and hydrogen atoms respectively.

Stable Modes of Adsorption	Top View	Side View	Adsorption Energy (eV/H_2S)
Adsorption of a single sulfur atom within a TFH site.	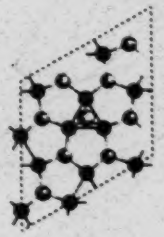		-1.64
Blockage of 50% of the total TFH sites by sulfur adatoms.	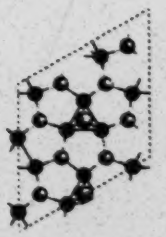		-1.64
Blockage of 75% of the total TFH sites by sulfur adatoms.	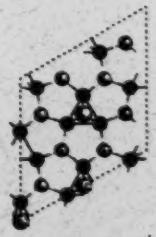	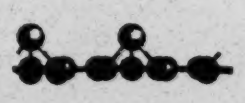	-1.63
All the TFH sites are blocked by atomic sulfur.	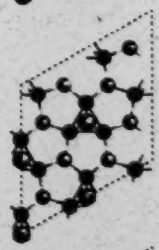		-1.58
Adsorption of additional sulfur atom at the bridging position between a nickel and a phosphorus atom.	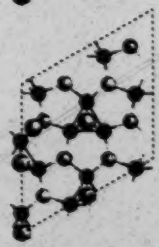	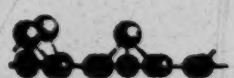	-1.21

Figure 4.7 Dissociative adsorption of H_2S as sulfur atom on the Ni_3P_2 surface. Cyan, purple, and yellow represent nickel, phosphorus and sulfur atoms respectively.

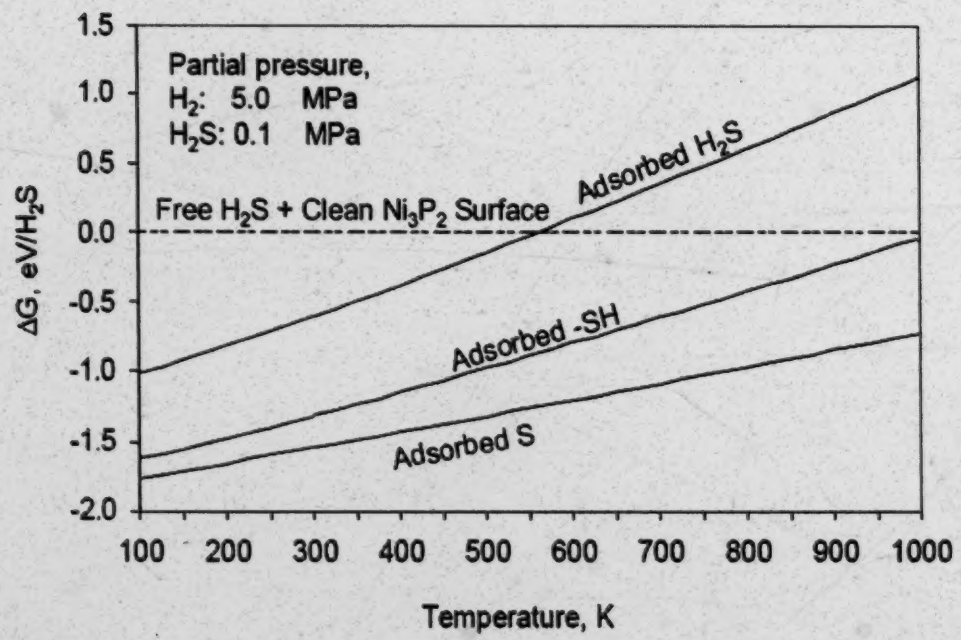

Figure 4.8 Free energy change for molecular and dissociative adsorption of H_2S on the Ni_3P_2 (001) surface, as a function of temperature at 5.0 MPa hydrogen and 0.1 MPa H_2S pressure. The pristine Ni_3P_2 surface, and gas-phase H_2S and H_2 are taken as the energetic references.

4.4.2 Replacement of Phosphorus Atoms from the Surface

An alternative way of incorporating of sulfur atoms on the Ni_3P_2 surface is by the reaction of the surface phosphorus atoms with the gas phase hydrogen present in the hydrotreating environment. The proposed process consists of multiple steps. In the first step, this reaction produces PH_3 creating a defect site on the Ni_3P_2 surface. Oyama et al.[34] detected the production of PH_3 in the gas phase during the temperature-programmed reduction (TPR) of the catalyst precursor, which is direct experimental evidence for this possibility. Next, the H_2S molecule undergoes a dissociation to adsorb as –SH on the defect site and a hydrogen atom. In the last step, the hydrogen desorbs from the surface to the gas phase. Therefore, the whole process results into the replacement of a single phosphorus atom from the surface by a sulfur atom from the gas phase H_2S. The steps are presented in Figure 4.9, and the associated energy changes are calculated using equation (3.46):

ΔE (Creation of the defect site) = +1.97 eV

ΔE (Dissociative adsorption of H_2S as –SH and hydrogen atom) = −2.43 eV

ΔE (Desorption of the hydrogen atoms as hydrogen gas) = +0.16 eV

ΔE (Overall) = −0.29 eV/H_2S molecule

The possibility of the replacement of more than one phosphorus atom was also taken into consideration. As shown in Figure 4.10, there are eight phosphorus atoms on the Ni_3P_2 surface of the 2x2x2 supercell used in this study. Phosphorus atoms located at the neighboring positions, such as positions 1 and 2, are bonded to the same nickel atom in the sublayer. On the other hand, phosphorus atoms at the distant positions, such as positions 1 and 7, are not bonded to the same nickel atom. After replacement of a single phosphorus atom from the surface, subsequent replacements had been tried at different positions and in various combinations. For example, for the replacement of two phosphorus atoms, the second replacement was tried at the positions of 2, 3, 4, 5, 6, 7 and 8, after the first replacement had been done at the position 1. It was found that the second replacement at any neighboring position to the first replacement position produces an energy change of -0.07 eV approximately. On the other hand, replacements at the distant

positions produced a subsequent energy change of -0.31 eV. Replacements were performed at three or more positions also, and each of the several possible combinations had been tried. The energy changes associated to all the possible replacement combinations are presented in Appendix C, and the energy changes for the most stable configurations for different number of replacements are presented in Table 4.2. It is apparent from the calculations that the substitutions take place preferentially at the distant atomic positions as long as they are available. After substitution had been done at all the four distant phosphorus positions present on the Ni_3P_2 surface (Figure 4.11), the overall energy change of the system is found to be -1.29 eV, which gives an approximate energy change of 0.32 eV per sulfur atom. However, a subsequent substitution at a neighboring position produces a positive energy change of +0.19 eV (Figure 4.13). Further substitutions also continued producing positive energy changes, and the overall energy change for complete substitution of all the eight phosphorus atoms was found to be -0.52 eV, which is approximately -0.06 eV per sulfur atom. Therefore, it is apparent from the calculations that the 50% phosphorus replaced Ni_3P_2 surface is thermodynamically the most stable configuration for the partial replacement scheme. Based on the stoichiometric composition, the surface is denoted as the Ni_3PS surface hereafter.

Having the most stable replaced configuration for the surface, phosphorous substitution was studied in the bulk phase (Figure 4.14). The energy change for this process was found to be +1.29 eV, indicating it thermodynamically unfavorable. This is concordant to the studies and findings of Oyama et al.[19], which involved XRD analysis of the spent samples of Ni_2P. By comparing the diffraction patterns of the spent and fresh samples (Figure 2.4), it was concluded in the study that the composition of Ni_2P remains unchanged in the bulk phase.

The relative stability of the Ni_3PS and the pristine Ni_2P surface is dependent on the reaction conditions and is calculated in terms of free energy change. The results are presented in Figure 4.12. Again, a typical hydrotreating condition, with hydrogen and H_2S partial pressures of 5.0 and 0.1 MPa respectively had been selected. The free energy change was calculated using Equation (3.48), and is shown in Figure 4.12. A negative free energy change indicates the favorability of the partial replacement over the pristine Ni_3P_2 surface. The results show that the partially sulfided surface is the more stable

configuration at low to moderate concentration of PH_3 in the gas phase, up to a very high temperature range. The formation of such a surface is also consistent with the findings of Koryani[35], who deduced the presence of a "PS" compound similar to Ph_3PS previously observed in the XPS spectra of $NiPS_3$.

4.4.3 Complete Sulfidation

The possibility of complete sulfidation of the bulk Ni_2P to bulk Ni_3S_2 at relevant conditions was also studied. The relative stability of the Ni_3S_2 structure had been calculated as a function of temperature, using Equations (3.47) and (3.49), and was illustrated in Figure 4.15. A negative free energy change in this case indicates that the formation of Ni_3S_2 crystal is more favorable as compared to the Ni_2P bulk phase. It is apparent from the results that the bulk Ni_2P phase is more stable at almost all temperature ranges at the chosen typical hydrotreating conditions, proving the complete sulfidation process unfavorable.

4.4.4 Summary of the Studies on Sulfur Incorporation in Ni_2P

Based on the results presented in Section 4.4.1, H_2S adsorbed on top of a nickel atom with the two hydrogen atoms pointing towards the other two nickel atoms, the –SH species adsorbed in the TFH, and the sulfur atoms adsorbed in the TFH are the three stable modes for molecular or dissociative adsorption of H_2S on Ni_3P_2 surface. At a high temperature range and the chosen hydrotreating conditions, the molecularly adsorbed H_2S becomes less stable than the gas-phase H_2S and desorbs from the surface. The atomic sulfur and the –SH species both adsorb within the TFH, and are stable up to high temperature ranges. However, as far as competitive adsorption is concerned, on the basis of the free energy calculations presented in Figure 4.8, the first of these two modes possesses a higher probability to be present on the Ni_2P surface at hydrotreating conditions. On the basis of Figure 4.15 presented in Section 4.4.3, complete sulfidation of Ni_2P to bulk Ni_3S_2 is thermodynamically unfavorable at the chosen hydrotreating conditions. Partial replacement of the surface phosphorus atoms by sulfur atoms from the

gas phase H_2S is stable up to a high temperature range, as shown in Figure 4.12, until 50% of the surface phosphorus atoms are replaced. Therefore, based on the results presented within Sections 4.4.1-4.4.3, all the possible modes for incorporation of sulfur in the Ni_2P structure can be narrowed down into two choices; (1) the adsorption of sulfur atoms at the TFH sites and evolution of gas phase hydrogen, and (2) the formation of a Ni_3PS surface by 50% partial replacement of surface phosphorus and evolution of PH_3 gas.

Several researchers[16,19,20,34] suggested the formation of a phosphosulfide overlayer of an unknown composition on Ni_2P at hydrotreating conditions, which supports the partial replacement model. However, the results presented in this study also prove that the possibility of presence of atomic sulfur on the surface is strong. Theoretical calculations by Liu et al, which revealed that the adsorption of sulfur atoms at the TFH sites on the Ni_3P_2 surface is energetically favorable, also supports this conclusion.[70] In order to determine which of these modes is present on the Ni_2P surface, both of the modes need to be validated on the basis of experimental evidences. Sun et al.[20] and Layman and Bussell[21] have conducted IR studies on DBT, and thiophene HDS, respectively, on silica supported reduced and sulfided Ni_2P catalysts, using CO as the probe molecule. Apart from the IR vibrational frequencies, Layman and Bussell also presented the adsorption enthalpies of CO on the reduced and sulfided Ni_2P surfaces. In the following sections, results of the theoretical studies on CO adsorption on the pristine and the two sulfided models of Ni_2P are presented and discussed in order to validate the two models under consideration with these experimental results.

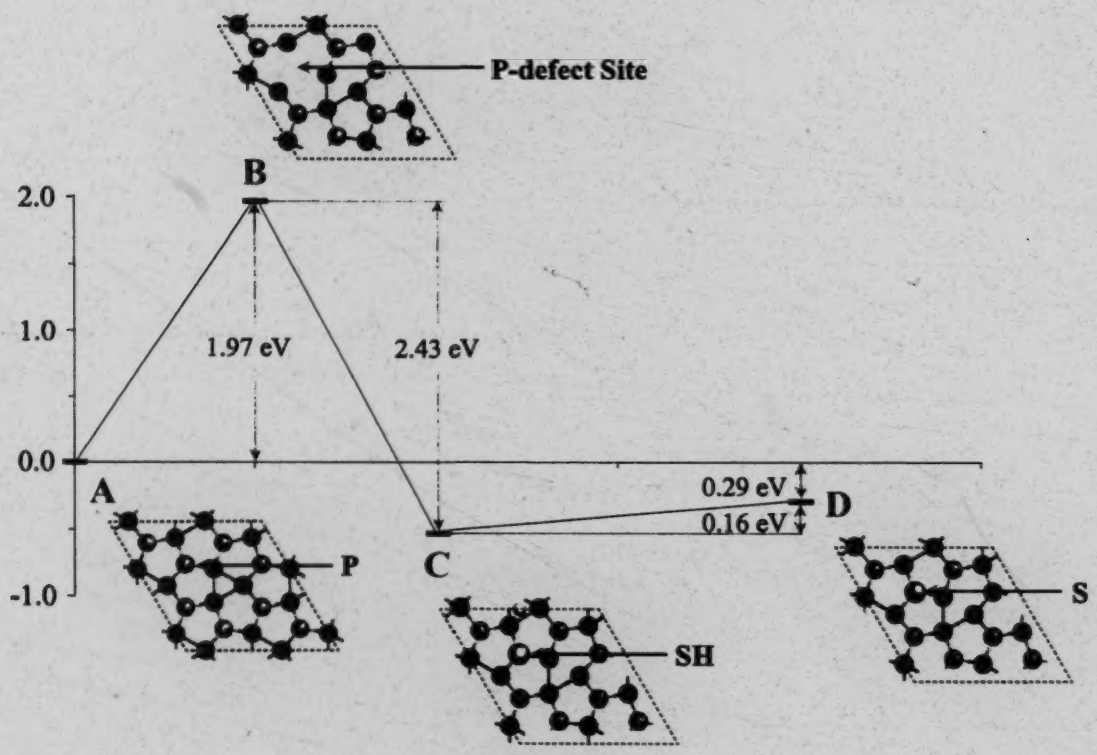

Figure 4.9 Energy changes related to the steps for replacement of phosphorus on the Ni_3P_2 surface by sulfur atoms from the gas phase H_2S.

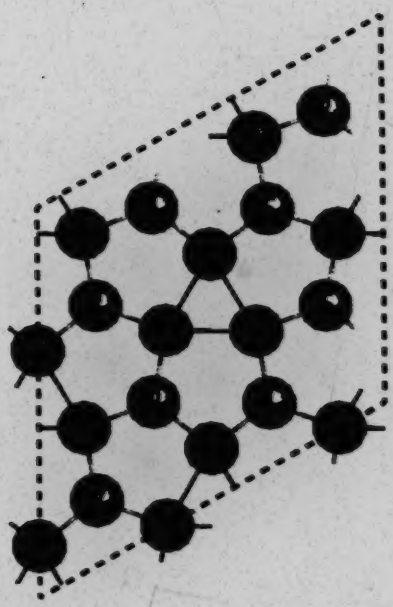

Figure 4.10 The Ni_3P_2 surface of the 2x2x2 Ni_2P supercell. The Phosphorus atoms are purple and numbered.

Table 4.2 Energy changes for the most stable configurations for the replacement of different number of phosphorus atoms from the surface.

Number of Phosphorus Atoms Replaced	Most Stable Configuration for Replacement	Total Energy (eV) of the Replaced Structure	Energy Change per Replacement (eV/S)
1	1 or equivalent	-295.12	-0.29
2	1,7 or eq.	-295.29	-0.30
3	1,5,7 or eq.	-295.50	-0.32
4	1,7,3,5 or eq.	-295.72	-0.32
5	1,2,3,5,6 or eq.	-295.40	-0.22
6	1,3,4,5,6,7 or eq.	-295.06	-0.15
7	1,2,3,4,5,6,7 or eq.	-294.67	-0.09
8	1,2,3,4,5,6,7,8	-294.96	-0.06

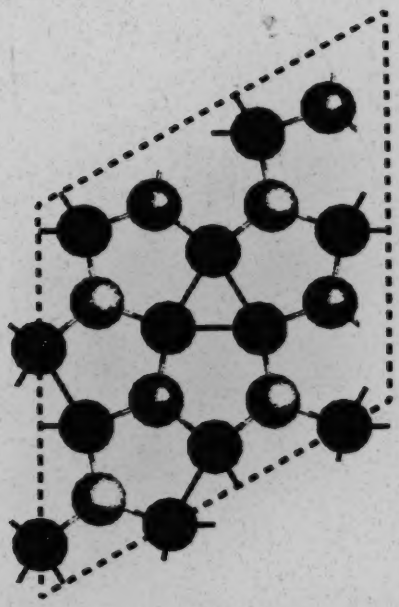

Figure 4.11 The 50% phosphorus replaced Ni_3P_2 surface (Ni_3PS). Replacements took place at all the available distant positions. Cyan, purple and yellow represent nickel, phosphorus and sulfur atoms respectively.

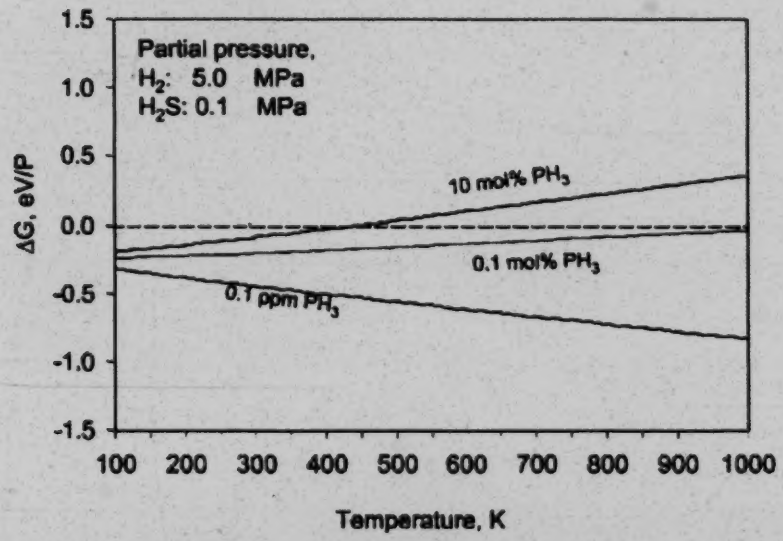

Figure 4.12 Free energy change of 50% phosphorus replaced Ni_2P (001) surface (Ni_3PS) as a function of temperature at 5.0 MPa hydrogen and 0.1 MPa H_2S. The pristine Ni_3P_2 surface, and gas phase H_2S and H_2 are taken as the energetic references.

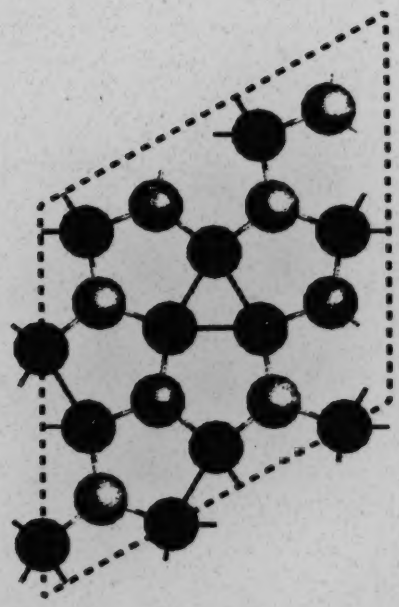

Figure 4.13 The 62.5% phosphorus replaced Ni_3P_2 surface, resulting from the replacement at a neighboring position, after replacing the phosphorus atoms from all the available distant positions on the supercell surface. Cyan, purple and yellow represent nickel, phosphorus and sulfur atoms respectively.

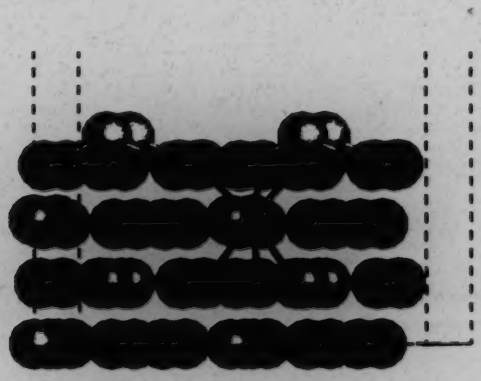

Figure 4.14 Replacement of a phosphorus atom from the bulk with a sulfur atom, after all the distant phosphorus atoms are replaced from the surface. Cyan, purple and yellow represent nickel, phosphorus and sulfur atoms respectively.

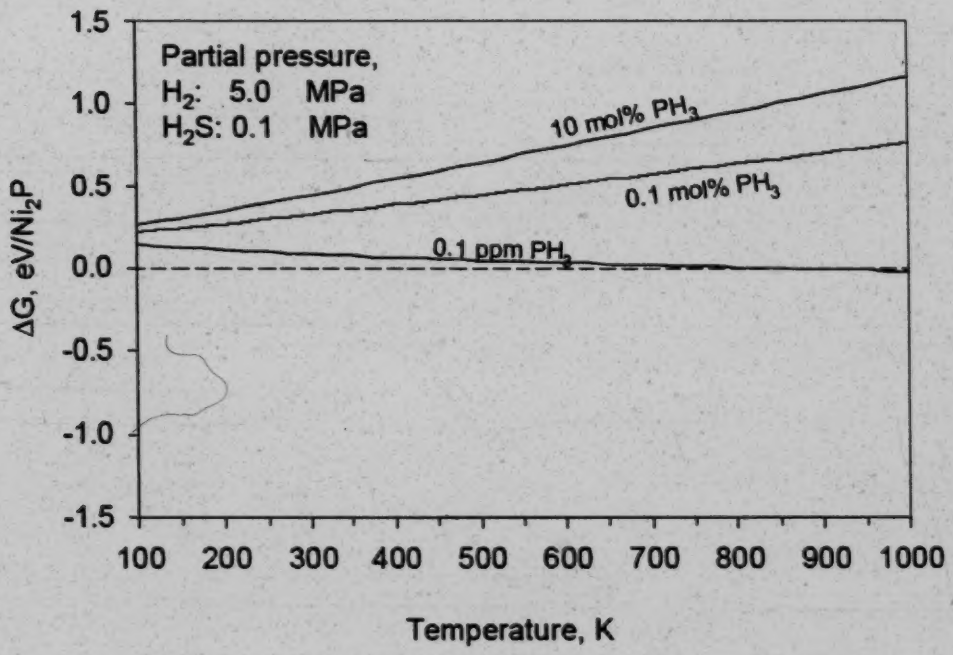

Figure 4.15 Free energy change for complete sulfidation of Ni_2P to Ni_3S_2, as a function of temperature at 5.0 MPa H_2 and 0.1 MPa H_2S, and with different PH_3 concentrations in the gas phase.

4.5 CO Adsorption

Since all of the three structures to consider for the CO adsorption studies, i.e., the pristine Ni_2P model, 50% surface phosphorus replaced model, and the sulfur adsorbed Ni_2P model, are symmetric in geometry each of them can be divided into four equal unit cell quarters. Conversely, the unit cells can be constructed for each of these models, as shown in Figure 4.16, each of which represents a quarter of the respective original supercell geometries. For a partially sulfided surface, the unit cell consists of one of the four replaced sulfur atoms present in the supercell, as shown in Figure 4.16 (b). Repeating the unit cell two times along the two directions of the surface would reproduce the same supercell geometry. Similarly, for the model with the atomic sulfur adsorbed at the TFH site, as shown in Figure 4.16 (c), a 2x2x1 repetition of the unit cell would reproduce the supercell with four sulfur atoms adsorbed at the TFH sites, which has the most stable configuration for that particular adsorption scheme. These geometries were used consistently throughout the CO adsorption studies to reduce the computational time while maintaining the same level of accuracy for the calculations.

4.5.1 Modes of CO Adsorption

All of the possible initial modes of CO adsorption had been attempted on the pristine, partially replaced, and atomic sulfur adsorbed Ni_2P surfaces. The surface coverages of the CO molecules had been defined based on the number of nickel atoms on the unit cells. Monolayer adsorption had been defined as the adsorption of one CO molecule per nickel site. Since a total of three nickel atoms are present in the only three-fold hollow on a unit cell surface, the adsorption of one, two, three, and four CO molecules can be defined as 0.33, 0.67, 1.00 and 1.33 ML of surface coverage, respectively. The calculated data for all the stable configurations of CO adsorption on the pristine and partially replaced surfaces for different surface coverages is provided in Appendix D. Only the most preferable modes of adsorption corresponding to different surface coverages are presented in Figure 4.17. It was found that the most stable modes are the same for the pristine and the partially replaced surface. At the low coverage of

0.33 ML, the CO molecule prefers to occupy in the TFH site. For a surface coverage of 0.67 ML, the preferred configuration is one CO molecule terminally bonded to a nickel site and another at the bridging position between two nickel atoms. At 1 ML coverage, three CO molecules are adsorbed, each terminally bonded to a nickel site in the TFH. However, for a surface coverage of 1.33 ML, a CO molecule occupies the TFH site in addition to the three terminally bonded molecules.

The configurations for CO adsorption on the surface with deposited sulfur atoms are shown in Figure 4.18. When the CO molecule was initially positioned to be linearly bonded to the nickel site, it formed bonds with both nickel and sulfur atoms during geometry optimization. However, no additional bonding was formed when the molecule had been placed at the bridging position between a nickel and a phosphorus site, or on top of a phosphorus atom.

4.5.2 Adsorption Energy

Although the stable configurations for the adsorption of CO molecules on the Ni_3P_2 and Ni_3PS surfaces are the same, the adsorption strength on the replaced surface was always lower than that on the pristine surface, corresponding to the same surface coverage. The adsorption energies of the most stable configurations on the pristine Ni_2P (001) surface (Ni_3P_2) and the 50% phosphorus replaced surface (Ni_3PS) are presented in Table 4.3. Adsorption energies for all the configurations are presented in Appendix D.

On the other hand, CO adsorption on the surface with adsorbed sulfur is not energetically favorable. The adsorption energies calculated for a CO terminally bonded on top of a nickel site, in the bridging position between a nickel and a phosphorus atom, and terminally bonded on top of a phosphorus atom are -0.05 eV, 0.00 eV, and +0.60 eV respectively. These results indicate that CO molecules are unable to adsorb on the Ni_2P surface spontaneously once the nickel sites are blocked by the sulfur atoms.

4.5.3 Vibrational Frequency Analysis

Since the model with adsorbed sulfur atoms cannot adsorb CO molecules spontaneously, the vibrational frequencies were calculated for adsorption on the pristine and partially replaced models only. The modes of vibration corresponding to different frequencies had also been identified, and the results are summarized in Table 4.4. The stable modes of adsorption corresponding to different surface coverages are presented in Figure 4.17. For 0.33 ML coverage, only one CO molecule is adsorbed on the TFH site. The frequency for the stretching of the C–O bond is 1858 cm^{-1} on the Ni_3P_2 surface, and 1821 cm^{-1} on the Ni_3PS surface. For 0.67 ML coverage, there are two adsorbed CO molecules; one at a Ni–Ni bridge site, and the other linearly on a single nickel site. The frequencies of 2088 cm^{-1} on the Ni_3P_2 surface, and 2066 cm^{-1} on the Ni_3PS surface, are due to the stretching vibration of the terminally bonded CO. The lower frequencies of 1875 and 1869 cm^{-1} for the Ni_3P_2 and the Ni_3PS surfaces respectively, are for the stretching of the bridged CO molecule. For the 1 ML coverage, each CO molecule is terminally bonded to one nickel site on both Ni_3P_2 and Ni_3PS surfaces. The frequencies of 2088 and 2084 cm^{-1} on the Ni_3P_2 and Ni_3PS surfaces respectively are attributed to the symmetric stretching of the molecules. On the other hand, asymmetric stretching results in lower frequencies of 2000 and 1980 cm^{-1} on the Ni_3P_2 surface, and 1995 and 1965 cm^{-1} on the Ni_3PS surface. For 1.33 ML CO coverage, one CO molecule occupies the TFH site and the other three CO molecules are terminally bonded to the nickel sites on both the Ni_3P_2 and Ni_3PS surfaces. In this case, the symmetric stretching of the three terminally bonded CO molecules produces frequencies of 2088 and 2090 cm^{-1} on the Ni_3P_2 and Ni_3PS surfaces, respectively, while the asymmetric stretching of the terminally bonded CO molecules results in the frequencies of 2026 and 1994 cm^{-1} on the Ni_3P_2 surface and 2030 and 2008 cm^{-1} on the Ni_3PS surface. CO at the TFH site has a vibrational frequency of 1690 cm^{-1} on the Ni_3P_2 surface, and 1692 cm^{-1} on the Ni_3PS surface. There is a large decrease in the frequency of the CO molecule at the TFH site, from 0.33 to 1.33 ML coverage, for both Ni_3P_2 and Ni_3PS surfaces. Moreover, an increase of 2-14 cm^{-1} is generally observed for terminally bonded CO at 1.33 ML coverage, from the pristine to the sulfided surface.

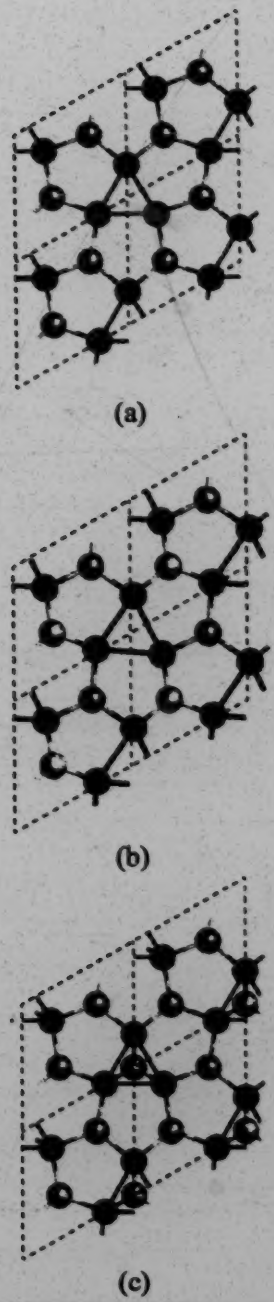

Figure 4.16 Top view of the surfaces of the unit cell models replicating the original supercell geometries, constructed for the CO adsorption studies: (a) pristine Ni_2P surface; (b) partially phosphorus replaced Ni_2P surface; and (c) Ni_2P surface with adsorbed atomic sulfur. Cyan, purple and yellow represent nickel, phosphorus and sulfur atoms respectively.

Surface Coverage	Top View	Side View
0.33 ML, with one CO within the TFH.	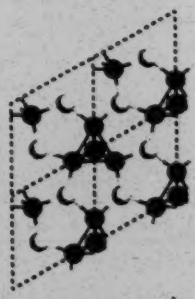	
0.67 ML, with one CO terminally bonded to a nickel site, and another bonded at the bridging position between two nickel sites in the TFH.	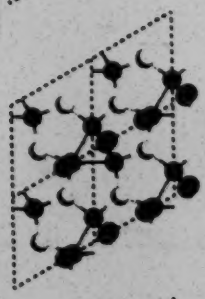	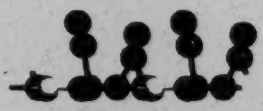
1 ML, with three CO bonded terminally to a nickel site each.	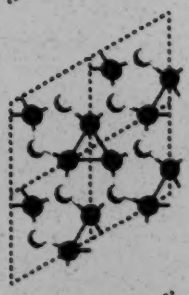	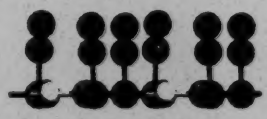
1.33 ML, with one CO within the TFH in addition to three CO, each bonded terminally to a nickel site.	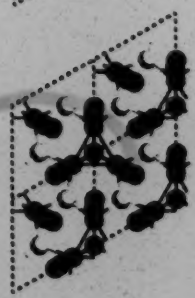	

Figure 4.17 Preferred configurations for adsorption of CO on the pristine Ni_3P_2 or partially sulfided Ni_3PS surfaces, corresponding to different surface coverages. Carbon, oxygen and nickel atoms are in gray, red and cyan respectively. White indicates phosphorus or sulfur atoms.

Optimized Mode	Top View	Side View	Adsorption Strength
CO bonded on top of a nickel site.	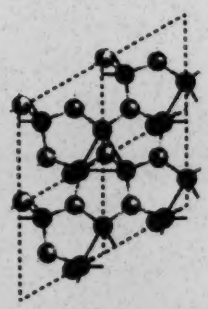		-0.05 eV
CO bonded at the bridging position between a nickel and a phosphorus atom.	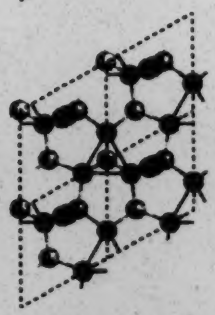		0.00 eV
CO bonded on top of a phosphorus site.	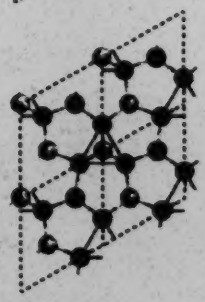		+0.60 eV

Figure 4.18 Configurations of CO adsorption on the Ni_3P_2 surface with adsorbed solid sulfur. Gray, red, cyan, purple and yellow represent carbon, oxygen, nickel, phosphorus and sulfur atoms, respectively.

Table 4.3 Adsorption energies of CO on the pristine Ni_3P_2, and the 50% phosphorus replaced Ni_3PS surfaces, corresponding to different surface coverages.

Coverage, ML	Adsorption energy, eV/CO	
	On Ni_3P_2	On Ni_3PS
0.33	-1.90	-1.78
0.67	-1.26	-1.07
1.00	-1.09	-0.95
1.33	-0.43	-0.36

Table 4.4 Calculated vibrational frequencies (cm^{-1}) of adsorbed CO molecule on the pristine Ni_3P_2 and the 50% phosphorus-replaced Ni_3PS surfaces, corresponding to different surface coverages.

Coverage, ML	Vibration frequency, (cm^{-1})			
	CO Molecule	Mode of Vibration	On Ni_3P_2	On Ni_3PS
0.33	In the TFH site	C-O stretching	1858	1821
0.67	On top of nickel site	C-O stretching	2088	2066
	Between nickel atoms	C-O stretching	1875	1869
1.00	On top of nickel sites	C-O symmetric stretching	2088	2084
		C-O asymmetric stretching	2000	1995
		C-O asymmetric stretching	1980	1965
1.33	On top of nickel sites	C-O symmetric stretching	2088	2090
		C-O asymmetric stretching	2026	2030
		C-O asymmetric stretching	1994	2008
	In the TFH site	C-O symmetric stretching	1690	1692

4.6 Hydrogen Adsorption

Studies were conducted on hydrogen adsorption on both the pristine and partially replaced unit cell surfaces. This involved determination of the stable configurations of molecular and atomic hydrogen adsorption on the surfaces, calculation of adsorption energies, and transition state search. To assure higher accuracy for transition state searches, medium quality parameters had been used consistently for all calculations involving hydrogen adsorption. The k-points associated to the medium quality calculations on the unit cell geometries are 4x4x1.

4.6.1 Modes of Adsorption

A hydrogen molecule, irrespective of the initial positioning, always dissociates when placed on the pristine Ni_3P_2 surface of the Ni_2P structure, if adsorbed. When molecular hydrogen was initially placed linearly bonding to a nickel, phosphorus or TFH site on the pristine Ni_2P, it did not adsorb on the surface during geometry optimization. The molecule dissociated into two hydrogen atoms and bonded separately to the same nickel atom if placed at the bridging position between a nickel and a phosphorus site. When placed at the bridging position between the two nickel atoms, it dissociated into two hydrogen atoms that adsorbed at two different Ni-Ni bridges within a single TFH on the pristine Ni_3P_2 surface, as shown in Figure 4.19. This is the most stable configuration for adsorption of hydrogen on the pristine Ni_3P_2 surface. Various initial positioning had been tried for the adsorption of atomic hydrogen on the pristine Ni_3P_2 surface. The most stable configuration was found to be the bridging position between the nickel sites, the same configuration for the molecular adsorption of hydrogen on the surface. Calculated data related to all the stable forms of hydrogen adsorption on the clean Ni_2P surface are presented in Table E.1 in Appendix E.

Hydrogen adsorption on the partially replaced surface is different from the adsorption on the pristine surface, and is more location sensitive. Hydrogen adsorbs molecularly on the surface if it is bonded linearly on a sulfur site, or vertically or horizontally along the plane on top of the TFH site. The horizontal position at the TFH

site is the most stable position for molecular adsorption of hydrogen on the Ni_3PS surface, and is shown in Figure 4.20 (a). When the hydrogen molecules had been initially bonded to a nickel or phosphorus site linearly, or placed at the bridging position between a nickel and a phosphorus atom, or a nickel and a sulfur atom, it didn't adsorb. However, if placed in the vicinity of any of the Ni-Ni bridges on the TFH, it dissociates into two atoms, each at a different bridging positions between two nickel sites. This is also the most stable configuration for adsorption of hydrogen as hydrogen atoms on the Ni_3PS surface, and is shown in Figure 4.20 (b). Calculated data for adsorption of molecular hydrogen and hydrogen atoms on the Ni_3PS surface are presented in Table E.2 and Table E.3 respectively, in Appendix E.

4.6.2 Adsorption Energy

The hydrogen molecules adsorb and always dissociate at the Ni_3P_2 surface, without requiring any external energy, i.e., the energy change calculated using Equation (3.51) is zero. After the dissociation process, the hydrogen atoms are adsorbed at the bridging positions between the nickel sites. The heat of adsorption is calculated using equation (3.50), approximately -0.62 eV per hydrogen molecule.

If the hydrogen molecule is not at the bridging position between two nickel atoms, the dissociation process on the Ni_3PS surface is activated. The adsorption energy for the most stable adsorption mode of the hydrogen molecule, which is on top of the TFH site as shown in Figure 4.20 (a), is -0.49 eV/H_2, calculated using Equation (3.50). The most stable configuration for the adsorption of hydrogen as atoms involves two hydrogen atoms sitting at two different Ni-Ni bridge sites, as shown in Figure 4.20 (b). Using the energy of the most stable configurations for the adsorptions of molecular and atomic hydrogen from Appendix E in Equation (3.51), the energy change for the dissociation process of the molecule is calculated as -0.02 eV/H_2. However, if the molecule is placed at the bridging position between two nickel atoms, it dissociates directly into hydrogen atoms, and adsorbs at the bridging positions, same as the configuration shown in Figure 4.20 (b). The dissociation is non-activated with zero energy change and the heat of adsorption in this case is -0.51 eV/H_2.

4.6.3 Transition State Search

From the results presented within Sections 4.6.1-4.6.2, it is clear that the dissociation process of a hydrogen molecule on the pristine Ni_2P surface is a non-activated process regardless of the mode of adsorption, and hence does not have any transient state. The dissociation process on the phosphorus-replaced Ni_2P surface is also non-activated if the hydrogen molecule is at the bridging position between the nickel sites. The transition state for the dissociation process is supposed to be of a form in between the stable modes of adsorption of hydrogen as a molecule and as atoms. They are considered as the reactant and the product of the dissociation reaction. These two modes are shown in Figure 4.20 (a) and (b), respectively. The Transition State Searching (TSS) via Synchronous Transit (ST) methods is more convenient if the initial and the final geometries of the reaction are known.[38] Therefore, this method is followed for the current study using the geometry optimized structures shown in Figure 4.20 (a) and (b) as the inputs for the reactant and the product, respectively. However, during the course of the search, the DMol^3 DFT quantum mechanical model engine failed to find the transition state within the reaction boundary. Such failure may result if the initial geometry is not adequately close to the structure of the transient state.[38] Since the transient state should posses a form somewhere in between the reactant and the product, other forms of the initial reactant geometry had been constructed for geometry optimization, as shown in Figure 4.21. The other stable mode of molecularly adsorbed hydrogen, which is the vertically bonded position on the TFH site, had also been used as the reactant for the TSS. However, in every attempt, the initial geometry either failed to achieve a stable form, or dissociated directly into the stable product structure after geometry optimization. Since this method of TSS must have unique optimized structures for both the reactant and the product geometries, the transient state for the hydrogen dissociation reaction could not be detected using these configurations.

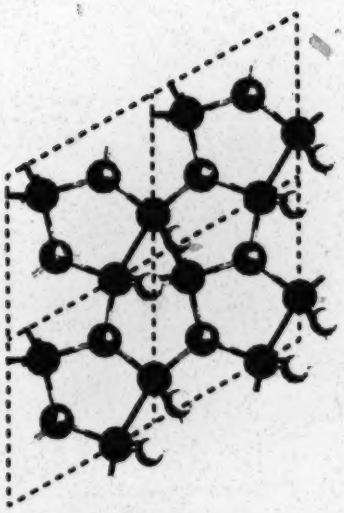

Figure 4.19 The most stable configuration for adsorption of hydrogen on the pristine Ni_3P_2 surface. Cyan, purple and white represent nickel, phosphorus and hydrogen atoms respectively.

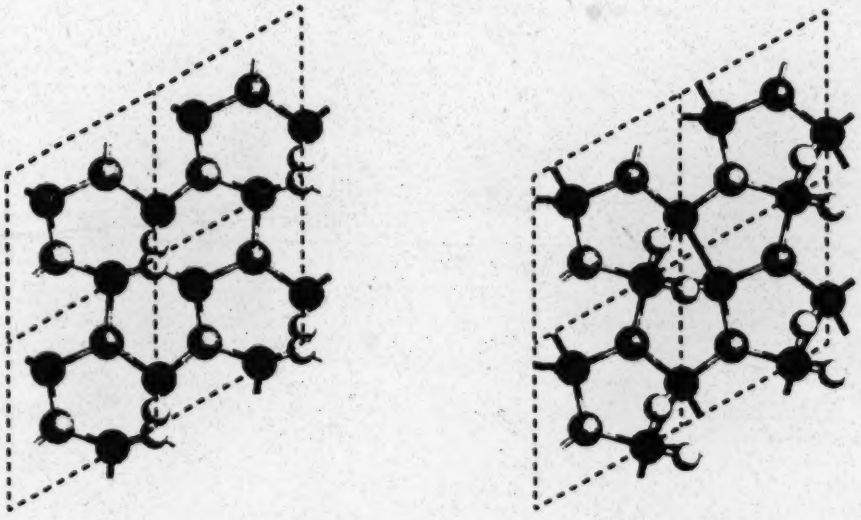

(a) (b)

Figure 4.20 The most stable configuration for adsorption of: (a) hydrogen molecule; (b) hydrogen atoms on the Ni_3PS surface. Cyan, purple, yellow and white represent nickel, phosphorus, sulfur, and hydrogen atoms respectively.

Top View of the Initial Reactant Geometry	Side View of the Initial Reactant Geometry	Result
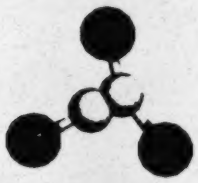		Failed to reach either an optimized reactant geometry, or a TS because of the initial geometry being too different from the TS
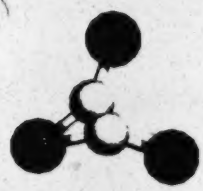		Directly dissociated into the product form after geometry optimization, initial geometry too close to the product form
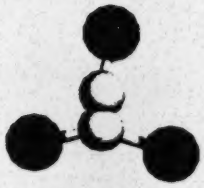		Directly dissociated into the product form after geometry optimization, initial geometry too close to the product form
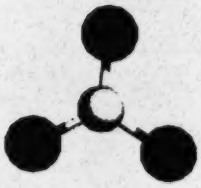		Failed to reach a TS, initial geometry too different from the TS

Figure 4.21 Input configurations for the reactant in the transient state search for the hydrogen dissociation reaction. Cyan and white represent nickel, and hydrogen atoms respectively.

4.7 Summary of the Results

The Ni_3P_2 termination is more stable than the Ni_3P termination on pristine Ni_2P. When H_2S is the sulfur-containing species, the two most favorable methods for incorporation of sulfur on this surface at typical hydrotreating conditions are dissociation of H_2S and adsorption of sulfur atoms at the TFH sites, and partial replacement of the surface phosphorus atoms by the sulfur atoms from gas phase H_2S. The structure with sulfur atoms adsorbed on the surface is stable up to high temperature range at the relevant hydrotreating conditions. The partially replaced model is favorable up to the replacement of 50% of the phosphorus atoms from the Ni_3P_2 surface. This model is stable at hydrotreating environment even at high temperature range, in presence of low to moderate PH_3 in the gas phase.

CO adsorption on the surface with adsorbed sulfur atoms is thermodynamically unfavorable. However, CO molecules adsorb favorably on the pristine and the 50% surface phosphorus replaced models. The adsorption strength of CO on the pristine Ni_3P_2 surface is always higher than that on the 50% phosphorus replaced Ni_3PS surface, corresponding to the same surface coverages on both the surfaces. There is a large decrease in the frequency values of the CO molecule at the TFH site, from 0.33 to 1.33 ML coverage, for both Ni_3P_2 and Ni_3PS surfaces. Moreover, particularly for terminally bonded CO molecules on the nickel sites for high coverage (1.33 ML), the wave numbers generally shift to a higher value of 2-14 cm^{-1} from the pristine to the sulfided surface.

The dissociation of molecular hydrogen on the pristine Ni_2P surface is non-activated and takes place spontaneously. The stable mode for adsorption of hydrogen on this surface is as hydrogen atoms at two different Ni-Ni bridging positions. The dissociation of molecular hydrogen on the Ni_3PS is location sensitive. If the molecule is placed at any position other than the vicinity of the bridge between two nickel sites, an activation energy remains for the process,. However, the exact form of the transition state could not be detected.

5 Discussion

5.1 Introduction

The following sections discuss the findings of this study sequentially on the basis of the results presented in Chapter 4, and the experimental and theoretical works found in the literature.

5.2 Structure and Surface of Pristine Ni_2P

As presented in Section 4.3, when exposed from the bulk phase geometry the Ni_3P_2 termination of the Ni_2P structure along the (001) plane undergoes an energy change that is -0.14 eV/Å^2 lower than that of the Ni_3P termination along the same plane. When the surface termination had been changed from Ni_3P to Ni_3P_2, the energy change associated was -0.026 eV/Å^2. Both the results indicate that the Ni_3P_2 is the more stable termination for Ni_2P structure. This is also consistent with the findings of the LEED and STM studies by Gomes et al., which revealed that the Ni_3P_2 surface was the exposed termination of Ni_2P in their study.[70] The subsequent DFT calculations by Liu et al. are also in agreement, whereby they found that the Ni_3P_2 terminated surface is more stable than the Ni_3P terminated surface by 2.75 eV/unit cell.[70] A very recently published STM study also confirms these results.[69] Based upon these experimental and theoretical evidences and our DFT calculation results, all the subsequent studies had been conducted on the Ni_3P_2 terminated structures.

5.3 Incorporation of Sulfur in Ni_2P Structure

As discussed in Section 4.4, the possible methods of incorporation of sulfur in the Ni_2P structure from the gas phase H_2S are by molecular or dissociative adsorption on the

surface, by partial replacement of the surface phosphorus atoms, or by complete sulfidation of the Ni_2P structure to bulk Ni_3S_2 structure.

5.3.1 Molecular and Dissociative Adsorption of H_2S

In accordance to the results presented in Section 4.4.1, it is clear that H_2S can adsorb stably on the Ni_3P_2 surface as a molecule, as -SH species or as a sulfur atom, according to the energetically favorable modes illustrated in Figure 4.5, Figure 4.6 and Figure 4.7, respectively. The related adsorption energies corresponding to these modes are -1.58, -0.70 and -1.40 eV/H_2S, respectively. The relative stabilities of the surfaces with these adsorbed species are presented in Figure 4.8 as a function of temperature, in terms of free energy change with respect to the pristine surface. Typical hydrotreating partial pressures of 5.0 MPa and 0.1 MPa had been chosen for H_2 and H_2S, respectively. A negative ΔG value on the plot indicates that the structure with the sulfur species on the surface is more favorable than the pristine Ni_2P surface plus the H_2S molecules in the gas phase. The relative stability over a low temperature range increases in the following order:

Free H_2S (gas) + Ni_2P clean surface (Ni_3P_2) < adsorbed molecular H_2S on Ni_2P surface < adsorbed –SH+1/2 free H_2 (gas) < adsorbed S atom+ free H_2 (gas).

At high temperatures, the molecularly adsorbed H_2S desorbs and prefers to be in the gas phase, but the dissociated –SH and sulfur atoms remain stable on the surface up to 1000 K. At a particular reaction condition, however, the population of these three species is dependent on the kinetics of dissociation of the H_2S molecule, and the hydrogenation of the adsorbed sulfur.

The adsorption of H_2S on the surface is a non-activated process and occurs spontaneously. The molecule is stable on the surface up to 550 K at 0.1 MPa H_2S and 5.0 MPa H_2 partial pressures, as shown in Figure 4.8. The stability changes with the temperature and partial pressure of H_2S in the gas phase. The highest temperature that the H_2S molecule can sustain as an adsorbed species on the surface increases or decreases

with the increasing or decreasing partial pressure of H_2S, respectively. Usually, a 10-fold increase in the partial pressure increases the highest temperature by 50°C.

The –SH species, or the sulfur atoms adsorb on the surface stably, but they only form if the activation energy required to dissociating the adsorbed H_2S molecule on the surface into one of these species is supplied. Once formed and adsorbed on the surface, both the species are stable until 1000 K at the chosen hydrotreating conditions, as shown in Figure 4.8. The atomic sulfur can, however, sustain a much higher temperature and still remain stably adsorbed on the surface. The stability of these species, similar to H_2S, is a function of the partial pressure of H_2S in the gas phase. Decreasing this pressure from 0.1 MPa to 0.1 ppm reduces the highest temperature for stable –SH and atomic sulfur on the surface to 650 and 850 K, respectively. On the basis of the free energy calculations presented in Figure 4.8, the surface with adsorbed atomic sulfur possesses the higher stability to be present on the Ni_2P surface at the hydrotreating environment compared to the –SH species.

The presence of different sulfur species adsorbed on the surface was also observed by other researchers[70]. Liu et al. have detected the presence of these species, and found that they desorb at different temperature ranges. Based on the XPS spectra taken after dosing H_2S on a Ni_2P surface, Liu et al. found that a strongly bound sulfur species bonds to the surface at low and high surface coverages, while a weakly bound sulfur species is found only at high surface coverages.[70] The weakly adsorbed species was found to desorb between the temperature ranges 400-450 K at Ultra High Vacuum (UHV), while the other stable species desorbed at temperatures beyond 700 K. They concluded that these are sulfur atoms adsorbed on the surface in different modes. One of the modes bonds strongly at the TFH site and desorbs at high temperature, while the other bonds weakly at the bridge site between a nickel and a phosphorus atom and desorbs at a lower temperature range. They also supported their conclusions by DFT calculations, which found the same two stable modes for adsorption of atomic sulfur on the surface. However, although these two modes are independently stable, the adsorption of sulfur at the Ni-P bridge sites after all the TFH sites are occupied was found to be exothermic, which is in well agreement with our results. This study did not cover the possibility of adsorption of molecular or dissociated species of H_2S.

In light of the experimental results discussed above, and the theoretical calculations presented in this study, it is evident that the sulfur at the Ni-P bridge is very unlikely to be present on the Ni_2P (001) surface at hydrotreating conditions. On the basis of the results presented in Section 4.4.1, the weakly bound sulfur species that desorbs at 400-450 K in the XPS experiments is most likely to be the molecular H_2S bonded linearly to nickel sites, and the strongly bound species that desorbs above 700 K in UHV atmosphere are the sulfur atoms adsorbed on the TFH sites. Considering that the theoretical calculations had been done for typical hydrotreating partial pressures of 5.0 MPa and 0.1 MPa for H_2 and H_2S, respectively, the experimental data reported by Liu et al.[70] agree very well with the results presented in Figure 4.8. However, the sulfur atoms adsorbed at the TFH sites is the more stable configuration than the molecularly adsorbed H_2S at hydrotreating conditions.

5.3.2 Replacement of phosphorus atoms from the surface

Gas phase hydrogen may react with the surface phosphorus atoms and remove them, creating defect sites which may eventually be filled by sulfur atoms from the gas phase H_2S, and making the overall process the replacement of surface phosphorus atoms by sulfur atoms. The details of the DFT calculations done on this proposed multiple-step scheme had been presented in Section 4.4.2, and the energy change associated to each of the steps had been presented in Figure 4.9.

The first step, the creation of a defect site by the reaction of the surface phosphorus with the gas phase hydrogen, creates gas phase PH_3 and has a positive energy change of +1.97 eV. However, the calculations show that the free energy change for this step is negative, approximately at 750 K and in presence of 100 kPa fresh hydrogen, and with a PH_3 partial pressure less than 10^{-7} Pa. Considering the usual methodologies of preparing Ni_2P catalysts by reducing the phosphate precursor in a hydrogen flow up to 850-923 K,[21,34] it is very much possible to supply this energy to generate some defect sites. Oyama et al.[34] detected the presence of gas phase PH_3 during the temperature-programmed reduction (TPR) of the catalyst precursor, which is also an evidence for this step in actual conditions.

The defect site is highly active as it is found to dissociate gas phase H_2S spontaneously during the course of geometry optimization with an energy of -2.43 eV. The dissociated hydrogen requires a small additional +0.16 eV to desorb from the surface to the gas phase. An overall energy change of -0.29 eV indicates the favorability of the process. This process continues to be thermodynamically favorable until all the distant phosphorus atoms, which are 50% of the surface phosphorus atoms, are replaced, as discussed in Section 4.4.2 and shown in Figure 4.11. Subsequent replacement at a neighboring position (Figure 4.13), or complete replacement of all the surface atoms are both unfavorable, with energy changes of +0.19 eV and -0.06 eV/atom respectively, in contrast to the -0.32 eV/atom for 50% surface phosphorus replacement. Any subsequent replacement in the bulk phase, as shown in Figure 4.14, is thermodynamically unfavorable, with an energy change of +1.29 eV per atom. This is also in agreement to the XRD studies conducted by Oyama et al.[19], which found experimental evidence of an unchanged Ni_2P bulk phase during hydrotreatment. Therefore, the 50% replaced surface can be considered as the most stable configuration for the replacement scheme.

The thermodynamic stability of the 50% phosphorus replaced Ni_3PS surface had been plotted in terms of free energy change in Figure 4.12. The relative stability of the Ni_3PS surface is dependent on the reaction conditions. At a very low concentration of PH_3 of less than 0.1 mol%, the partially sulfided replaced surface is always more stable than the pristine surface. If the PH_3 concentration is higher than 0.1 mol% but less than 10 mol%, the replaced surface is stable up to a high temperature range of 1000 K. Only at a very high concentration of PH_3, approximately about 10 mol%, and at a temperature higher than 450 K, the pristine surface becomes more stable than the replaced surface. Therefore, if no additional phosphorus is provided to the reactor, 50% of the phosphorus on the pristine surface is expected to be gradually replaced by sulfur to form the phosphosulfide overlayer. Previous studies by Koryani[35] found the presence of a "PS" compound similar to Ph_3PS previously observed in the XPS spectra of $NiPS_3$. The stoichiometry of the partially sulfided surface, determined in the current study, is also consistent to the findings of the experimental study.

5.3.3 Complete Sulfidation

As presented in Figure 4.15 in Section 4.4.3, as long as the PH_3 concentration in the hydrotreating environment is kept at a minimum of 0.1 ppm, the free energy change for the complete sulfidation process is positive at least until 825 K. This indicates that the complete sulfidation process of Ni_2P to convert to bulk Ni_3S_2 will not take place even at the presence of trace amount of PH_3. The excess phosphorus present in the fresh catalyst[34] or the phosphorus replaced from the surface can easily supply this trace amount of PH_3. This implies that the possibility of complete sulfidation of the Ni_2P catalyst at common hydrotreating environment is at a minimum.

On the basis of the discussions within Sections 5.3.2-5.3.3, in combination with the results presented in Figure 4.12 and Figure 4.15, it can be concluded that Ni_2P is stable against complete sulfidation, but the 50% partial replacement of surface phosphorus creating a partially sulfided Ni_3PS surface is favorable at hydrotreating conditions.

5.4 CO Adsorption

On the basis of the results presented in Section 4.4, and the discussions presented in Section 5.3, it can been concluded that the adsorption of sulfur atoms in the TFH sites and evolution of gas phase hydrogen, and the formation of Ni_3PS surface by 50% partial replacement of surface phosphorus and evolution of phosphine gas are thermodynamically the two most favorable processes for formation of sulfur species on the Ni_3P_2 surface. Several researchers[16,19,20,34] suggested the formation of a phosphosulfide overlayer of an unknown composition on Ni_2P at hydrotreating conditions, which supports the partial replacement model. XPS results and DFT calculations by Liu et al., however, strongly supports the possibility of the presence of atomic sulfur on the surface.[70] In order to determine which of these models is present as the Ni_2P surface in actual hydrotreating environment, they need to be validated against experimental data. Sun et al.[20] and Layman and Bussell[21] have conducted IR vibrational frequency calculations on silica supported reduced and sulfided Ni_2P catalysts using CO

as the probe molecule. Layman and Bussell also presented the adsorption enthalpies of CO on the reduced and sulfided Ni_2P surfaces. Therefore, the adsorption strengths and vibrational frequencies associated to CO adsorption on these two sulfur incorporation models were calculated using DFT for validation against the reported experimental data.

The results of CO adsorption on the stable models were presented in details within Sections 4.5.1-4.5.3. The most stable modes of adsorption for different CO coverages on the pristine and partially replaced surfaces are the same, as presented in Figure 4.17. It had been found that corresponding to 0.33, 0.67, 1.00 and 1.33 ML coverages, one, two, three, and four CO molecules adsorb respectively on the TFH site, at the Ni-Ni bridge and linearly to another nickel site, linearly to three nickel sites, and to a nickel site in addition to the three linearly bonded molecules. The initial modes attempted for adsorption of CO on the surface with sulfur atoms had been presented in Figure 4.18.

The adsorption energies and vibrational frequencies of the CO molecules on the pristine surface, partially replaced surface, and the surface with adsorbed sulfur atoms are discussed in details in the following sections.

5.4.1 Adsorption Energy

The adsorption energies corresponding to different coverages of CO on the pristine and replaced surfaces was summarized in Table 4.3. It is apparent from the results that the adsorption strengths of CO on the phosphorus replaced Ni_3PS surface are always weaker than those on the pristine Ni_3P_2 surface, corresponding to the same coverage. This reveals the general trend of the CO molecules to adsorb on the pristine surface more strongly than on the replaced surface.

The calculated results are compared to the experimental data found in the literature. Layman and Bussell had conducted some IR spectroscopic experiments on reduced and sulfided Ni_2P catalysts in UHV.[21] They reported that the adsorption enthalpies of CO on the reduced and sulfided Ni_2P are -31.4±1.5 $kJmol^{-1}$ (-0.33±0.02 eV) and -30.5±1.5 $kJmol^{-1}$ (-0.32±0.02 eV) respectively, which are very close to the values of -41.08 $kJmol^{-1}$ (-0.43 eV) and -34.95 $kJmol^{-1}$ (-0.35 eV) calculated in this study for 1.33 ML coverage. More importantly, the calculated adsorption strength on the replaced

surface had been found to be lower compared to that on the pristine surface, which is in excellent agreement with the general trend revealed in the experimental studies.

The adsorption strengths of CO molecules bonded both to a nickel and a sulfur atom, bonded linearly to a phosphorus atom, and bonded at the Ni-P bridge site on the surface with adsorbed sulfur atoms, as shown in Figure 4.18, are -0.05 eV, 0.00 eV, and +0.60 eV, respectively. Therefore, it is apparent that the adsorption of CO molecules on the surface with the adsorbed sulfur atoms is not favorable.

Based on all these calculated energetic data, combined with the experimental CO adsorption studies on the reduced and sulfided surfaces, the sulfur replacement model better describes the form of Ni_2P at hydrotreating conditions.

5.4.2 Vibrational Frequency

The calculated vibrational frequencies of CO molecules adsorbed on the pristine and replacement models, along with the corresponding modes of vibration, were presented in Table 4.4. The wave numbers varied by 2-37 cm^{-1} from the pristine to the replaced surface for the corresponding coverages. A large decrease in the vibrational frequency of the CO molecule at the TFH site had been observed for a change of coverage from 0.33 ML to 1.33 ML, for both Ni_3P_2 and Ni_3PS surfaces, and this is attributed to the interference arising from the presence of three linearly bonded neighboring CO molecules at 1.33 ML.

As seen from Table 4.4, particularly for the CO molecules terminally bonded to the nickel sites at 1.33 ML, the wave numbers generally shift to higher frequency values by 2-14 cm^{-1} from the pristine to the sulfided surface. This indicates that the incorporation of sulfur on the surface causes withdrawal of additional electron density from the surface Ni species, reducing the adsorption strength of the CO molecules, and therefore increasing the IR vibrational frequencies. This is also supported by the IR studies done by Layman and Bussell, who observed a strong absorbance at about 2083 cm^{-1} in their IR spectra for CO adsorbed on the reduced Ni_2P/SiO_2 sample.[21] They attributed this to the stretching of the terminally bonded CO molecules on the reduced Ni_2P surface. Upon sulfidation, this peak shifted to higher frequency of 2093 cm^{-1}, causing an increase of 10

wave numbers. They reached a similar conclusion that the presence of sulfur species on the surface causes the reduction in the electron density of the Ni species on the surface, causing the increase in the vibrational frequencies of CO. Sun et al. also observed a shift in the frequency values from 2082 cm^{-1} to 2094 cm^{-1} for the stretching of CO molecules adsorbed on the reduced and sulfided Ni_2P surfaces respectively (Figure 2.5).[20] The results from both the experimental studies are in excellent agreement with the present calculated results.

Layman and Bussell, and Sun et al. (Figure 2.5) had also observed a sharp decrease in the intensity of absorbance for the terminally bonded CO molecules upon sulfidation of the reduced surface.[20,21] This is inexplicable with respect to the partially sulfided model, since the partial replacement does not reduce the amount the CO molecule adsorbing on the Ni_2P surface. The same modes and number of CO molecules stably adsorb on the pristine and the partially replaced surfaces, as presented in Figure 4.17. Therefore, the partial replacement model fails to explain this sharp decrease in the intensity of absorbance of the linearly bonded CO molecules on the nickel sites. On the basis of the adsorption energies calculated for adsorption of CO on the surface with the adsorbed sulfur atoms, it can be concluded that the presence of these sulfur atoms at the TFH sites prevents adsorption of the CO molecules. Based on the experimental evidence for the reduction in the number of linearly bonded CO on the surface upon sulfidation, it can be concluded that sulfur atoms are also present on the surface at the TFH sites.

Therefore, combining the DFT calculation results and the experimental results published in literature, it can be concluded that the two models may be present simultaneously on the Ni_2P catalyst surface during hydrotreatment. A balance may also exist between the extents to which these two surfaces can be present. The formation of the partially phosphorus replaced model weakens the sulfur-TFH interaction by +0.30 eV, which may limit the population of atomic sulfur on the surface. However, the sulfur replaced Ni_3PS surface plus the sulfur atom deposited surface is a consistent model for the so-called NiP_xS_y phase, which is believed to be the active phase of Ni_2P catalyst at hydrotreating conditions. A qualitative representation of the combined model for the surface is illustrated in Figure 5.1.

The sulfur atoms adsorbed at the TFH sites on the surface block the other molecules (as CO molecules) to adsorb on the surface, and therefore are not beneficial for hydrotreating reactions. On the contrary, incorporation of the sulfur atoms as replacement for surface phosphorus keeps the TFH sites open, and would be the ideal structure to promote hydrotreating reactions. The replacement reduces the interaction between the adsorbed species and the surface, as seen from both the calculated and experimental adsorption energies of CO on the replaced surface, as compared to the pristine surface. This may impart a positive effect according to Sabatier's principle[71], which states that the interaction between the reactant and the catalytic surface should not be too strong so the desorption of products from the surface is hindered, and should not be too weak so the intermediates do not form, and there exist an optimum interaction for which the reaction rate is maximum. This is concordant to the conclusion of the IR studies done by Layman and Bussell, which recommended that the controlled formation of a surface phosphosulfide phase is beneficial to the catalytic properties of Ni_2P.[21]

The next logical steps for this study are therefore to observe hydrogen adsorption and dissociation, and hydrotreating reactions of sulfur and nitrogen containing compounds on the partially sulfided surface, possibly with additional atomic sulfur at the TFH sites—the true form of the active phase of Ni_2P at hydrotreating conditions.

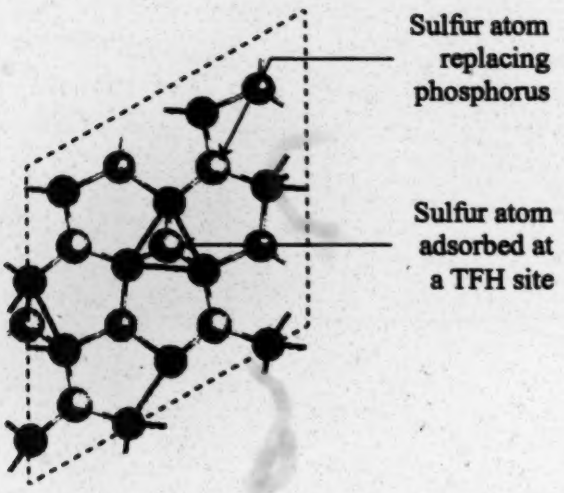

(a)

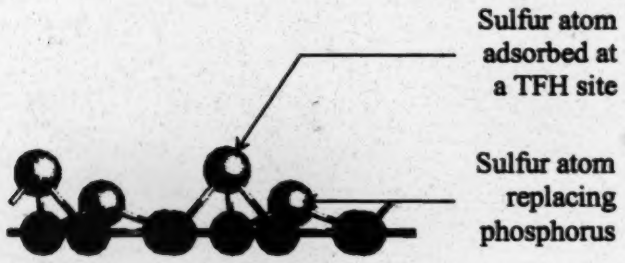

(b)

Figure 5.1 A qualitative representation of the true active phase of Ni_2P at hydrotreating conditions, a combination of the partial replacement model, and the model with adsorbed sulfur atoms: (a) top view; (b) side view. Cyan, purple and yellow represent nickel, phosphorus and sulfur atoms respectively.

5.5 Hydrogen Adsorption

Based on the discussions in the previous sections, hydrogen adsorption and dissociation studies to be done on the combined model are presented in Figure 5.1. However, studies should also be done on the partially replaced surface, which is ideal for hydrotreatment reactions, and on the pristine Ni_3P_2 surface for comparison. The results presented in Section 4.6 are for studies on hydrogen adsorption and dissociation on the pristine and the Ni_3PS surfaces. Due to the time constraints of the project, studies on the combined model could not be conducted.

The most stable modes for hydrogen adsorption on these surfaces are presented in Figure 4.19 and Figure 4.20, respectively. Molecular hydrogen always dissociates and prefers to adsorb at the Ni-Ni bridge positions on the pristine surface. On the other hand, the molecular hydrogen adsorbs most stably horizontally along the surface at the TFH site on Ni_3PS, with an adsorption energy of -0.49 eV/H_2. Atomic hydrogen prefers the Ni-P bridge position, just as on the pristine surface. All the stable modes of adsorption and the related adsorption strengths of atomic and molecular hydrogen are presented in Appendix E. The adsorption strengths of hydrogen atoms on the pristine and the partially replaced model are 0.62 and 0.51 eV per molecule, respectively, which also supports the conclusion drawn from both theoretical and experimental studies that the incorporation of sulfur on the surface decreases the interaction of the surface with the adsorbed species. It had been found that the dissociation of the hydrogen molecule on the pristine surface is a non-activated and spontaneous process. On the other hand, the dissociation process on the partially sulfided surface is location sensitive. Other than the vicinity of the bridging position between two nickel atoms, the dissociation process is activated on Ni_3PS, and hence, transient state/states for the dissociation process is/are supposed to be present between the reactant and product forms shown in Figure 4.20 (a) and (b) respectively.

However, as described in Section 4.6.3, the transient state of the dissociation process could not be determined in this study. It is apparent that the activation energy barrier is quite significant for the dissociation process of molecular hydrogen adsorbed at the TFH site (reactant) to form the atomic hydrogen bonded to two Ni-Ni bridging positions (product), as shown in Figure 4.20. It is also clear that a subtle variation in the

orientation of the reactant can approach the product form, since the geometry optimization of the differently oriented reactants led to the dissociated hydrogen atoms directly, presented in Figure 4.21. Possibilities for presence of more than one reaction intermediates also prevail. Therefore, very careful and explicit studies on the variations of the reactant orientation on the TFH site are required in order to determine the transition state. Within the time line of this project it was not possible to conduct extensive studies on transition state search for hydrogen dissociation reaction.

6 Conclusions

6.1 Conclusions from the Current Study

The objective of this study was to conduct DFT investigations to determine the exact chemical composition of the surface and structure of the sulfur-incorporated active phase of Ni_2P at typical hydrotreating conditions. Adsorption, desorption, dissociation, and hydrotreating reactions of hydrogen, and sulfur containing compounds were also to be studied on this active phase.

Based upon the results of the current study, the stable modes of incorporation of sulfur on the more stable Ni_3P_2 termination of the Ni_2P (001) surface had been found to be atomic sulfur adsorbed at the TFH sites, or sulfur atoms replacing 50% phosphorus from the Ni_3P_2 surface. DFT calculations revealed that CO adsorption on the partially sulfided model is possible for different coverages, whereas, the adsorption is energetically unfavorable on the sulfur atom adsorbed model. The adsorption strength generally decreases from the pristine to the partial replacement model. The calculated vibrational frequencies for the terminally bonded CO molecules at 1.33 ML coverage showed a general tendency to increase by 2-14 wave numbers from the pristine to the replaced sulfided model. Comparison with the values reported in experimental studies[20,21] on the reduced and sulfided Ni_2P confirms the existence of the partially replaced Ni_3PS surface. However, this model could not explain the decrease in the absorbance intensity of CO when the reduced surface is sulfided, as reported in the literature[20,21]. On the other hand, the surface with the adsorbed sulfur atoms can explain this nicely, because the DFT calculations showed that the presence of sulfur atoms in the TFH sites prevents the adsorption of the CO molecules. Therefore, the active phase of Ni_2P at hydrotreating conditions is suggested to be a combination of both of these stable models. A balance between these two forms exists, as the partially replaced model reduces the interaction of the atomic sulfur with the TFH site on the surface in a significant amount.

While the model with adsorbed sulfur atoms opposes the adsorption of further species, the Ni_3PS model does not. But compared to the pristine surface, the Ni_3PS model does reduce the adsorption strength of the adsorbed species, like CO, on the surface. Probably the Ni_3PS model provides an optimum reactant-surface interaction according to Sabatier's principle[71]. Therefore, the Ni_3PS model is the ideal surface for hydrotreatment, and it is necessary to study hydrogen adsorption and dissociation and reaction of the sulfur and nitrogen containing compounds on this ideal surface. However, studies should also be conducted on the combined model representing the active phase, and the pristine surface, for comparison.

Hydrogen dissociation had been found to be non-activated on the pristine surface, and location sensitive on the partially replaced surface. The adsorption strength of the hydrogen atoms were higher on the pristine surface than on the partially replaced model, once again supporting the conclusions that the reactant-surface interaction decreases upon incorporation of sulfur in the structure of the pristine surface.

6.2 Recommendations and Future Works

Since it has been concluded that the combined model (Figure 5.1) is a good qualitative representation of the active phase of Ni_2P at hydrotreating conditions, more studies should be done to determine the exact composition of the model. The ratio of the atomically adsorbed sulfur to surface-phosphorus replacing sulfur can be determined. Having known the qualitative form, such studies should be done on larger cell geometries in order to accommodate more variation to determine the exact composition.

Hydrogen adsorption and dissociation, and HDS and HDN reactions of the sulfur and nitrogen containing compounds should be performed on the combined model in order to observe the hydrotreating reactions on this active phase. Similar investigations should be done on the pristine surface and the partially sulfided ideal hydrotreatment model to conduct comparative studies. As a part of the current work, studies had been done on the hydrogen adsorption and dissociation on the pristine and partially sulfided model. Attempts had also been made in the current study to determine the transient state for hydrogen dissociation reaction on the pristine and partially sulfided models. It had been

found that the hydrogen dissociation reaction on the pristine surface does not have any identifiable transition state, whereas the transient state on the other model could not be determined exactly due to time constraints. However, the form of the transition state is deducible from the results presented in the current study, and further studies should reveal the exact form. Similar studies should be done on the combined model representing the actual surface at hydrotreating conditions. Detailed investigation into the HDS and HDN reactions on the pristine, partially replaced, and the combined models, involving the major sulfur and nitrogen containing contaminant molecules shown in Figure 2.1, can be significant future works in this field.

Similar theoretical studies can be done on the other transition metal phosphides, which would enable us to comprehend the general trends, if any, present in the structure-activity relationship of these catalysts. This would also provide us a better understanding of the exceptional activity of these so-designated "next generation hydrotreating catalysts"[16], as compared to the established conventional sulfide catalysts. This would also provide insights for future modifications for the structure or composition of the phosphides in order to attain better stability at industrial hydrotreating environment.

Bibliography

(1) Webster, D. E. 25 Years of Catalytic Automotive Pollution Control: A Collaborative Effort. *Top. Catal.* **2001**, *16/17* (1-4), 33-38.

(2) Greening, P. European Vehicle Emission Legislation–Present and Future. *Top. Catal.* **2001**, *16/17* (1-4), 5-13.

(3) Booth, M.; Buglass, J. G.; Unsworth, J. F. Tailoring Fuels for the New Millennium. *Top. Catal.* **2001**, *16/17* (1-4), 39-46.

(4) Weisner, O; Landa, S. *Sulphide Catalysts, Their Properties and Applications;* Pergamon Press: Prague, 1973.

(5) Wisconsin Department of Natural Resources. http://dnr.wi.gov/org/aw/air/health/sulfurdiox.htm (accessed July 19, 2006), Sulfur Dioxide.

(6) The Acid Rain Report. http://www.angelfire.com/ks3/acidrainreport/acid.html (accessed July 18, 2006).

(7) Speight, J. G. *The desulfurization of Heavy Oils and Residua*, 2nd Edition; Marcel Dekker Inc.: New York, 2000.

(8) U.S. Environmental Protection Agency. http://www.epa.gov/nonroad-diesel/2004fr/420r04007f.pdf (accessed May 20, 2006). Final Regulatory Analysis: Control of Emissions from Nonroad Diesel Engines: Chapter 5: Fuel and Standard Feasibility.

(9) Bertelsen, I. B. US Motor Vehicle Emission Standards and the Role of Advanced Emission Control Technology in Meeting Those Standards. *Top. Catal.* **2001**, *16/17* (1-4), 15-22.

(10) Control of Air Pollution From New Motor Vehicles: Heavy-Duty Engine and Vehicle Standards and Highway Diesel Fuel Sulfur Control Requirements: Final Rule. *Fed. Regis.* **2001**, *66* (12), 5001-5194.

(11) Kabe, T.; Ishihara, A.; Qian, W. *Hydrodesulfurization and Hydroprocessing Chemistry and Engineering*; Wiley-VCH: Tokyo, 1999.

(12) (a) Bearden, Jr.; Roby; F.; Thomas E. Alkali Metal Desulfurization Process for Petroleum Oil Stocks Using Low Pressure Hydrogen. US Patent 3,787,315, 1974. (b) Baird Jr.; William, C.; Bearden Jr.; Roby. Desulfurization and Hydroconversion of Residua with Sodium Hydride and Hydrogen. US Patent 4,003,824, 1977.

(c) Bearden Jr.; Roby. Combined Desulfurization and Conversion with Alkali Metals. US Patent 4,076,613, 1978.

(13) Brons, G.; Myers, R. D.; Bearden Jr., R.; MacLeod, J. B. Process for Desulfurization of Petroleum Feeds Utilizing Sodium Metal. US Patent 6,210,564, 2001.

(14) Desulfurization, the New-Fashioned Way. *Chem. Eng. Prog.* **April 2006**, 12-13.

(15) McFarland, B. L.; Boron, D. J.; Deever, W.; Meyer, J. A.; Johnson A. R.; Atlas, R. M. Biocatalytic Sulfur Removal from Fuels: Applicability for Producing Low Sulfur Gasoline. *Crit. Rev. Microbio.* **1998**, *24* (2), 99–147.

(16) Oyama, S. T. Novel catalysts for advanced hydroprocessing: transition metal phosphides. *J. Catal.* **2003**, *216* (1-2), 343-352.

(17) Oyama, S. T.; Wang, X.; Requejo, F. G.; Sato, T.; Yoshimura, Y. Hydrodesulfurization of Petroleum Feedstocks with a New Type of Nonsulfide Hydrotreating Catalyst. *J. Catal.* **2002**, *209* (1), 1-5.

(18) Sawhill, S. J.; Phillips, D.C.; Bussell, M. E.; Thiophene hydrodesulfurization over supported nickel phosphide catalysts. *J. Catal.* **2003**, *215* (2), 208-219.

(19) Oyama, S. T.; Wang, X.; Lee, Y.-K.; Bando, K.; Requejo, F.G. Effect of Phosphorus Content in Nickel Phosphide Catalysts Studied by XAFS and Other Techniques. *J. Catal.*, **2002**, *210* (1), 207-217.

(20) Sun, F.; Wu, W.; Wu, Z.; Guo, J.; Wei, Z.; Yang, Y.; Jiang, Z.; Tian, F.; Li, C. Dibenzothiophene hydrodesulfurization activity and surface sites of silica-supported MoP, Ni_2P, and Ni_Mo_P catalysts. *J. Catal.*, **2004**, *228* (2), 298-310.

(21) Layman, K. A.; Bussell, M. E. Infrared Spectroscopic Investigation of CO Adsorption on Silica-Supported Nickel Phosphide Catalysts. *J. Phys. Chem. B.* **2004**, *108* (30), 10930-10941.

(22) Kabe, T.; Ishihara, A.; Tajima, H. Hydrodesulfurization of sulfur-containing polyaromatic compounds in light oil. *Ind. & Ind. Chem. Res.* **1992** *31* (6), 1577-1580.

(23) National Institute of Standards and Technology Scientific and Technical Database: Chemistry Webbook, http://webbook.nist.gov/chemistry/name-ser.html (accessed May 10, 2006), NIST Standard Reference Database Number 69, June 2005 Release.

(24) Bergius, F. Neue Methode zur Verarbeitung von Mineralöl und Kohle. *Z. Angew. Chem.* **1921**, *34* (53), 341-347.

(25) Byrns, A. C.; Bradley, W. E.; Less, M. W. Catalytic Desulfurization of Gasolines by Cobalt Molybdate Process. *Ind. Eng. Chem.* **1943**, *35* (11), 1160-1167.

(26) Ishii, M. *Petrotech.* **1994**, *17*, 174-176.

(27) Sun, M.; Nelson, A. E.; Adjaye, J. On the incorporation of nickel and cobalt into MoS_2-edge structures. *J. Catal.* **2004**, *226* (1), 32-40.

(28) Update: Process Technology. *Chem. Eng. Prog.* **March 2006**, 13.

(29) Pecoraro, T. A.; Chianelli, R. R. Hydrodesulfurization catalysis by transition metal sulfides. *J.Catal.*, **1981**, *67* (2), 430-445.

(30) Suchanek, A. J.; Granniss, E. L. Customized Hydroprocessing with SYNSAT. Presented at the Annual Meeting of the National Petrochemical and Refiners Association, San Francisco, California, U.S.A., March 19-21, 1995; p.AM-95-40.

(31) Plantenga, F. L.; Cerfontain, R.; Eijsbouts, S.; Houtert, F.; Riley, K.; Soled, S.; Miseo, S.; Anderson, G.; Fujita, K. Nebula: A Hydroprocessing Catalyst With Breakthrough Activity, Presented at the Akzo Nobel Catalysts Symposium ECO-MAGIC, The Netherlands, June 2001; H-7.

(32) S. Ramanathan and S.T. Oyama, New Catalysts for Hydroprocessing: Transition Metal Carbides and Nitrides. *J. Phys. Chem.*, **1995**, *99* (44), 16365-16372.

(33) Topsøe, H.; Clausen, B; Massoth, F. E. Hydrotreating Catalysis. In *Catalysis: Science and Technology;* Anderson, J. R.; Boudart, M., Eds.; Springer: Berlin, 1996; Vol. 11.

(34) Oyama, S. T.; Wang, X.; Lee, Y.-K.; Chun, W.-J. Active phase of Ni_2P/SiO_2 in hydroprocessing reactions. *J. Catal.* **2004**, *221* (2), 263-273.

(35) Korányi, T.I. Phosphorus promotion of Ni (Co)-containing Mo-free catalysts in thiophene hydrodesulfurization. *Appl. Catal. A.* **2003**, *239* (1-2), 253-267.

(36) Santen, R. A. van. Computational advances in catalyst modelling. *Chem. Eng. Sci.* **1990**, *45* (8), 2001-2011.

(37) Broadbelt, J. L.; Snurr, R. Q. Applications of molecular modeling in heterogeneous catalysis research. *Appl. Catal., A.* **2000**, *200* (1-2), 23-46.

(38) *Materials Studio*, version 3.2; Online Help; Accelrys: San Diego, CA, USA, 2005.

(39) Accelrys® Materials Studio Modeling Page. http://www.accelrys.com/products/mstudio/modeling (accessed March 2, 2006).

(40) Wikipedia: Molecular Modeling Page. http://en.wikipedia.org/wiki/Molecular_modeling (accessed March 3, 2006).

(41) Cramer, C. J.; *Essentials of Computational Chemistry, Theories and Models,* 2nd ed.; John Wiley and Sons Ltd.: West Sussex, England, 2002.

(42) House, J. E. *Fundamentals of Quantum Chemistry,* 2nd ed.; Elsevier Academic Press: San Diego, CA, USA, 2004.

(43) Koch, W.; Holthausen, M. C. *A Chemist's Guide to Density Functional Theory,* 2nd ed.; Wiley-VCH: Weinheim, Germany, 2001.

(44) Department of Chemistry Queen Mary, University of London. An Introduction to Molecular Orbital Theory. http://www.chem.qmul.ac.uk/software/download/mo/, (accessed March 10, 2006).

(45) Jensen, F. *Introduction to Computational Chemistry*; John Wiley & Sons, 1999Chichester, West Sussex, England.

(46) Lewars, E.; *Computational Chemistry: Introduction to the Theory and Applications of Molecular and Quantum Mechanics*; Boston Kluwer Academic Publishers: Boston, USA, 2003.

(47) Pople J. A.; Beveridge, D. L. *Approximate Molecular Orbital Theory*, McGraw–Hill: New York, 1970.

(48) Lowe, J. P. *Quantum Chemistry*, 2nd Edition; Academic Press: New York, 1993.

(49) Roothaan, C. C.; New Developments in Molecular Orbital Theory. *Rev. Mod. Phys.* **1951**, *23* (2), 69-89.

(50) Hall, G. G. The molecular orbital theory of chemical valency. VIII - A Method of calculating ionization potentials. *Proc. R. Soc.London, Ser. A.* **1951**, 205 (1043), 541-552.

(51) Møller, C.; Plesset, M. S. Note on an Approximation Treatment for Many-Electron Systems. *Phys. Rev.* **1934**, *46* (7), 618-622.

(52) Binkley, J. S.; Pople, J. A. Møller-Plesset theory for atomic ground state energies. *Int. J. Quantum Chem.* **1975**, *9* (2), 229-236.

(53) Levine, I. N.; *Quantum Chemistry*, 5th ed.; Prentice Hall: New Jersey, USA, 2000.

(54) Bader, R. F. W. *Atoms in Molecules*; Oxford Science Publications, Clarendon Press Press: London, 1990.

(55) Parr, R. G.; Yang, G. *Density Functional Theory of Atoms and Molecules.* Oxford University Press: New York, 1989.

(56) Kohn, W.; Becke, A. D.; Parr, R. J. Density Functional Theory of Electronic Structure*J. Phys. Chem.* **1996**, *100* (31), 12974-13322.

(57) Friesner, R. A.; Murphy, R. B.; Beachy, M. D.; Ringnalda, M. N.; Pollard, W. T.; Dunietz, B. D.; Cao, Y. Correlated ab Initio Electronic Structure Calculations for Large Molecules. *J. Phys. Chem. A.* **1996**, *103* (13), 1913-2174.

(58) Slater, J. C. A Simplification of the Hartree-Fock Method. *Phys. Rev.* **1951**, *81* (3), 385-390.

(59) Hohenberg, P.; Kohn, W. Inhomogeneous electron gas. *Phys. Rev. B.* **1964**, *136*, 864-871.

(60) Matyushov, D.; Chapter 27, CHM 341: Elementary Physical Chemistry Lecture Notes, Fall 2002, Department of Chemistry and Biochemistry, Arizona State University.http://www.public.asu.edu/~dmatyus/teaching/chm341/lecture_notes/chapter27/chapter27.pdf (accessed April 5, 2006)..

(61) Kohn, W.; Sham, L. J.; Self-consistent equations including exchange and correlation effects. *Phys. Rev. A.* **1965**, *140*, 1133-1138.

(62) Bauschlicher Jr., C.W.; Ricca, A.; Patridge, H.; Langhoff, S.R. In *Recent Advances in Density Functional Methods*; Chong, D. P., Ed.; World Scientific: Singapore, 1995; Part II.

(63) Frenking, G.; Pidun, U. Ab Initio Studies of Transition Metal Compounds: The Nature of the Chemical Bond to a Transition Metal. *J. Chem. Soc. Dalton Trans.* **1997**, 1653-1662.

(64) Capelle, K. A Bird's-Eye View of Density Functional Theory, *Condens. Matter Phys.*, Submitted for publication, revised v4, 2005.

(65) Ayala, P. Y.; Schlegel, H. B. A combined method for determining reaction paths, minima, and transition state geometries. *J. Chem. Phys.* **1997**, *107* (2), 375-384.

(66) Franzen, S. Density Functional Theory Modules, MultiScale Modeling Course Pages, Department of Chemistry, North Carolina State University,

http://chsfpc5.chem.ncsu.edu/~franzen/CH795N/dft_modules/dft_general/dft_input (accessed April 13, 2006).

(67) Kanama, D.; Oyama, S. T.; Otani, S.; Cox, D. F. Photoemission and LEED characterization of Ni_2P(0 0 0 1). *Surf. Sci.* **2004**, *552* (1-3), 8-16.

(68) Wyckoff, R.W.G. *Crystal Structures*; Interscience Publishers: New York, 1963; Vol. 1.

(69) Moula, M.G.; Suzuki, S.; Chun, W.J.; Otani, S.; Oyama, S.T.; Asakura, K. The First Atomic-scale Observation of a Ni2P(0001) Single Crystal Surface. *Chem. Lett.* **2006**, *35* (1), 90-91.

(70) Liu, P.; Rodriguez, J. A.; Asakura, T.; Gomes, J.; Nakamura, K. Desulfurization Reactions on Ni_2P(001) and α-Mo_2C(001) Surfaces: Complex Role of P and C Sites. *J. Phys. Chem. B.* **2005**, *109* (10), 4575-4583.

(71) Santen, R. A. van. Catalysis: Closing the Molecular and Macroscopic Sciences Gap. *Chem. Eng. Sci.* **1995**, *50* (24), 4027-4044.

Appendix A

Optimization of k-point Parameters

Table A.1 Variation of adsorption energy and frequency values for 1 ML CO adsorbed on the sulfided and unsulfided Ni_2P unit cell surface, for changing k-point parameters.

Surface	k-points	Adsorption energy per CO molecule (eV)	Frequency (cm^{-1})
Unsulfided	3x3x1	-1.10	2109
	4x4x1	-1.09	2088
	5x5x1	-1.09	2089
Sulfided	3x3x1	-0.96	2085
	4x4x1	-0.95	2085
	5x5x1	-0.95	2089

Appendix B

Dissociative Adsorption of H_2S as Atomic Sulfur on Ni_2P

Total Energy of the Pristine Ni_2P Supercell Structure = -294.95 eV

Total Energy of H_2S Molecule = -7.95 eV

Total Energy of H_2 Molecule = -4.56 eV

Table B.1 Calculated data for dissociative adsorption of H_2S as atomic sulfur on pristine Ni_2P supercell surface.

Stable Modes of Adsorption	**Total Energy (eV) of the Sulfur-adsorbed Structure**	**Adsorption Energy (eV/H_2S) of Atomic Sulfur**
In TFH	-299.99	-1.64
Bridge between a nickel and a phosphorus atom	-298.59	-0.25

Appendix C

Replacement of Phosphorus by Sulfur Atoms from Ni_2P Surface

Total Energy of the Pristine Ni_2P Supercell Structure = -294.95 eV

Total Energy of PH_3 Molecule = -10.36 eV

Total Energy of H_2S Molecule = -7.95 eV

Total Energy of H_2 Molecule = -4.56 eV

Table C.1 Calculated data for the replacement of the phosphorus atoms from the Ni_3P_2 surface by the sulfur atoms from the gas phase H_2S.

Number of Phosphorus Atoms Replaced	Replaced Positions	Total Energy (eV) of the Replaced Structure	Total Energy Change (eV/S) per Sulfur Atom
1	1	-295.12	-0.29
	2	-295.11	-0.29
	3	-295.12	-0.29
	4	-295.12	-0.29
	7	-295.11	-0.29
2	1,2	-295.06	-0.18
	2,7	-295.06	-0.18
	6,7	-295.06	-0.18
	1,4	-295.13	-0.22
	1,7	-295.29	-0.30
3	1,5,7	-295.50	-0.32
	1,6,7	-295.11	-0.18
	2,3,7	-295.10	-0.18
	2,7,8	-295.07	-0.17
4	1,2,3,4	-294.96	-0.13
	1,2,3,5	-295.19	-0.19
	1,2,3,6	-294.96	-0.13
	1,2,3,7	-295.25	-0.20
	1,2,3,8	-295.00	-0.14
	1,2,4,8	-295.20	-0.19
	1,3,5,7	-295.72	-0.32
	1, 4,6,7	-294.95	-0.12
	2,5,7,8	-294.94	-0.13

Table C.1(Cont.) Calculated data for the replacement of the phosphorus atoms from the Ni_3P_2 surface by the sulfur atoms from the gas H_2S.

Number of Phosphorus Atoms Replaced	Replaced Positions	Total Energy (eV) of the Replaced Structure	Total Energy Change (eV/S) per Sulfur Atom
5	1,2,3,4,8	-294.97	-0.13
	1,2,3,5,6	-295.40	-0.22
	2,3,4,5,6	-294.91	-0.12
	7,2,3,5,8	-294.90	-0.12
	7,3,4,5,6	-294.96	-0.13
6	1,2,3,4,5,6	-294.70	-0.09
	1,3,4,5,6,7	-295.06	-0.15
	2,3,4,5,6,7	-294.75	-0.10
7	1,2,3,4,5,6,7	-294.67	-0.09
8	1,2,3,4,5,6,7,8	-294.96	-0.06

Appendix D

CO Adsorption on Pristine and Partially Sulfided Ni_2P

Energy of the pristine Ni_2P unit cell = -74.45 eV

Energy of the partially phosphorus replaced Ni_2P unit cell = -74.59 eV

Energy of CO molecule = -11.98 eV

Table D.1 Calculated data for the stable modes of CO adsorption on the pristine Ni_2P surface, for different surface coverages.

Surface Coverage	Stable Modes of Adsorption	Total Energy (eV) of the Structure	Adsorption Energy (eV/CO) per Molecule
0.33	Single CO molecule bonded on top of the TFH	-88.33	-1.90
0.67	Two CO molecules, each bonded linearly to a nickel atom	-100.90	-1.24
	Two CO molecules, each bonded at the bridging position between two nickel atoms	-100.84	-1.21
	One CO molecule bonded linearly to a nickel atom, another at the bridging position between two nickel atoms	100.94	-1.26
1.00	Three CO molecules, each bonded on top of a nickel atom	-113.68	-1.09
	Three CO molecules, each bonded between two nickel atoms at the bridging position	-112.66	-0.76
	Two CO molecules each bonded linearly to a nickel atom, and one other bonded at the bridging position between two nickel atoms	-113.65	-1.08

Table D.1(Cont.) Calculated data for the stable modes of CO adsorption on the pristine Ni_2P surface, for different surface coverages.

Surface Coverage	Stable Modes of Adsorption	Total Energy (eV) of the Structure	Adsorption Energy (eV/CO) per Molecule
1.00	One CO molecule bonded on top of the TFH, one bonded linearly to a nickel atom, and one at the bridging position between two nickel atoms	-112.95	-0.85
1.33	One CO molecule bonded on top of the TFH, three other bonded linearly to a nickel atom each	-124.08	-0.43

Table D.2 Calculated data for the stable modes of CO adsorption on the partially phosphorus replaced Ni_2P surface, for different surface coverages.

Surface Coverage	Stable Modes of Adsorption	Total Energy (eV) of the Structure	Adsorption Energy (eV/CO) per Molecule
0.33	Single CO molecule bonded on top of the TFH	-88.34	-1.78
0.67	Two CO molecules, each bonded linearly to a nickel atom	-100.61	-1.03
	One CO molecule bonded on top of the TFH, one linearly to a nickel atom	-100.65	-1.05
	One CO molecule bonded linearly to a nickel atom, one at the bridging position between two nickel atoms	100.68	-1.07
1.00	Three CO molecules, each bonded on top of a nickel atom	-113.39	-0.95
	Three CO molecules, each bonded between two nickel atoms at the bridging position	-112.44	-0.64
	Two CO molecules each bonded linearly to a nickel atom, and one other bonded at the bridging position between two nickel atoms	-113.00	-0.82
1.33	One CO molecule bonded on top of the TFH, three other bonded linearly to a nickel atom each	-123.97	-0.36

Appendix E

Hydrogen Adsorption on Pristine and Partially Sulfided Ni_2P

Energy of hydrogen molecule = -4.56 eV

Energy of the Pristine Ni_2P structure = -74.44 eV

Energy of the partially phosphorus replaced Ni_2P unit cell = -74.55 eV

Table E.1 Calculated data for the stable modes of hydrogen adsorption on the pristine Ni_2P unit cell surface.

Stable Modes of Adsorption	Total Energy (eV) of the Hydrogen Adsorbed Structure	Adsorption Energy (eV/H_2) per Molecule
Two hydrogen atoms bonded linearly on the same nickel site	-79.34	-0.34
Two hydrogen atoms bonded at two different bridging sites between nickel atoms	-79.62	-0.62
One hydrogen atom bonded on the TFH site, the other linearly bonded to a phosphorus atom	-79.41	-0.41
One hydrogen atom bonded on the TFH site, the other bonded linearly to a nickel atom	-79.43	-0.43
One hydrogen atom bonded linearly to a nickel atom, another bridged between the other two nickel sites	-79.40	-0.40
One hydrogen atom bonded on the TFH site, the other bridged between a nickel and a phosphorus atom	-79.57	-0.56

Table E.2 Calculated data for the stable modes of adsorption of molecular hydrogen on the partially replaced Ni_2P unit cell surface.

Stable Modes of Adsorption	Total Energy (eV) of the Hydrogen Adsorbed Structure	Adsorption Energy (eV/H_2) per Molecule
Terminally bonded to a sulfur atom	-79.13	-0.03
Vertically bonded at the TFH site	-79.15	-0.04
Horizontally bonded at the TFH site	-79.60	-0.49

Table E.3 Calculated data for the stable modes of adsorption of hydrogen atoms on the partially replaced Ni_2P unit cell surface.

Stable Modes of Adsorption	Total Energy (eV) of the Hydrogen Adsorbed Structure	Adsorption Energy (eV/H_2) per Molecule
One hydrogen atom bonded linearly to a nickel site, the other bonded linearly to a phosphorus atom	-79.31	-0.20
Two hydrogen atoms bonded at two different bridging sites between nickel atoms	-79.62	-0.51
One hydrogen atom bonded on the TFH site, the other linearly bonded to a sulfur atom	-79.28	-0.17
One hydrogen atom bonded on the TFH site, the other bridged between a nickel and a phosphorus site	-79.43	-0.32
One hydrogen atom bonded on the TFH site, the other linearly bonded to a nickel atom	-79.25	-0.15

Table E.3(Cont.) Calculated data for the stable modes of adsorption of hydrogen atoms on the partially replaced Ni_2P unit cell surface.

Stable Modes of Adsorption	Total Energy (eV) of the Hydrogen Adsorbed Structure	Adsorption Energy (eV/H_2) per Molecule
One hydrogen atom bonded on the TFH site, the other terminally bonded to a phosphorus site	-79.31	-0.20
One hydrogen atom bonded to a nickel site, and the other bridged between two other nickel sites	-79.42	-0.31
Two hydrogen atoms each bonded linearly to a separate nickel site	-79.27	-0.16
One hydrogen atom bonded on the TFH site, the other bridged between another nickel and a phosphorus site	-79.42	-0.31